

DESIGN OF A COMPLEX MODULUS TEST SYSTEM FOR VISCOELASTIC
MATERIALS

A THESIS SUBMITTED TO
THE GRADUATE SCHOOL OF NATURAL AND APPLIED SCIENCES
OF
MIDDLE EAST TECHNICAL UNIVERSITY

BY

BİLGEHAN ERDOĞAN

IN PARTIAL FULFILLMENT OF THE REQUIREMENTS
FOR
THE DEGREE OF MASTER OF SCIENCE
IN
MECHANICAL ENGINEERING

DECEMBER 2019

Approval of the thesis:

**DESIGN OF A COMPLEX MODULUS TEST SYSTEM FOR
VISCOELASTIC MATERIALS**

submitted by **BİLGEHAN ERDOĞAN** in partial fulfillment of the requirements for the degree of **Master of Science in Mechanical Engineering Department, Middle East Technical University** by,

Prof. Dr. Halil Kalıpçılar

Dean, Graduate School of **Natural and Applied Sciences**

Prof. Dr. M. Sahir ARIKAN

Head of Department, **Mechanical Engineering**

Assist. Prof. Dr. Gökhan O. ÖZGEN

Supervisor, **Mechanical Engineering, METU**

Examining Committee Members:

Prof. Dr. Ender CİĞEROĞLU

Mechanical Engineering, ODTÜ

Assist. Prof. Dr. Gökhan O. ÖZGEN

Mechanical Engineering, METU

Prof. Dr. Y. Samim ÜNLÜSOY

Mechanical Engineering, ODTÜ

Assist. Prof. Dr. Orkun ÖZŞAHİN

Mechanical Engineering, ODTÜ

Assoc. Prof. Dr. Yiğit TAŞÇIOĞLU

Mechanical Engineering, TED University

Date: 04.12.2019

I hereby declare that all information in this document has been obtained and presented in accordance with academic rules and ethical conduct. I also declare that, as required by these rules and conduct, I have fully cited and referenced all material and results that are not original to this work.

Name, Surname: Bilgehan Erdoğan

Signature:

ABSTRACT

DESIGN OF A COMPLEX MODULUS TEST SYSTEM FOR VISCOELASTIC MATERIALS

Erdoğan, Bilgehan
Master of Science, Mechanical Engineering
Supervisor: Assist. Prof. Dr. Gökhan O. ÖZGEN

December 2019, 143 pages

In this thesis, the design of test devices for dynamic characterization of elastomer materials and elastomer vibration control components are designed. For this purpose, two different studies are conducted. In the first study, an already installed test setup is modified to provide preloading capability. In the second study, a completely new test setup is established. Conceptual design studies are carried out based on the information obtained in the literature and related standards, then the validity of the design has been investigated with finite element eigenvalue extraction analysis. The consistency of the results is evaluated by frequency dependent comparative tests. Error analysis study is carried out accordingly because the results were not consistent as expected. The effects that could cause these distortions are discussed and comments are made about possible changes. The outputs are aimed to guide the people who will work on this subject.

Keywords: Complex modulus, Dynamic stiffness, Dynamic tests, Viscoelastic materials

ÖZ

VİSKOELASTİK MALZEMELER İÇİN KARMAŞIK MODÜL ÖLÇÜM TEST DÜZENEGİ TASARIMI

Erdoğan, Bilgehan
Yüksek Lisans, Makina Mühendisliği
Tez Danışmanı: Dr. Öğr. Üyesi Gökhan O. ÖZGEN

Aralık 2019, 143 sayfa

Bu tez kapsamında elastomer malzemelerin ve elastomer titreşim kontrol bileşenlerinin dinamik karakterizasyonu amacıyla kullanılacak test düzeneklerinin tasarımı yapılmıştır. Bu amaçla iki farklı çalışma yürütülmüştür. Birinci çalışmada halihazırda kurulu bir test düzeneği önyükleme özelliği kazandırmak amacıyla modifiye edilmiştir. Diğer çalışma kapsamında tamamen yeni bir düzenek kurulmuştur. Literatürde elde edilen bilgiler ve ilgili standartlara bağlı olarak kavramsal tasarım çalışmaları yapılmış ve sonlu eleman analizleriyle tasarımın geçerliliği araştırılmıştır. Düzeneklerin üretimi yapılmış ve frekansa bağlı kıyaslamalı testler ile sonuçların tutarlılığı değerlendirilmiştir. Sonuçların beklendiği gibi tutarlı gelmemesinden dolayı hata ayıklama çalışmaları yürütülmüştür. Bu çalışmalar ile bu bozulmalara sebep olabilecek etkenler üzerinde tartışılmış ve olası değişiklikler hakkında yorumlarda bulunulmuştur. Elde edilen çıktıların bu konu ile ilgili çalışacak kişilere yol göstermesi amaçlanmaktadır.

Anahtar Kelimeler: Karmaşık modül, Dinamik direngenlik, Dinamik testler, Viskoleastik malzemeler

This work is dedicated to those who support me insistently to continue this work to
the end.

ACKNOWLEDGEMENTS

This study was carried out under SAN-TEZ R&D Program supported by Ministry of Science, Industry and Technology of Turkish Republic in collaboration with ROKETSAN Missiles Inc. (Project No: 00947.STZ.2011-2, Elastomer Titreşim Takozlarının Tasarımı)

I am grateful to Halil ARDIÇ and Eren KOÇAK for performing modal tests in modal characterization studies.

I would like to thank Kemal ÇENLİ for the manufacturing of the assemblies and for correcting some mistakes in the design and Haşim ÖZEL for helping me during the assembly process.

I would like to thank Gökhan KARAPISTİK for receiving great support in error analysis.

I would like to express my gratitude to Asst. Prof. Gökhan ÖZGEN, the esteemed supervisor for whom I have worked together during all conceptual and detail design, who contributed personally to all the works both as a colleague and a guide, who financed me during the working process and who supported morally at any time.

I would like to thank my family for their persistent support of me on everything else.

TABLE OF CONTENTS

ABSTRACT.....	v
ÖZ	vi
ACKNOWLEDGEMENTS	viii
TABLE OF CONTENTS	ix
LIST OF TABLES	xii
LIST OF FIGURES	xiii
CHAPTERS	
1. INTRODUCTION	1
1.1. Introduction	1
1.2. Objective of the Thesis.....	2
1.3. Motivation of the Thesis.....	3
1.4. Structure of the Thesis.....	4
2. LITERATURE REVIEW	5
2.1. Introduction	5
2.2. Linear Viscoelastic Behavior	5
2.2.1. Mathematical Models for Viscoelastic Behavior.....	5
2.2.2. Definition of Complex Modulus.....	8
2.2.3. Dependency of Complex Modulus on Environmental Factors.....	9
2.2.4. Temperature & Frequency Equivalence	10
2.2.5. Nonlinear Behavior of Elastomers.....	11
2.3. Testing Methods for Viscoelastic Properties.....	13
2.3.1. Measuring Time-Dependent Properties	14
2.3.2. Measuring Frequency-Dependent Properties.....	14

2.4. Design Considerations about Dynamic Testing.....	23
2.5. Factors Influencing Measurements	24
2.6. Previous Studies about the Topic of Interest	25
3. DESIGN EFFORTS FOR A PRELOADING MECHANISM FOR AN ALREADY EXISTING TEST SETUP FOR VISCOELASTIC MATERIAL CHARACTERIZATION.....	31
3.1. Introduction.....	31
3.2. Unmodified Version of the Test Setup	31
3.3. Design Objectives, Requirements and Constraints	32
3.4. Design Efforts	32
3.4.1. Conceptual Design	32
3.4.2. Structural Design.....	34
3.4.3. Instrumentation and Measurement	35
3.4.4. Design of Preloading Mechanism	38
3.5. Design Evaluation.....	40
3.6. Design Revision	41
3.6.1. Design of a Preloading Mechanism with Elastomeric Bands	41
3.6.2. Calculation of Internal Resonance Frequency of Preloading Mechanism.....	43
3.7. Re-Evaluation of the Design	47
3.8. Conclusions.....	48
4. DESIGN EFFORTS FOR A NEW TEST SETUP.....	49
4.1. Introduction.....	49
4.2. Design Objectives, Requirements and Constraints	50
4.3. Design Efforts	51

4.3.1. Conceptual Design	51
4.3.2. Investigation of the Validity of the Structural Design using Finite Element Based Simulations.....	52
4.3.3. Instrumentation and Measurement.....	69
4.4. Design Evaluation	70
4.5. Determination of the Dynamic Effects of Structural Features on Accuracy of Dynamic Stiffness Measurements	73
4.5.1. Simulation of Dynamic Stiffness Measurements using Reduced-Order Models Developed to Represent Dynamics of the Test Setup.....	74
4.5.2. Modal Characterization.....	100
4.5.3. Simulation of Dynamic Stiffness Measurements in the Test Setup Using Finite Element Based Harmonic Response Analysis.....	112
4.5.4. Comments on Analysis Results	123
4.6. Design Re-Evaluation & Validation.....	123
4.6.1. Design of a Calibration Specimen	124
4.6.2. Dynamic Stiffness Validation Tests	129
4.7. Conclusions	132
5. CONCLUSION.....	135
REFERENCES.....	137
APPENDICES	
A. COMPARISON OF DYNAMIC STIFFNESS MEASUREMENTS MADE USING THE TWO TEST SETUPS STUDIED IN THIS THESIS	141

LIST OF TABLES

TABLES

Table 2.1. The comparison of test methods in ASTM D5992.....	23
Table 3.1. Estimated force vs stroke for elastomeric bands	42
Table 3.2. Internal resonance frequency calculations for decoupling springs with coil spring	46
Table 3.3. Internal resonance frequency calculations for decoupling springs with elastomeric bands.....	46
Table 4.1. Mode frequencies and shapes obtained by FE analysis.....	64
Table 4.2. Transmitted force values at frequency limits	68
Table 4.3. Maximum deflection values at frequency limits	68
Table 4.4. System Parameters.....	77
Table 4.5. Calculated natural frequencies for Two-Axial DOF Point Mass Model ..	78
Table 4.6. Calculated natural frequencies for Four-Axial DOF Point Mass Model ..	81
Table 4.7. Calculated natural frequencies for Model with Two Beam Elements.....	86
Table 4.8. Calculated natural frequencies for Model with Two Beam Elements Supported by Transverse Beam	90
Table 4.9. Calculated natural frequencies for Model with Two Beam Elements Supported by Transverse Beam, Constrained Actuator.....	96
Table 4.10. Mode frequencies and shapes obtained by modal test.....	110
Table 4.11. List of correlated modes	112
Table 4.12. Specimen properties used in the test simulation model.....	115
Table 4.13. Analysis configurations used in test simulation	116
Table 4.14. Measurement methods used in the analysis mode and their details	117
Table 4.15. Parameters and results for quadruple beam spring.....	126
Table 4.16. Parameters and results for ring spring	127

LIST OF FIGURES

FIGURES

Figure 2.1. Essential spring-dashpot models to represent viscoelastic behavior	6
Figure 2.2. Temperature dependence of a typical elastomeric material	10
Figure 2.3. Hysteresis loop observed in rubber stress-strain relationship (Banks, Pinter, Potter, Gaitens, & Yanyo, 2013)	11
Figure 2.4. Typical behavior of an elastomeric material at high strain deformation (SIMULIA, 2016)	12
Figure 2.5. Change of storage and loss modulus with strain amplitude for different filler portions (Roland, 2016).....	13
Figure 2.6. General layout of a forced non-resonant test system.....	17
Figure 2.7. Schematic representation of Direct Method	18
Figure 2.8. Direct method, force measurement from ground.....	19
Figure 2.9. Direct method with resilient fixture where force measurement on actuator side (a) and fixture side (b)	19
Figure 2.10. Direct method with resilient fixture and decoupling springs.....	21
Figure 2.11. Tension-compression specimen.....	22
Figure 2.12. Double-shear specimen.....	22
Figure 2.13. Detail view of the test system on temperature chamber	26
Figure 2.14. Final design of the test fixture as a result of optimization study	27
Figure 2.15. Overview of the test system designed by Uz (2013)	28
Figure 2.16. General layout of the test system designed by Bilgi (2016).....	29
Figure 3.1. Overview of the modified design	33
Figure 3.2. Detailed view and the components of the setup	34
Figure 3.3. First bending mode, 376 Hz	35
Figure 3.4. First torsional mode 657 Hz	35
Figure 3.5. Instrumentation layout of the modified test setup	36

Figure 3.6. Flowchart of the amplitude control code.....	37
Figure 3.7. Detailed view of the preload mechanism	39
Figure 3.8. Stress distribution on the preload mechanism.....	39
Figure 3.9. System with coil springs	40
Figure 3.10. Real stiffness measurements vs frequency at the first attempt.....	41
Figure 3.11. Loss factor measurements vs frequency at the first attempt	41
Figure 3.12. Preloading mechanism with elastomeric bands	43
Figure 3.13. Mechanical representation of the preloading mechanism	43
Figure 3.14. Real stiffness and loss factor measurements for the system with elastomeric bands.....	47
Figure 4.1. Overview of the test setup	51
Figure 4.2. FE model of test system	53
Figure 4.3. Modelling electrodynamic-actuator	54
Figure 4.4. Region where specimen is mounted.....	55
Figure 4.5. Analysis results, 1st-(left) and 2nd (right) mode shapes, 12.3 Hz, 16.5 Hz	55
Figure 4.6. Analysis results, 3rd-(left) and 4th (right) mode shapes, 19.8 Hz, 19.9 Hz	56
Figure 4.7. Analysis results, 5th-(left) and 6th (right) mode shapes, 27.1 Hz, 28.4 Hz	56
Figure 4.8. Analysis results, 7th-(left) and 8th (right) mode shapes, 28.9 Hz, 57.1 Hz	57
Figure 4.9. Analysis results, 9th-(left) and 10th (right) mode shapes, 59.8 Hz, 59.9 Hz	57
Figure 4.10. Analysis results, 11th-(left) and 12th (right) mode shapes, 74.2 Hz, 75.8 Hz.....	58
Figure 4.11. Analysis results, 13th-(left) and 14th (right) mode shapes, 75.9 Hz, 82.9 Hz.....	58
Figure 4.12. Analysis results, 15th-(left) and 16th (right) mode shapes, 121.9 Hz, 152.3 Hz.....	59

Figure 4.13. Analysis results, 17th-(left) and 18th (right) mode shapes, 155.3 Hz, 166.6 Hz	59
Figure 4.14. Analysis results, 19th-(left) and 20th (right) mode shapes, 184.5 Hz, 187.8 Hz	60
Figure 4.15. Analysis results, 21st-(left) and 22nd (right) mode shapes, 216.9 Hz, 217.5 Hz	60
Figure 4.16. Analysis results, 23rd-(left) and 24th (right) mode shapes, 235.4 Hz, 288.9 Hz	61
Figure 4.17. Analysis results, 25th-(left) and 26th (right) mode shapes, 290.6 Hz, 305.4 Hz	61
Figure 4.18. Analysis results, 27th-(left) and 28th (right) mode shapes, 343.8 Hz, 370.1 Hz	62
Figure 4.19. Analysis results, 29th-(left) and 30th (right) mode shapes, 380.5 Hz, 380.5 Hz	62
Figure 4.20. Analysis results, 31st-(left) and 32nd (right) mode shapes, 411.3 Hz, 437.1 Hz	63
Figure 4.21. Analysis results, 33rd mode shape, 449.5 Hz	63
Figure 4.22. 2 DOF model used for determination of force capacity	66
Figure 4.23. Force profile of APS 400 Shaker	66
Figure 4.24. Transmitted force vs frequency for three stiffness configurations	67
Figure 4.25. Maximum deflection for three stiffness configurations	67
Figure 4.26. Instrumentation layout for test setup	69
Figure 4.27. Assembled test setup and its components.....	70
Figure 4.28. Real stiffness measurements for AM 009-14, compared with MTS 831.50	71
Figure 4.29. Loss factor measurements for AM-009-14, compared with MTS 831.50	71
Figure 4.30. Accelerometer locations	72
Figure 4.31. Dynamic stiffness measurements for LORD AM-009	72
Figure 4.32. Loss factor measurements for LORD AM-009	73

Figure 4.33. Two-Axial DOF Point Mass Model	78
Figure 4.34. Mode shapes for Two-Axial DOF Point Mass Model	78
Figure 4.35. Stiffness calculation for Two-Axial DOF Point Mass Model.....	79
Figure 4.36. Deviation of calculated stiffness from reference for Two-Axial DOF Point Mass Model.....	79
Figure 4.37. Four-Axial DOF Point Mass Model.....	80
Figure 4.38. Mode shapes for Four-Axial DOF Point Mass Model	81
Figure 4.39. Stiffness calculation for Four-Axial DOF Point Mass Model.....	82
Figure 4.40. Deviation of calculated stiffness from reference for Four-Axial DOF Point Mass Model.....	82
Figure 4.41. Model with Two Beam Elements.....	83
Figure 4.42. Schematic representation of frame element or generalized beam element	84
Figure 4.43. First nine modes, 1-4,6-7th modes are bending and 5,8,9th are axial...	87
Figure 4.44. Stiffness calculation for Model with Two Beam Elements.....	88
Figure 4.45. Deviation of calculated stiffness from reference for Model with Two Beam Elements	88
Figure 4.46. First nine modes for Model with Two Beam Elements	91
Figure 4.47. Stiffness calculation for Model with Two Beam Elements Supported by Transverse Beam, 0-2000 Hz	92
Figure 4.48. Stiffness calculation for Model with Two Beam Elements Supported by Transverse Beam, 0-400 Hz	92
Figure 4.49. Deviation of calculated stiffness from reference between 0-400 Hz for Model with Two Beam Elements Supported by Transverse Beam.....	93
Figure 4.50. Stiffness calculation for Model with Two Beam Elements Supported by Transverse Beam, with Sensor offset	94
Figure 4.51. Deviation of calculated stiffness from reference for Model with Two Beam Elements Supported by Transverse Beam, with Sensor offset.....	94
Figure 4.52. First nine modes for Model with Two Beam Elements Supported by Transverse Beam, Constrained Actuator	97

Figure 4.53. Stiffness calculation for Model with Two Beam Elements Supported by Transverse Beam, Constrained Actuator.....	98
Figure 4.54. Deviation of calculated stiffness from reference for Model with Two Beam Elements Supported by Transverse Beam, Constrained Actuator.....	98
Figure 4.55. Stiffness calculation for Model with Two Beam Elements Supported by Transverse Beam, Constrained Actuator, Sensor Offset.....	99
Figure 4.56. Deviation of calculated stiffness from reference for Model with Two Beam Elements Supported by Transverse Beam, Constrained Actuator, Sensor Offset	99
Figure 4.57. Overview of the test system.....	101
Figure 4.58. Locations of accelerometers to be used in modal tests.....	102
Figure 4.59. Test results, 1st mode shape, 16.6 Hz.....	102
Figure 4.60. Test results, 2nd mode shape, 24.5 Hz	103
Figure 4.61. Test results, 3rd mode shape, 42.9 Hz	103
Figure 4.62. Test results, 4th mode shape, 48.2 Hz	104
Figure 4.63. Test results, 5th mode shape, 60.1 Hz	104
Figure 4.64. Test results, 6th mode shape, 80.9 Hz	105
Figure 4.65. Test results, 7th mode shape, 93.9 Hz	105
Figure 4.66. Test results, 8th mode shape, 116.5 Hz	106
Figure 4.67. – Test results, 9th mode shape, 122.5 Hz	106
Figure 4.68. Test results, 10th mode shape, 192.7 Hz	107
Figure 4.69. Test results, 11th mode shape, 259.4 Hz	107
Figure 4.70. Test results, 12th mode shape, 328.5 Hz	108
Figure 4.71. Test results, 13th mode shape, 343.0 Hz	108
Figure 4.72. Test results, 14th mode shape, 369.6 Hz	109
Figure 4.73. Test results, 15th mode shape, 443.2 Hz	109
Figure 4.74. Test results, 16th mode shape, 463.8 Hz	110
Figure 4.75. MAC numbers between analysis and test.....	111
Figure 4.76. General configuration of the analysis model.....	113
Figure 4.77. Electrodynamic actuator model	114

Figure 4.78. Engineering element definition between mounting blocks to represent resilient specimen	114
Figure 4.79. Configuration without offset between armature force axis and transmission rods (left) and with offset (right)	116
Figure 4.80. Measurement locations used in the analysis, vibrating blocks at left, armature on the middle and frame at right	117
Figure 4.81. Real stiffness calculations for analysis configuration #1	118
Figure 4.82. Deviations of real stiffness from reference for analysis configuration #1	118
Figure 4.83. Real stiffness calculation for analysis configuration #2.....	119
Figure 4.84. Deviation of real stiffness from reference for analysis configuration #2	119
Figure 4.85. Real stiffness calculation for analysis configuration #2.....	120
Figure 4.86. Deviation of real stiffness from reference for analysis configuration #2	120
Figure 4.87. Damping coefficient calculations for analysis configuration #1.....	121
Figure 4.88. Deviations of damping coefficient from reference for analysis configuration #1	121
Figure 4.89. Damping coefficient calculations for analysis configuration #2.....	122
Figure 4.90. Deviations of damping coefficient from reference for analysis configuration #2.....	122
Figure 4.91. Damping coefficient calculations for analysis configuration #3.....	122
Figure 4.92. Deviations of damping coefficient from reference for analysis configuration #3.....	123
Figure 4.93. Spring types proposed for a calibration spring.....	124
Figure 4.94. Quadruple beam spring with design dimensions.....	125
Figure 4.95. Ring spring with design dimensions	126
Figure 4.96. Ring spring calibration specimen	128
Figure 4.97. Force-deflection curve of the calibration spring	128

Figure 4.98. Real stiffness measurements and deviation from the reference value, 50N/mm130

Figure 4.99. Damping coefficient measurements and deviation from the reference value, 0.01N.s/mm131

Figure A.1. Real stiffness measurements for LORD AM-009141

Figure A.2. Loss factor measurements for LORD AM-009141

Figure A.3. Real stiffness measurements for custom-made vibration mount, room temperature.....142

Figure A.4. Loss factor measurements for custom-made vibration mount, room temperature.....142

Figure A.5. Dynamic stiffness measurements for custom-made vibration mount, 70°C143

Figure A.6. Loss factor measurements for custom-made vibration mount, 70°C ...143

CHAPTER 1

INTRODUCTION

1.1. Introduction

Elastomer materials are widely used in vibration control applications. Because these materials have high damping properties, are easy to apply and economical at the same time, making them attractive for these applications. However, it is possible to use these materials in vibration control applications only by measuring their dynamic properties accurately. The mechanical behavior of these materials is dependent on various environmental conditions and type of deformation.

When elastomer materials are deformed, they store and absorb mechanical energy. This is defined as viscoelastic behavior. The frequency-dependent stress-strain relationship of viscoelastic materials is defined by the concept of complex modulus. Complex moduli of elastomers are dependent on environmental and mechanical conditions such as temperature, frequency, dynamic amplitude and amount of carried preload.

Dynamic characterization of the vibration control devices is essential for correct application of these solutions to vibration problem in case. For design and application of vibration damping elements and other vibration control applications (surface damping treatment, tuned mass dampers) the measurement of the complex module is necessary.

Characterization of viscoelastic materials and components for vibration control applications can be performed by exciting these components by cyclic loads and measuring the deformations and applied or transferred forces. The devices that are specialized for characterization of these components are dynamic characterization test setups and dynamic mechanical analyzers for material characterization. Mechanical,

electrodynamic and hydraulic exciters could be utilized to generate necessary harmonic load on the specimen in these systems. Some auxiliary components could be used in order to control other variables such as temperature and preload. Dynamic properties could be gathered either directly measuring force and displacement of the specimen or deriving from modal characteristics of the setup depending on the test method.

The topic of this thesis is presentation of the efforts for design and development of test systems specialized for dynamic characterization of viscoelastic materials and viscoelastic components such as vibration isolators. The test systems for measurement of viscoelastic properties can be used both for complex modulus measurement and for vibration isolator characterization. There is a relationship between isolator and material behavior related to geometry. Therefore, the information presented in this study is related with both design of test system for complex modulus measurement and isolator characterization.

1.2. Objective of the Thesis

In this thesis, it is aimed to design two test setups for dynamic characterization of viscoelastic components and explain the studies to gather experience about this context. Therefore, experiences gathered by the development of two different test setups will be expressed. In addition, it is expected to determine the design considerations for dynamic characterization test systems of viscoelastic materials and viscoelastic components, and then to provide guidance for the people working in this field. For this purpose, two different design studies were carried out.

In the first study, a test setup developed in ODTÜ Mechanical Engineering Department is modified in order to introduce manual preloading mechanism. In addition, software of the setup developed in LabVIEW environment is updated to enable amplitude-controlled sine sweep tests. The modified design has been verified by comparing the results obtained from the original test setup.

In the second study, a test setup was designed from scratch. This setup is aimed for both viscoelastic material characterization and dynamic characterization of vibration isolators with respect to temperature, frequency, strain amplitude and preload. It was observed that the mechanism designed within the scope of the second study did not work as expected in the target frequency range. For this reason, analysis and test studies were carried out to find the source of the problem. The sources of the problems were tried to be identified and solution suggestions were presented.

1.3. Motivation of the Thesis

Special testing devices are required to measure these properties. Commercial products are available on the market for this purpose, but people can install their own special test devices if these devices are not economically affordable. The structural properties of the test system used affect the measurements. For this reason, dynamic effects must be taken into consideration in the design of these devices.

General insight about structural characteristics of a dynamic test setup is that structural modes should be out of the frequency range of measurement. However, the effects of structural behavior on measurements are not clearly stated if any structural coupling occurs within the range of interest. Possibly there are some distinct behavior that should be strictly avoided, whereas some structural behavior could be allowed. General approach is to avoid some structural behavior by making structures rigid; however, heavy and bulky structural elements would be created. Determination of the characteristics that influence results may facilitate less conservative designs for viscoelastic testing. In addition, the measurement techniques and the locations where the measurements are gathered potentially affect the test results. More correct and consistent results will be obtained with the knowledge of correct points and techniques for measurement.

Therefore, clarification of the points mentioned above is important for better test system designs.

1.4. Structure of the Thesis

This thesis consists of five chapters. The details of these chapters are explained below:

- In Chapter 1 introduction of the study is presented.
- In Chapter 2 mechanical behavior of the rubbers, viscoelastic behavior and the models used to represent the viscoelastic behavior are expressed. The methods used to determine complex modulus are briefly discussed. The practical considerations used in the literature are also expressed.
- In Chapter 3 design efforts of a test setup, which is modification of an already existing viscoelastic material test setup is presented. The modification is aimed to introduce preloading capability to previous setup. The design of decoupling springs is explained in detail and influences of dynamic characteristics of decoupling springs on the measurements are discussed.
- In Chapter 4 design efforts of a new test setup are presented. The structural design of this setup is carried by Finite Element (FE) based analysis studies; however, real stiffness and loss factor measurements is not obtained as accurate as expected within the frequency range of interest. An error analysis study is carried out in order to determine possible reasons of problematic results. In this context, reduced-order models are used for determination of dynamic characteristics of the design. Modal characteristics of the structure are evaluated by eigenvalue analysis and correlation between modal tests is established. Test simulations are performed by linear harmonic analysis with FE Method. Test results with metallic calibration specimen is presented and compared with the analysis studies for validation.
- In Chapter 5 achievements and comments of the studies are briefly discussed.

CHAPTER 2

LITERATURE REVIEW

2.1. Introduction

In this thesis, test system design studies will be performed in order to determine the dynamic properties of rubber materials and components consisting of rubber materials. For this reason, a literature survey was conducted to obtain information about the mechanical properties of the materials to be tested and tests methods. In this study, general properties of viscoelastic materials, complex modulus concept, temperature-frequency equivalence of viscoelastic properties, viscoelastic component testing methods and design criteria determined about these tests will be given.

2.2. Linear Viscoelastic Behavior

Viscoelasticity is the term expressing the stress-strain relation depends on both strain and strain rate. Elastomers both store and dissipate strain energy during deformations and time dependent behavior of elastomers are due to energy dissipation of strain energy, which is treated as viscoelastic behavior. The constitutive relationship between harmonic forces and deformations could be expressed by complex modulus concept.

2.2.1. Mathematical Models for Viscoelastic Behavior

2.2.1.1. Spring-Dashpot Models – Generalized Maxwell Model

Viscoelastic behavior could be modeled with combination of spring and dashpot elements. These models describe the behavior of a typical polymer (Nashif, Jones, & Henderson, 1985) (Jones, 2001) (Ferry, 1980). (Bower, 2010) and illustrated in Figure 2.1.

Spring and dashpot element in series represents the Maxwell model (See Figure 2.1.(a)). The Maxwell model represents the response of an uncrosslinked polymer: for a constant strain the stress reaches to zero when time goes to infinite – which is the relaxation behavior. Constitutive relationship for Maxwell model is given in Eq. (2-1). Kelvin-Voigt model is spring and dashpot element in parallel. (See Figure 2.1.(b)). Kelvin-Voigt model behaves like a crosslinked polymer. For a step force input material gives no response immediately then reaches in a particular strain i.e. creep. The constitutive relationship for Kelvin-Voigt model is given in Eq. (2-2). The combination of Maxwell and Voigt elements resembles the Standard model or Generalized Maxwell model (See Figure 2.1.(c)) with constitutive relationship given in (2-4). There can be infinite number of Maxwell elements in parallel in Standard Model, and its number determines the complexity of the model. Higher order models show both types behavior for proper selection of model parameters.

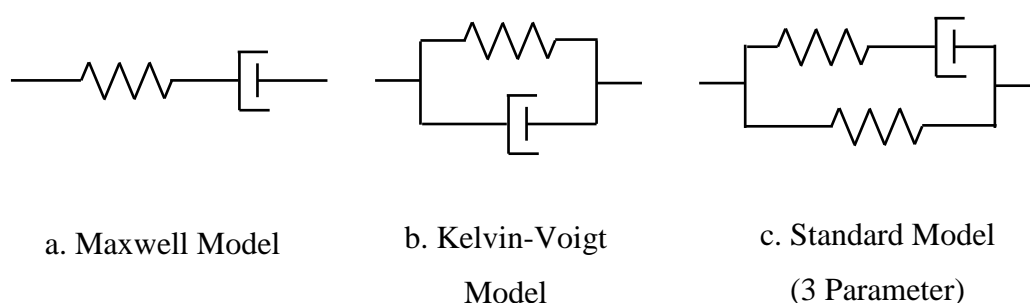


Figure 2.1. Essential spring-dashpot models to represent viscoelastic behavior

$$k\sigma + \eta \frac{d\sigma}{dt} = k\eta \frac{d\epsilon}{dt} \quad (2-1)$$

$$\sigma = k\epsilon + \eta \frac{d\epsilon}{dt} \quad (2-2)$$

$$k\sigma + \eta \frac{d\sigma}{dt} = k_1 k_2 \epsilon + (k_1 + k_2) \eta \frac{d\epsilon}{dt} \quad (2-3)$$

For Eq. (2-1).(2-3), k, k_1 and k_2 are the stiffness of the spring elements, η is the structural damping parameter. By arranging these equations, the relaxation modulus representations for Maxwell and 3-parameter Standard model are given in Eq. (2-4) and (2-5) respectively. For standard model modulus relation is a series representation, which is called **Prony series** (See Eq. (2-6)). Kelvin-Voigt model do not have an explicit modulus relationship.

$$G(t) = k e^{-kt/\eta} \quad (2-4)$$

$$G(t) = k_2 + k_1 e^{-k_1 t/\eta} \quad (2-5)$$

$$G(t) = G_\infty + \sum_{i=1}^N G_i e^{-t/t_i} \quad (2-6)$$

Prony Series representation is converted into frequency domain in Eq. (2-7). Real part of Prony series in frequency domain represents the storage part (See. Eq. (2-8)) and imaginary part corresponds to loss part, which is given in Eq. (2-9).

$$G^* = G\phi + \frac{G\eta}{\omega} i\omega\phi = G(1 + i\eta)\phi \quad (2-7)$$

$$Re(G^*) = G'(\omega, T) = G_\infty + \sum_{i=1}^N \frac{G_i \omega^2 t_i^2}{1 + \omega^2 t_i^2} \quad (2-8)$$

$$Im(G^*) = G''(\omega, T) = \sum_{i=1}^N \frac{G_i \omega t_i}{1 + \omega^2 t_i^2} \quad (2-9)$$

2.2.1.2. Fractional Derivative Model

It is slightly cumbersome to fit the Prony series parameters to compliance measurements. (Bagley, 1989) Fractional derivative models enable accurate description of viscoelastic properties over wide frequency range. They are effective when broad range of experimental data is used since better fit with less parameter is achieved. Both time and frequency domain formulations are present.

Stress strain relationship in fractional derivative form in time-domain is represented in Eq. (2-10) and frequency domain relationship is given in Eq. (2-11). The fractional derivative of a function is represented in Eq. (2-12).

$$\sigma(t) + \sum_{m=1}^M b_m \frac{d^m \sigma(t)}{dt^m} = E_0 \epsilon(t) + \sum_{n=1}^N E_n \frac{d^n \epsilon(t)}{dt^n} \quad (2-10)$$

$$\sigma^*(i\omega) = \frac{E_0 + E_1(i\omega)^\alpha}{1 + b(i\omega)^\beta} \epsilon^*(i\omega) \quad (2-11)$$

$$\frac{d^\alpha x(t)}{dt^\alpha} = \frac{1}{\Gamma(1-\alpha)} \frac{d}{dt} \int_0^t \frac{x}{(t-\tau)^\alpha} d\tau \quad (2-12)$$

The constants E_0, E_1, α and β could be determined by curve fit procedures by using test data.

2.2.2. Definition of Complex Modulus

The constitutive relationship of viscoelastic materials for uniaxial stress state is given in Eq. (2-10) (Bagley, 1989). For harmonic response, stress and strain could be written in the form of $\sigma = \sigma_0 e^{i\omega t}$ and $\epsilon = \epsilon_0 e^{i\omega t}$ respectively, then the relation could be expressed in a compact form by Eq (2-13).

$$\sigma_0 = (E'(\omega) + iE''(\omega))\epsilon_0 \quad (2-13)$$

In (2-13) E' is the storage modulus, E'' is the loss modulus term and ω is the frequency. By rearranging, the expression becomes in Eq (2-14).

$$E^* = E'(1 + i\eta) \quad (2-14)$$

In Eq (2-14), E^* is the complex modulus, η is the loss factor which expressed in (2-15)

$$\eta = \frac{E''}{E'} \quad (2-15)$$

2.2.3. Dependency of Complex Modulus on Environmental Factors

The mechanical properties of elastomeric materials are seriously affected by temperature. Elastomer materials have characteristic properties depending on the temperature. Strain energy at high temperatures is stored by making the polymer chains more regular i.e. entropically, so it can be easily deformed by smaller forces. This temperature range is called the rubbery region. As temperature drops, bond interactions and damping forces increase significantly. This zone is called the transition region. As temperature goes down further strain energy is stored only in bonds while deforming the material because the polymers are interlocked with each other. For that reason, material behaves very stiff. The temperature range at which this behavior is indicated is called the glassy region. There could be 1.10^3 to 1.10^6 times difference between glassy and rubbery region stiffness values. Figure 2.2 shows the typical E' and η value of an elastomeric material depending on the temperature.

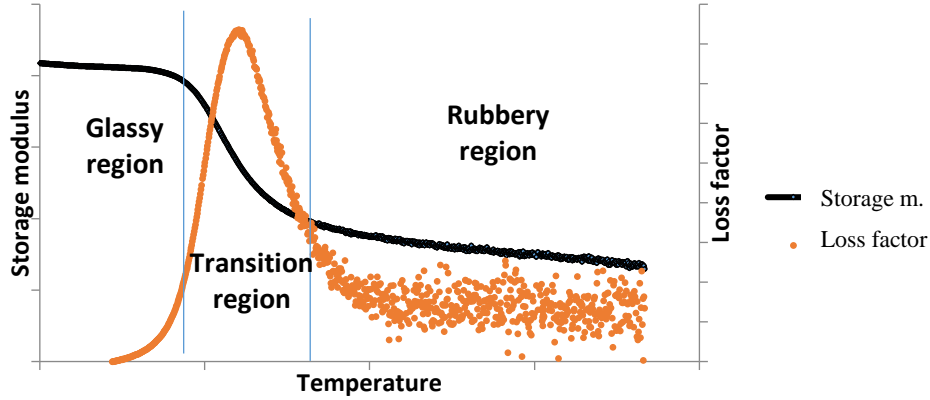


Figure 2.2. Temperature dependence of a typical elastomeric material

2.2.4. Temperature & Frequency Equivalence

Dynamic stiffness measurements are usually performed in limited range of frequency and temperature. Temperature-frequency equivalence could be utilized in order to interpolate or extrapolate the results over a broad range of temperature and frequency. The assumption is that complex modulus of any frequency f_1 at a temperature T_1 is equal to those at any frequency f_2 and temperature T_2 . This assumption has no physical reason, but it works in elastomers (Jones, 2001).

$$G^*(f_1, T_1) = G^*(f_2 \alpha(T_2)) \quad (2-16)$$

$$f_{reduced} = f \alpha(T) \quad (2-17)$$

The expression of temperature and frequency terms by a single parameter forms the reduced frequency definition (See Eq. (2-17)). The term $\alpha(T)$ is called the shift factor. WLF (Williams-Landel-Ferry) and Arrhenius relationships are commonly used for this term. WLF relation is represented by Eq. (2-18) (Williams, Landel, & Ferry, 1955). WLF relation have a curved relationship in temperature extremes. Arrhenius have a linear relationship.

$$\log_{10}(\alpha(T)) = \frac{-C(T - T_0)}{(B + T - T_0)} \quad (2-18)$$

2.2.5. Nonlinear Behavior of Elastomers

Elastomeric materials show stress-strain relationship dependent on deformation history. This is called hysteretic behavior and illustrated in Figure 2.3 (Banks, Pinter, Potter, Gaitens, & Yanyo, 2013). The elliptical shape is due to viscous effect of viscoelastic solid. Dynamic modulus of elastomers is generally strain sensitive and it may be more significant for materials with high stiffness and damping.

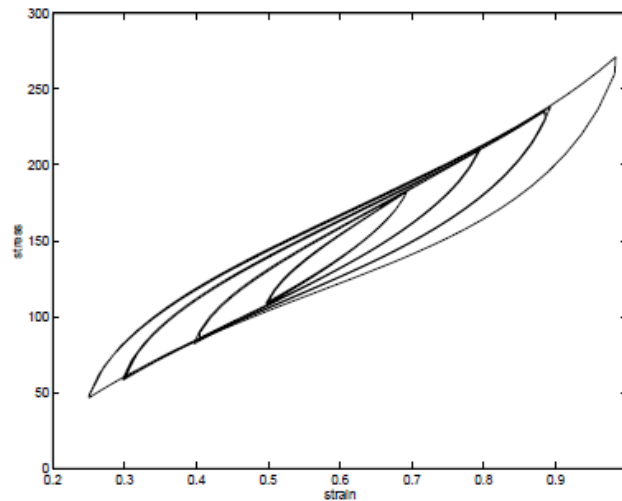


Figure 2.3. Hysteresis loop observed in rubber stress-strain relationship (Banks, Pinter, Potter, Gaitens, & Yanyo, 2013)

At high strains -for example close to 100% stretch different material deformation behaviors are observed. These are illustrated in Figure 2.4 (SIMULIA, 2016).

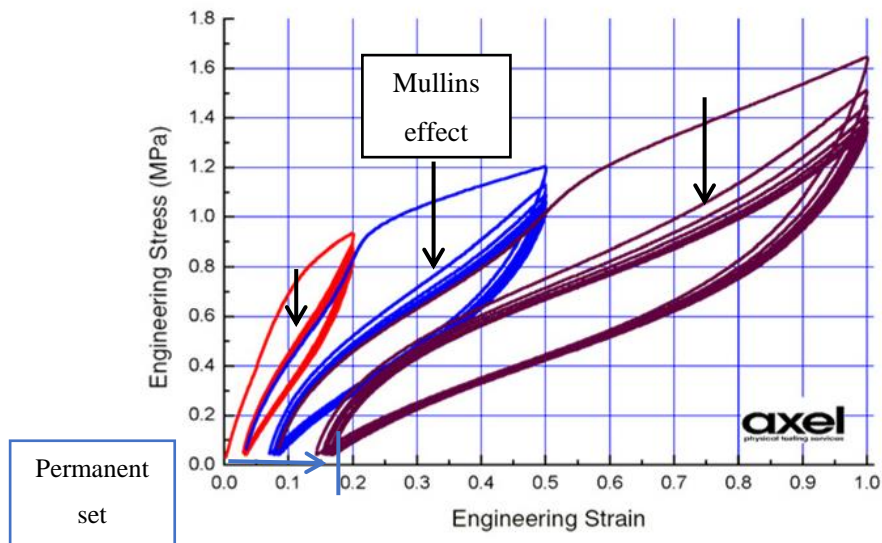


Figure 2.4. Typical behavior of an elastomeric material at high strain deformation (SIMULIA, 2016)

Some assumptions could be made in order to model large strain effects. Long term modulus is function of static prestrain and frequency dependent part of modulus is independent from prestrain. Linear expression for modulus is still present; however, only varies with preload. This simple assumption could be applicable for many materials. If this assumption is not valid, frequency dependent properties at particular prestrain could be used.

2.2.5.1. Mullins effect

A deformed elastomeric material behaves more softly in the second cycle, reducing the amount of hysteresis, i.e., the rate of damping. This behavior is called the Mullins effect. This effect is observed in various types of polymeric materials in various types of deformation methods. Although mechanism of Mullins Effect is not clearly understood, it is presumed that the weak bond between the polymer and the filling material breaks and the resulting material behaves softer (Diani, Fayolle, & Gilormini, 2008). The amount of softening depends on material and could be seen even on low stretch levels. There is also no general model valid at each case. Mullins effect is healed by exposing high temperature over some period or immersing on solvent;

however, no recovery is observed in room temperature. Mullins effect must be considered in dynamic testing because it greatly affects the stiffness.

2.2.5.2. Payne effect

When an elastomeric material deformed under harmonic forces material behaves softer at high strain levels. Damping effects are observed more aggressive until some strain level then damping decreases at very large strains. This behavior is commonly called as Payne Effect (Roland, 2016) and observed more significant when the filler portion of the rubber increases. Change of storage and loss modulus with strain is illustrated in Figure 2.5 by different filler portions.

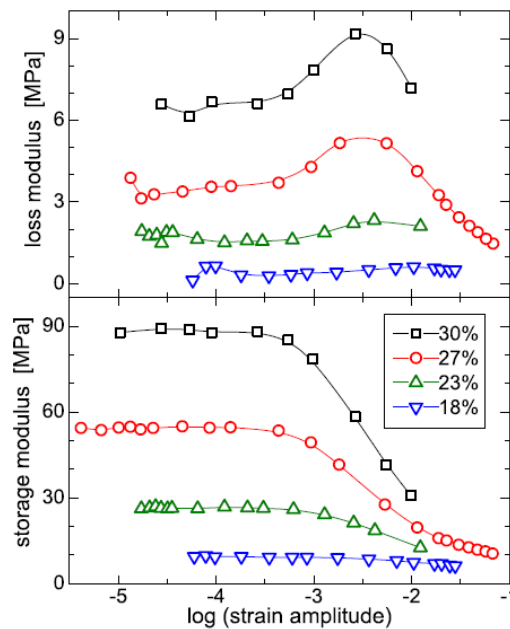


Figure 2.5. Change of storage and loss modulus with strain amplitude for different filler portions (Roland, 2016)

2.3. Testing Methods for Viscoelastic Properties

Characterization and verification of vibration isolators are necessary for the design of the system solution. If the geometric properties of the specimen are known, the complex modulus can be obtained by measuring the dynamic stiffness. Therefore,

dynamic stiffness and complex modulus measurements are interrelated [4]. Therefore, the test methods described in this section may apply to both complex modulus and dynamic stiffness measurements.

In the field of acoustics, the vibration amplitudes are small therefore linear viscoelastic behavior is applicable. In vibration isolation systems excitation amplitudes may be large or small depending on the application. In addition, since isolator must support the isolated device it will perform under significant preload then amplitude-dependent properties must be in consideration.

In this section, some test methods used in vibration control applications will be discussed. The test methods for measuring frequency-dependent properties are specifically included in this section.

2.3.1. Measuring Time-Dependent Properties

Time dependent behavior of viscoelastic materials could be determined by creep and relaxation tests. These tests could be utilized to obtain the parameters of Prony Series (See Eq (2-6)). Within the scope of the thesis, there will be no study about evaluation of the time-dependent behavior of viscoelastic materials; therefore, these tests are out of the scope of this thesis.

2.3.2. Measuring Frequency-Dependent Properties

Dynamic stiffness can be obtained by many methods depending on the test specimen and test conditions, and many of these methods are included by the standards. There are three types of methods used for dynamic modulus measurement: Resonant methods, non-resonant methods and wave propagation methods.

2.3.2.1. Indirect Methods-Resonant Methods

Resonant methods dynamic properties are obtained from the modal characteristics of the test setup. In the literature, it is called Transfer function method by (Pritz, 1980), indirect methods by (ISO 10546-3:2002 Acoustics and vibration -- Laboratory measurement of vibro-acoustic transfer properties of resilient elements -- Part 3:

Indirect method for determination of the dynamic stiffness of resilient supports for translatory motion, 2002) and resonant methods by (ASTM D5992 - Standard Guide for Dynamic Testing of Vulcanized Rubber and Rubber-Like Materials Using Vibratory Methods, 2011). Among these methods, the dynamic modulus is obtained from the modal character of the beam treated with the viscoelastic material by Oberst test setup (Oberst & Frankenfeld, 1952) and the standardized version of this method by ASTM (ASTM E756 - 05 Standard method for measuring vibration-damping properties of materials, 2005). In the methods defined by ASTM and ISO standards (ISO 10546-3:2002 Acoustics and vibration -- Laboratory measurement of vibro-acoustic transfer properties of resilient elements -- Part 3: Indirect method for determination of the dynamic stiffness of resilient supports for translatory motion, 2002) (ASTM D5992 - Standard Guide for Dynamic Testing of Vulcanized Rubber and Rubber-Like Materials Using Vibratory Methods, 2011) (ISO 10846-5:2008(E) Acoustics and vibration – laboratory measurement of vibro-acoustic transfer properties of resilient elements – part 5: driving point method for determination of low-frequency transfer stiffness of resilient supports for translatory mot, 2008), dynamic modulus is obtained from the transmissibility relationship of a single DOF resilient element-mass system. By these methods, dynamic properties are measured with cheap and practical test apparatus. However, there are some difficulties to take measurements over wide frequency ranges and to provide amplitude control to determine nonlinear effects.

ASTM D5992 Free resonance offers a simple and cheap method to measure stiffness and damping of resilient material. It consists of specimen material as stiffness (and damping) element and a mass. Vibrations are created by applying an initial displacement then releasing. Free oscillations of single DOF mass-spring system are recorded then damping is obtained from logarithmic decrement method. This method is so easy to apply because it requires little equipment and instrumentation. However, there are two main disadvantages: Since method is based on decay of free oscillations dynamic strain amplitude could not be controlled then strain amplitude dependent

material properties could not be measured. The other problem is that damping ratio of high damping materials could not be measured properly since the oscillations are damped in few cycles. By this method; however, only the properties at a specific frequency is measured. Adjustment of frequency is done by changing the quantity of mass, but it may practically impossible since resonance frequency changes by square root of mass. For example, the increasing the resonance frequency by a factor of two requires four times greater mass. Resilient element may not support adding this amount of mass.

The problems having insufficient amount of cycles with free resonant method are overcome by addition of a shaker for creating forced vibrations. This is forced resonant method. System could be excited in two ways: Motion or force excitation. Motion excitation refers to base motion which the specimen-mass system is connected to shaker table. Main advantage of forced resonant method over free method is that resonant amplitude could be adjusted. However, since the method requires steady-state vibration the specimen temperature may change due to heat generation. This should be taken into consideration as it may cause material properties to change. This method is not practical for measurements over wide frequency range because of same reasons in free resonant method.

2.3.2.2. Direct Methods-Non-Resonant Methods

Dynamic stiffness is obtained by applying dynamic forces directly to the sample. It is called Direct Complex Stiffness test systems by (Allen, 1996) and these methods are standardized by ISO (ISO 4664-1:2011 Rubber, vulcanized or thermoplastic -- Determination of dynamic properties -- Part 1: General guidance, 2011) (ISO 10846-2:2008(E) Acoustics and vibration – laboratory measurement of vibro-acoustic transfer properties of resilient elements – part 2: direct method for determination of the dynamic stiffness of resilient supports for translatory motion, 2008) (ISO 18437-3:2005(E) Mechanical vibration and shock – characterization of the dynamic mechanical properties of visco-elastic materials – part 4: dynamic stiffness method,

2005) (ISO 6721-1:2019 Plastics -- Determination of dynamic mechanical properties -- Part 1: General principles, 2019) and ASTM (ASTM D5992 - Standard Guide for Dynamic Testing of Vulcanized Rubber and Rubber-Like Materials Using Vibratory Methods, 2011) (ASTM D4065 – 12 Standard Practice for Plastics: Dynamic Mechanical Properties: Determination and Report of Procedures, 2012). In these methods, the sample can be deformed in extension, shear and torsion. Dynamic stiffness is obtained by measuring the force and deformation of the specimen at a specific frequency. Deforming force can be generated by mechanical, electrodynamic and hydraulic actuators. Dynamic modulus can be measured over wide frequency range with controlled amplitude and preload. Deforming force could be created by means of crank-link mechanism, servohydraulic or electrodynamic actuator. Latter two have ability of strain adjustment. General outline of a forced non-resonant system with a hydraulic actuator is given in Figure 2.6.

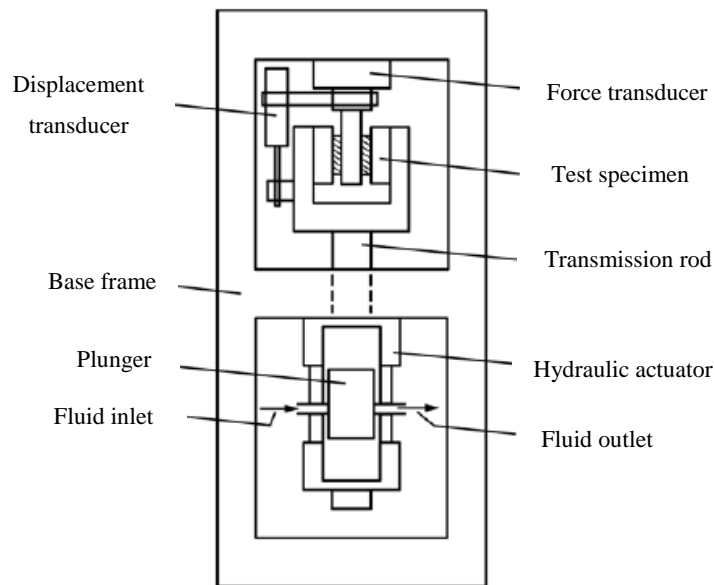


Figure 2.6. General layout of a forced non-resonant test system

Schematic representation of Direct Method is illustrated in Figure 2.7 and the stiffness relationship for the viscoelastic specimen is given in Eq (2-19) (Jones, 2001)

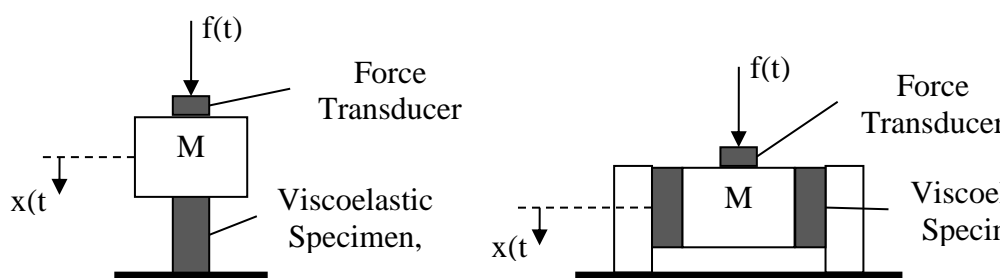


Figure 2.7. Schematic representation of Direct Method

$$k^* = \frac{F + \omega^2 M_e X}{X} \quad (2-19)$$

$$M_e = M + \frac{m}{3} \quad (2-20)$$

For Eq (2-20), M is the mass of the force transmission element and m/3 corresponds to the effective mass of the specimen. If force is measured at the point where specimen is connected to the ground (See Figure 2.8) then dynamic stiffness relationship becomes in Eq (2-21).

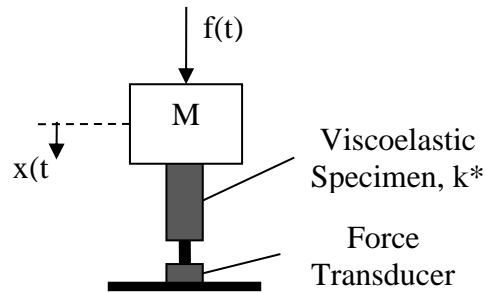


Figure 2.8. Direct method, force measurement from ground

$$k^* = \frac{F}{X} \quad (2-21)$$

In most cases the fixture that supports the specimen has resilience (Ozgen, Design and Development of a Complex Shear Modulus Measurement Setup For Viscoelastic Materials, 2005) (Ozgen, Erol, & Batihan, Dynamic Stiffness-Based Test Systems for Viscoelastic Material Characterization: Design Considerations, 2012), then the deformation of the fixture should also be considered. This condition is illustrated in Figure 2.9 and the equation of motion can be written as in (2-22).

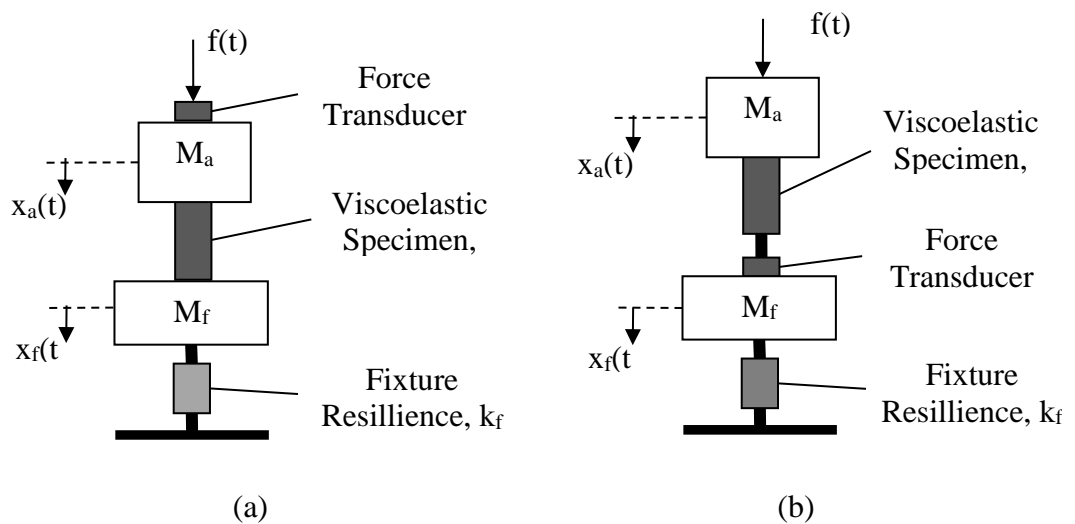


Figure 2.9. Direct method with resilient fixture where force measurement on actuator side (a) and fixture side (b)

$$\begin{bmatrix} M_a & 0 \\ 0 & M_f \end{bmatrix} \begin{Bmatrix} \ddot{x}_a \\ \ddot{x}_f \end{Bmatrix} + \begin{bmatrix} k^* & -k^* \\ -k^* & k_f + k^* \end{bmatrix} \begin{Bmatrix} x_a \\ x_f \end{Bmatrix} = \begin{Bmatrix} f \\ 0 \end{Bmatrix} \quad (2-22)$$

In Eq (2-22) specimen mass is lumped into the connecting masses. For a harmonic force input, $f = Fe^{i\omega t}$ and single harmonic output, $x = Xe^{i\omega t + \phi}$ the equation of motion is rewritten as in Eq (2-23).

$$\begin{bmatrix} -\omega^2 M_a + k^* & -k^* \\ -k^* & -\omega^2 M_f + (k_f + k^*) \end{bmatrix} \begin{Bmatrix} X_a \\ X_f \end{Bmatrix} = \begin{Bmatrix} F \\ 0 \end{Bmatrix} \quad (2-23)$$

In this case force could be measured from either actuator side, X_a or fixture side, X_f . For the case where force is measured from the point where actuator force is applied, dynamic stiffness is obtained from Eq (2-24). If the force is measured from fixture connection, force transducer records the signal corresponds to $F_s = k_f X_f$ then dynamic stiffness relation becomes in Eq (2-25).

$$k^* = \frac{F + \omega^2 M_a X_a}{X_a - X_f} \quad (2-24)$$

$$k^* = \frac{F_s - \omega^2 M_f X_f}{X_a - X_f} \quad (2-25)$$

Deformation of the sample can be achieved by direct measurement of displacement or by double integration of data from accelerometers (ASTM D5992 - Standard Guide for Dynamic Testing of Vulcanized Rubber and Rubber-Like Materials Using Vibratory Methods, 2011). If acceleration data is to be used for deformation, the conversion given by Eq (2-26) must be performed. In Eq (2-26) A is the acceleration measurement at that degree of freedom.

$$X = -\frac{A}{\omega^2} \quad (2-26)$$

For the case with decoupling springs (Figure 2.10) dynamic stiffness relation is given as Eq (2-27) for force measurement taken on actuator side. If the measurement is taken from the fixture, the relation is same as Eq (2-25). An extra term, k_d , is introduced in relation and any error in determination of that value will affect the dynamic stiffness calculation. Therefore, it is more convenient to take force measurement at fixture connection.

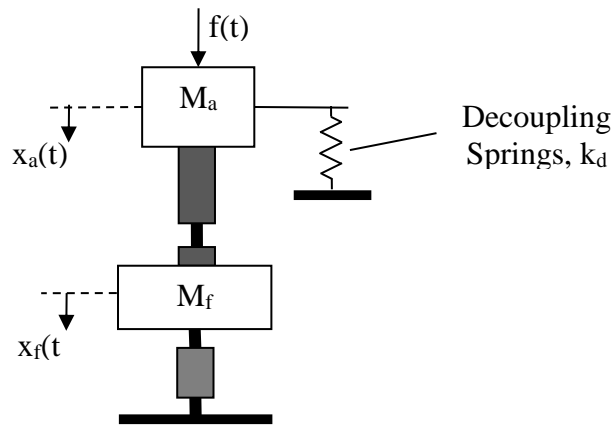


Figure 2.10. Direct method with resilient fixture and decoupling springs

$$k^* = \frac{F + (\omega^2 M_a - k_d) X_a}{X_a - X_f} \quad (2-27)$$

2.3.2.3. Obtaining Modulus of the Material from Dynamic Stiffness Measurements

Material storage modulus and loss factor could be obtained from dynamic stiffness measurements by knowing the geometrical properties of the viscoelastic specimen. The relationships for obtaining these properties are provided in ASTM D5992 (ASTM D5992 - Standard Guide for Dynamic Testing of Vulcanized Rubber and Rubber-Like Materials Using Vibratory Methods, 2011).

Tension-compression specimen is represented in Figure 2.11. Tensile modulus of tension-compression specimen could be obtained from the relationship given in Eq (2-28).

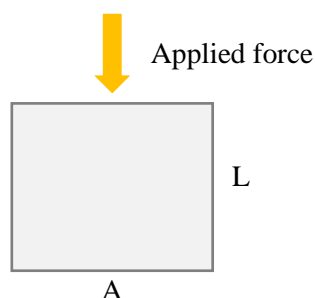


Figure 2.11. Tension-compression specimen

$$E^* = K^* \frac{L}{A} \quad (2-28)$$

In Eq (2-28) L is the length of tensile specimen and A is the bonded area of one face of the specimen. Specimen bond area may be rectangular or circular. Storage modulus and the loss factor of the material is obtained from Eq (2-14) & (2-15) respectively.

The specimen tested in double-shear configuration is represented in Figure 2.12. Shear modulus of the material could be obtained from Eq (2-29)

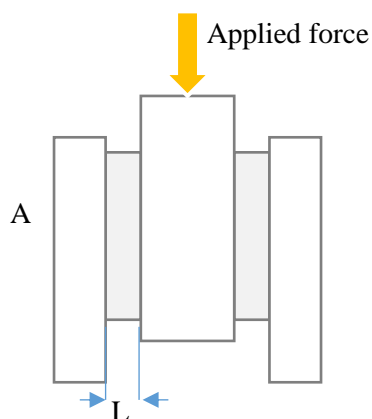


Figure 2.12. Double-shear specimen

$$G^* = K^* \frac{L}{2A} \quad (2-29)$$

In Eq (2-29) A is the bond area of the single elastomer specimen. For double shear specimen, total area is equal to two times bond area of single elastomer component.

2.3.2.4. Wave Propagation Methods

Wave propagation and attenuation properties in viscoelastic environment are used in these methods. Wave speed is related to elastic modulus and wave attenuation character is related to damping. The principles and details are given by Lakes (Lakes, 2004).

2.4. Design Considerations about Dynamic Testing

Direct and indirect methods are compared in ASTM D5992 by considering the cost, availability of amplitude control and applicable frequency range. It is stated that these methods are applicable over temperature range from -70 to 200°C and frequency range between 0.01 and 100 Hz. The intended real modulus range is also from 0.1 to 100 MPa. Qualitative comparison of these methods is given in Table 2.1.

Table 2.1. *The comparison of test methods in ASTM D5992*

Feature	<i>Free Method</i>	<i>Forced Resonant Method</i>	<i>Non-resonant Method</i>
Constant Amplitude	Not applicable	Possible	Possible
Cost	Low	Moderate	High
Frequency Range	Narrow	Narrow	Wide

There are additional conclusions that are stated by D5992 and Frampton (Frampton). The first issue is about linearity of the specimen behavior. When applying preload to specimen some time is allowed before starting to test because preload stress will be settled in a particular value. This is important when the material have significant

nonlinearity. Also, material configurations in shear have more linear behavior than configuration in tension-compression.

Since small strains and high frequencies are in concern signal noise rejection is another important issue to minimize the contribution. First method for minimizing the noise error is averaging the results. Frampton says that noise error will reduce by factor of square root of average number. Other way is to reduce noise is filtering the signal. For periodic signals band-pass filters improves the signal contribution by factor K, given in Eq.(2-30). Also extracting parameters from Fourier transform works better than hysteresis loop.

$$K = \sqrt{\frac{\text{total bandwidth}}{\text{filter bandwidth}}} \quad (2-30)$$

The last issue is that test machine should be as heavy as possible whereas transmission rods must be light in order to avoid mass loading effect. In addition, suspending the whole body on anti-vibration mounts could create mass coupling to load cell. It is better to mount whole system to a rigid solid floor.

2.5. Factors Influencing Measurements

Some remarks in the standard regarding accuracy of the results are listed below:

- Accuracy of stiffness measurement depends on correct measurement of force and deflection. It must be considered that displacements and transmitted forces are small at high frequencies.
- Accuracy of modulus measurement depends on correct measurement of specimen dimensions.
- Accuracy of damping measurement depends on attachment between specimen and test fixture. No slipping must occur in connections since this creates additional source of damping.

The other remarks about measurements about Signal to noise ratio (SNR): Measured magnitude should exceed inherent noise of signal. There is no specifically given SNR ratio. Multiple-cycle averaging could be used for enhancing SNR. Measurements and display of signal must be in phase. Out of phase measurements could be corrected by suitable hardware or software.

The remarks about motion transducer are that measurements should be taken from as close as possible to the specimen. Since this is practically not possible for most cases there are additional components that introduce stiffness.

For displacement measurements double integration of acceleration signal could be utilized depending on the input signals are sinusoids. Distortion of the signals should be properly controlled if double-integration is used.

Additionally, for non-resonant method forcing and deflection are sinusoidal for linear case, force and displacement produce elliptical hysteresis loop, phase angle between sinusoidal motions give loss factor. In frequency domain analysis only fundamental frequency should be used. In case of any nonlinearity the sinusoidal shapes are distorted, methods using waveshape and peak amplitudes are prone to be influenced.

FFT works well for all cases linear or nonlinear. Its advantages are it have good repeatability and insensitive to exact shape of waveform. Peak-peak methods are gives correct result only in sinusoidal case.

Choice of specimen depends on how much uniformly stress and strain is distributed and how much important this condition.

2.6. Previous Studies about the Topic of Interest

Previous studies related with the test system design for complex modulus measurement is discussed in this topic. These studies were carried out in ODTÜ Mechanical Engineering Department.

In the study by Erol (2014), a test system design for complex modulus measurements is proposed (Erol, 2014) - first study carried out within this thesis is based on this test

setup. The system is designed to be used in 1-200Hz frequency range and -55/+150°C temperature range and in accordance with ISO 10846-3 Driving Point Method. The system is applicable for measurements with low amplitudes and without preload. Specimen is enclosed by a temperature chamber to achieve temperature control of the specimen. The detailed view of the section of the test system in temperature chamber is given in Figure 2.13.

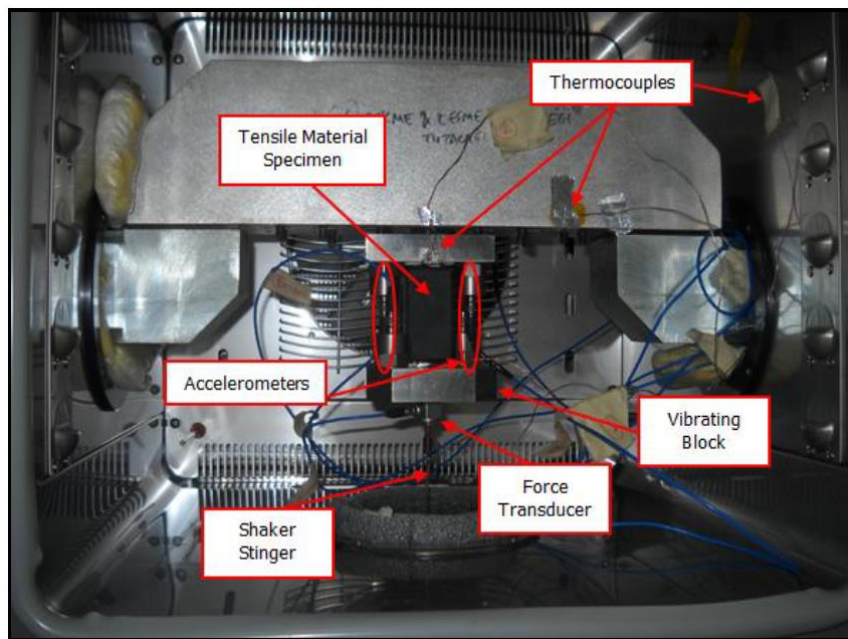


Figure 2.13. Detail view of the test system on temperature chamber

As a design objective, structural modes are avoided in the frequency range. Limited volume and openings of the temperature chamber creates mechanical constraint mechanical assembly. Under these constraints desired modal characteristics are achieved by topology optimization method based on a finite-element model. As a result of the optimization study the fixture layout given in Figure 2.14 is achieved. Analysis-test correlation is performed for validating the model and successful measurements are obtained within the prescribed conditions.

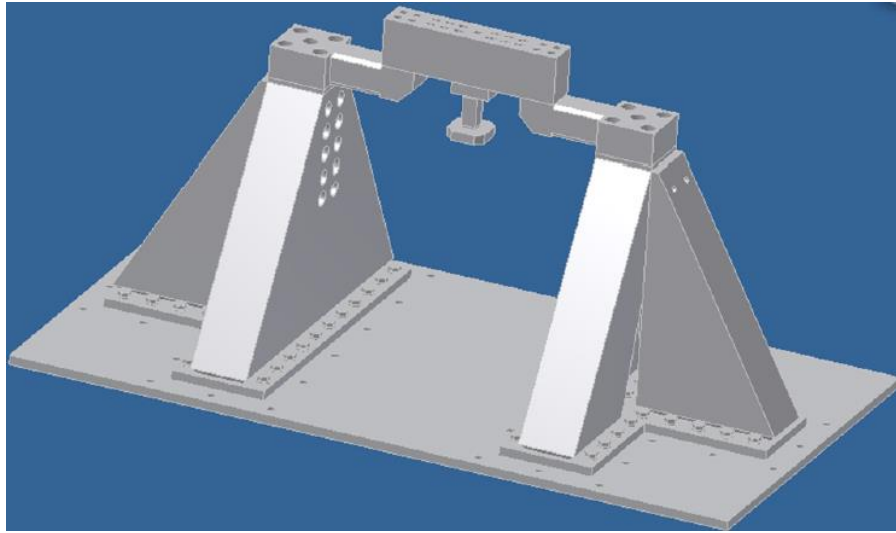


Figure 2.14. Final design of the test fixture as a result of optimization study

In the study by Uz (2013) the effect of system parameters on complex modulus measurements are investigated (Uz, 2013). A system design is proposed then these variations are studied on that design. The system is in accordance with ISO 10846-2 Direct method. Design conditions for this setup are within 1-1000Hz frequency range, in room temperature and under preload. A lumped mass model is created by obtaining the equivalent mass and spring representations of mechanical features along deformation direction of the specimen. The effects of variations of fixture dimensions and specimen properties on measurements are illustrated by sine-sweep test simulations. The model is correlated with finite-element model to ensure modal characteristics. By this study local distortions on measurements due to structural modes are illustrated; therefore, structural modes within the frequency range of interest are expected to be avoided. However, the effect of bending motion of the crosshead that connected to the specimen is reduced by considering the mass and acceleration of the connecting block to the calculation. In addition, it is stated that specimen stiffness and mass have a great influence on measurement errors.

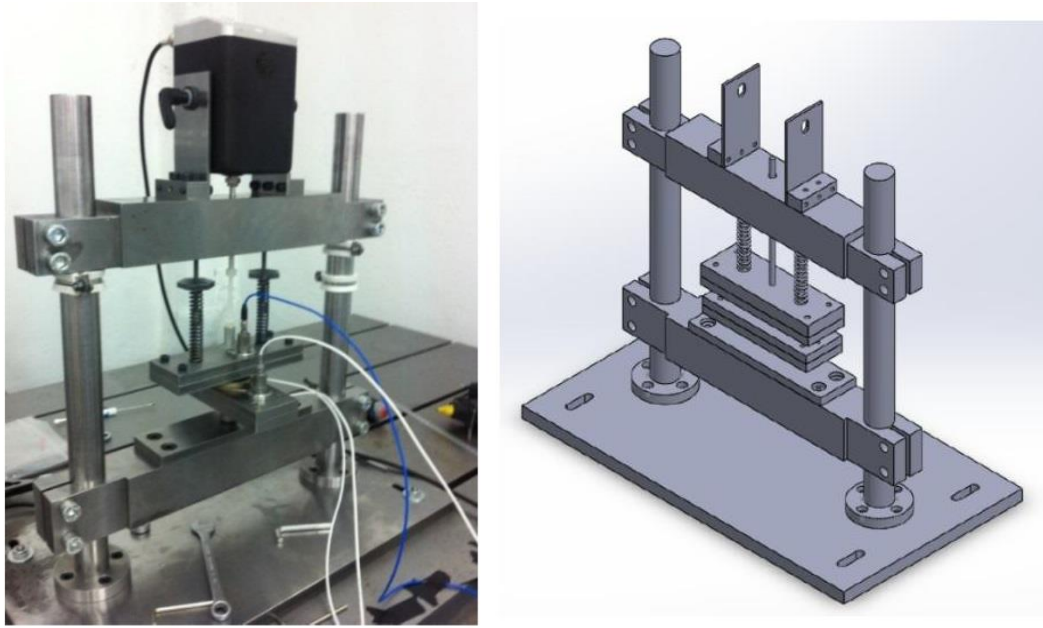


Figure 2.15. Overview of the test system designed by Uz (2013)

In the study by Bilgi (2016), a mechanical solution is proposed for temperature-controlled and preloaded complex modulus measurements in accordance with ISO 10846-2 under limited volume due to temperature chamber (Bilgi, 2016). Preloading force is provided by a resilient element made of elastomers deformed by a linear actuating mechanism. Virtual sine-sweep tests are performed to represent the system performance within the frequency range of interest and results are compared with viscoelastic material model used in the model. Some distortions are observed within the frequency range due to structural characteristics of the system, but no specific conclusion is drawn about which specific mode is influenced on which distortion.

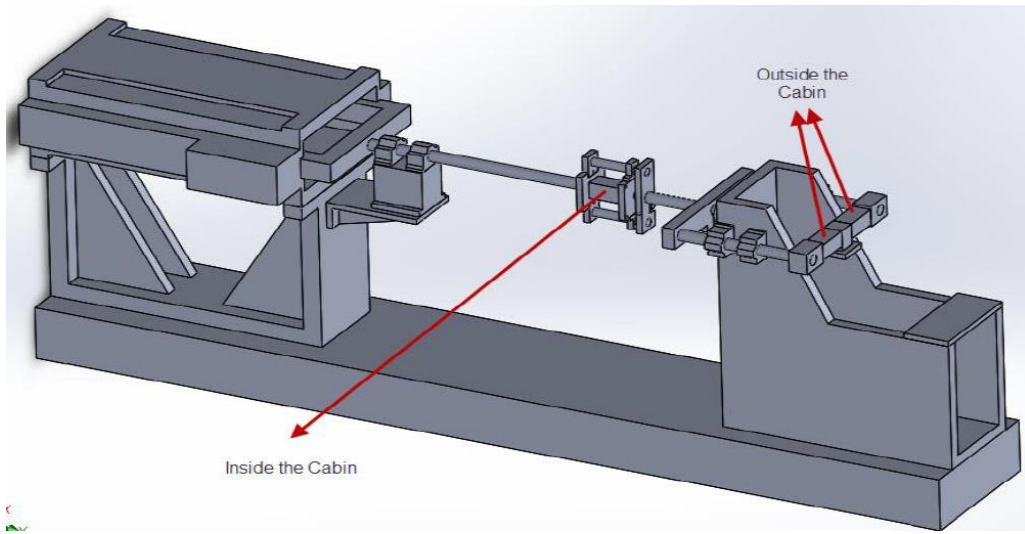


Figure 2.16. General layout of the test system designed by Bilgi (2016)

CHAPTER 3

DESIGN EFFORTS FOR A PRELOADING MECHANISM FOR AN ALREADY EXISTING TEST SETUP FOR VISCOELASTIC MATERIAL CHARACTERIZATION

3.1. Introduction

In this chapter design efforts for a preloading mechanism for an already existing viscoelastic material characterization test setup is presented. Firstly, the details of the unmodified test system will be given, then design studies, verification tests, revision of the design and re-evaluation of the results will be discussed.

The original setup is developed by Erol (2014) in ODTÜ Mechanical Engineering Department. This system is planned to be used first to serve project (Project No: 00947.STZ.2011-2, Elastomer Titreşim Takozlarının Tasarımı). This test system is planned to be revised to be able to measure dynamic stiffness of vibration isolators under preload. This planned modification study is presented in this thesis.

The aim of this study is to provide original setup the capability of characterization of viscoelastic materials under preload. In addition, dynamic stiffness values of vibration mounts can be measured. Furthermore, software in the previous test system has been redesigned and updated to perform amplitude-controlled sweep sine testing. The test system software is based on LabVIEW as in the previous design.

3.2. Unmodified Version of the Test Setup

The unmodified version of the test system is developed for complex modulus measurements, which is designed to be used in 1-200Hz frequency range and -55/+150°C temperature range and in accordance with ISO 10846-3 Driving Point Method (Erol, 2014). The system is applicable for measurements with low amplitudes

and without preload. Specimen is enclosed by a temperature chamber to achieve temperature control of the specimen. The detailed view of the section of the test system in temperature chamber is given in Figure 2.13.

Structural design of this setup is carried by avoiding the structural modes in the frequency range. Limited volume and openings of the temperature chamber creates mechanical constraint mechanical assembly. Under these constraints desired modal characteristics are achieved by topology optimization method based on a finite-element model. As a result of the optimization study the fixture layout given in Figure 2.14 is achieved. Analysis-test correlation is performed for validating the model and successful measurements are obtained within the prescribed conditions.

3.3. Design Objectives, Requirements and Constraints

The main objective of the study is to design a preloading mechanism by modifying existing test setup. The preloading mechanism has flexible elements which are connected between fixture and the specimen loading plate. Preloading force is planned to be applied manually. Max preload value is set as 1000 N.

Frequency range is set as 5-200 Hz. The structural modes are to be out of frequency range of interest. Temperature range is set as -55/+150°C

The temperature control of the specimen is to be provided by a temperature chamber same as the unmodified setup, which imposes some geometrical constraints. This mechanism had to be packed into a volume of 400x400x300mm. The holes in the side walls of the chamber are used for fixture connections, while the hole in the bottom wall permits the actuator connection.

3.4. Design Efforts

3.4.1. Conceptual Design

In this study, the region of the previous design enclosed by the temperature chamber has been completely redesigned. Direct method has been adapted to that setup and a mechanism has been designed to apply preloading force. The general view of the

designed test system is given in Figure 3.1. In this figure, test specimen is enclosed by a temperature chamber. The region enclosed by the temperature chamber is connected to the ground through the openings in the temperature chamber. The temperature chamber is supported on a table, but not shown in the figure. An electrodynamic shaker is used as actuator and located at the bottom of the temperature chamber.

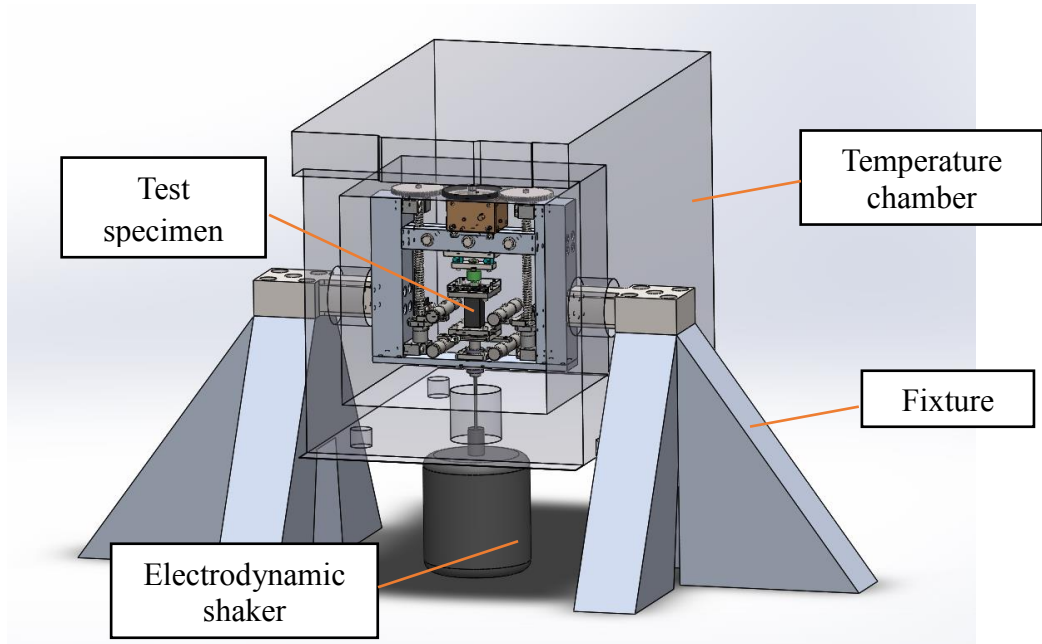


Figure 3.1. Overview of the modified design

In Figure 3.2. detailed view of the enclosed region by temperature chamber is illustrated. The test specimen is connected to the fixture via a force transducer assembly. The assembly consists of two piezoelectric force transducers for dynamic load measurement and one strain gage force transducer to measure static preload. The electrodynamic shaker is connected to the specimen through a connecting rod which is guided by a linear shaft bearing.

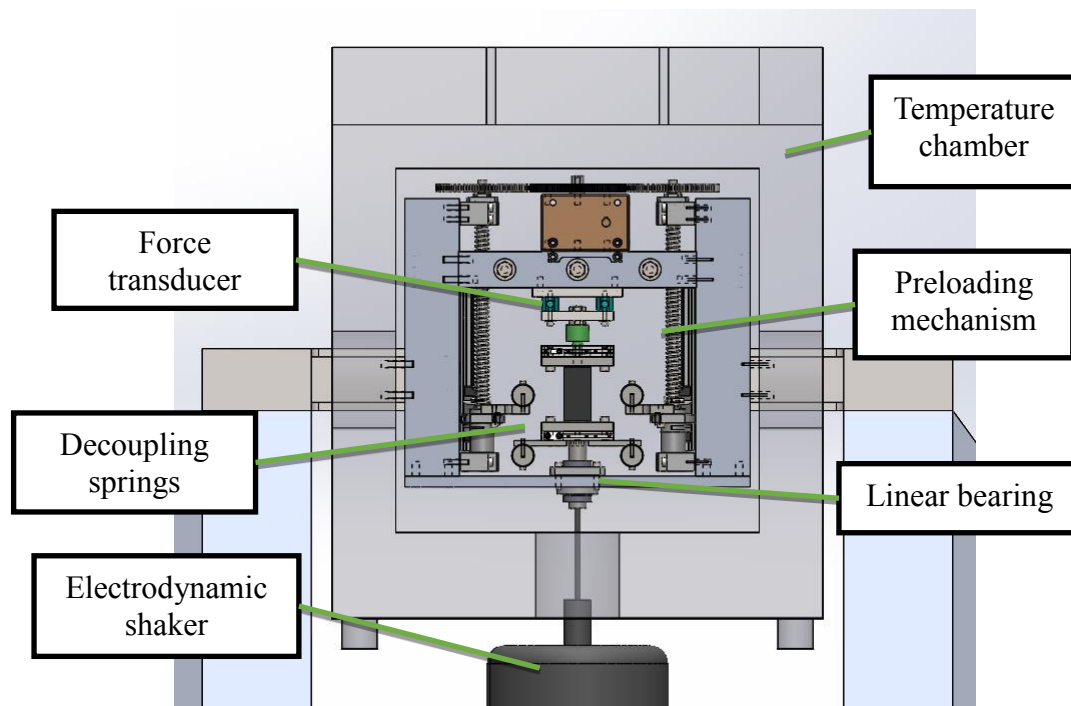


Figure 3.2. Detailed view and the components of the setup

The preloading mechanism is a ball screw-linear guidance assembly. The screw is supported by two bearings on the shaft ends, which is driven by a manual gearbox. By rotating the screw, end point of the decoupling spring makes reciprocating motion and the spring is tensioned. Coil springs are planned to be used as flexible elements.

3.4.2. Structural Design

The objective of the structural design is to avoid fixture bending modes in the frequency range of interest (Ozgen, Erol, & Batihan, Dynamic Stiffness-Based Test Systems for Viscoelastic Material Characterization: Design Considerations, 2012). Recall that the frequency range of interest is set as 5-200Hz. In order to ensure structural modes are beyond this range, modal analysis of the whole assembly is performed. The analysis is performed by Solidworks Simulation software package, using “Frequency” module. The mode shapes for first bending and torsional modes are shown in Figure 3.3 & Figure 3.4. By the analysis study the first bending mode of the

preloading force a strain-gage based force transducer is utilized, whereas dynamic force is to be measured by PZT force transducers. PZT sensor with IEPE acquired with a high-pass filter then they could not be used below 5Hz. Deflection measurement is derived from acceleration and in order to measure acceleration data PZT accelerometers are utilized.

Force and acceleration data is collected by NI 9234 analog data acquisition device. Electrodynamic shaker is driven by NI 9621 analog output device. Thermocouple data is collected by a separate card, NI 9211. PC with LabVIEW software is used to generate the signal necessary to drive electrodynamic shaker and collect analog signals. The instrumentation layout is given in Figure 3.5.

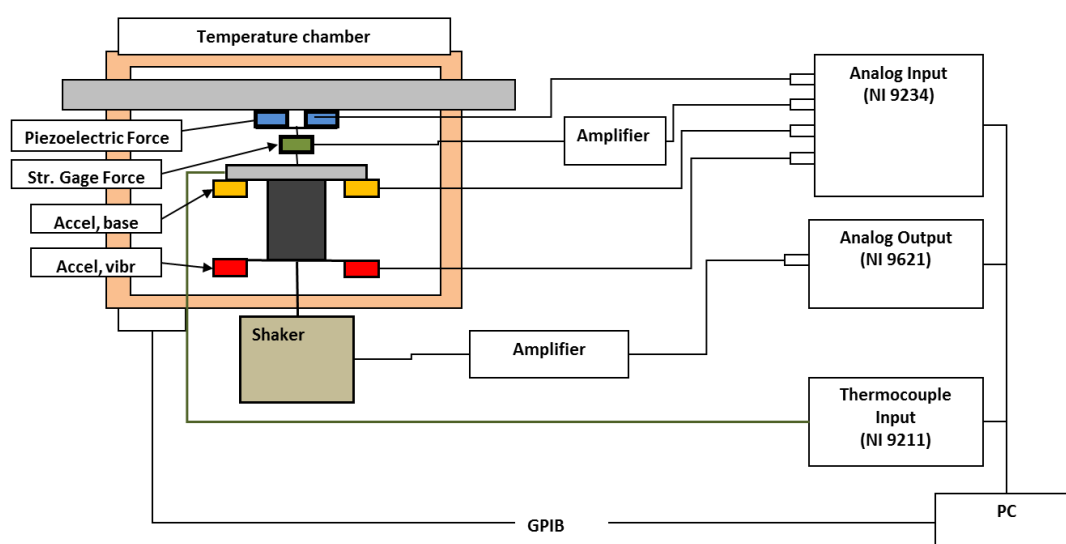


Figure 3.5. Instrumentation layout of the modified test setup

The software of the system is developed in LabVIEW platform. A P-control based algorithm is used for obtaining desired strain amplitude level, the flowchart is given in Figure 3.6.

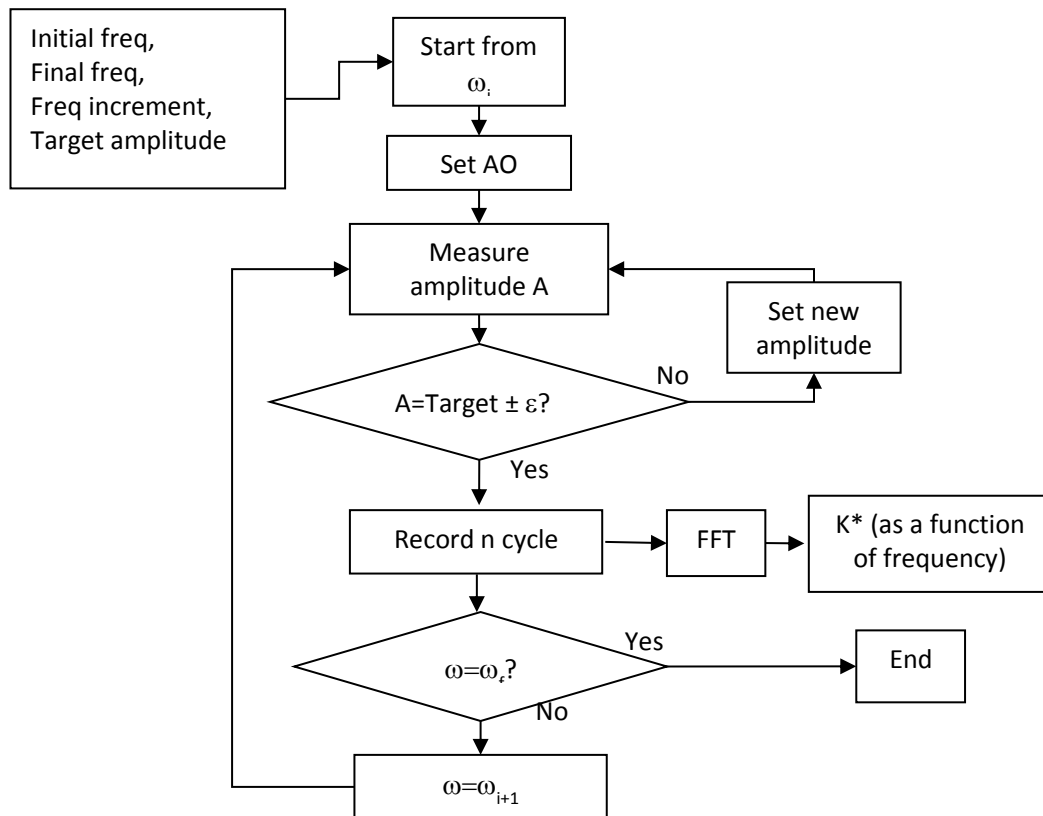


Figure 3.6. Flowchart of the amplitude control code

In this method, initially test parameters are defined. These parameters are initial and final frequency, frequency increment and target displacement amplitude. Test starts from initial frequency and specimen is deformed on an arbitrary level initially. Peak amplitude is measured from harmonic signal acquired from displacement sensor, which is accelerometer in this case. Amplitude is divided to square of frequency in order to get displacement. Amplitude of the signal is obtained by using Fast Fourier Transform algorithm. The difference between current and target amplitude is taken as error, which must be below a specified level. If error level is larger than specified, new amplitude is determined according to Eq (3-1).

$$A_{new} = K \frac{A_{ref}}{A_{current}} \quad (3-1)$$

The parameter K is the gain and determined by trial and error. If the error level is smaller than the specified level, then force and displacement data is recorded with duration equal to n number of cycles and transformed into frequency domain by FFT algorithm. Complex modulus is calculated by the Eq (3-2), which is derived by combining Eq (2-25) and Eq (2-26). In this equation F^* , A_a^* and A_f^* are the FFT transforms of measurements for force, acceleration at force plate and acceleration at base plate respectively.

$$K^* = \frac{F^* - mA_f^*}{(A_f^* - A_a^*)/\omega^2} \quad (3-2)$$

3.4.4. Design of Preloading Mechanism

In this study max preload value is set as 1000 N. The stiffness of the decoupling spring should be kept as minimum, because the force produced by the actuator is shared between the decoupling spring and the spring, and as the decoupling spring stiffness decreases, more force is transferred to the specimen. For this setup, the maximum stroke for the preload mechanism is 85mm due to mechanical packaging constraints. For 1kN preload, required total spring stiffness value is approx 11.7 N/mm.

Preloading is aimed to be provided by metal tension coil springs connected to force-transmission plate. There are 8 tension springs to provide 1 kN preload. Decoupling spring stiffness k_d used in this study is 1.18 N/mm for wire diameter $d = 2.5mm$ with outer diameter $D = 25mm$ and with active coils $N_a = 25$.

Tension force is generated by a manual linear actuation mechanism connected to the other end of the springs and driven by ball-screw. Detailed view of the preload mechanism is given in Figure 3.7.

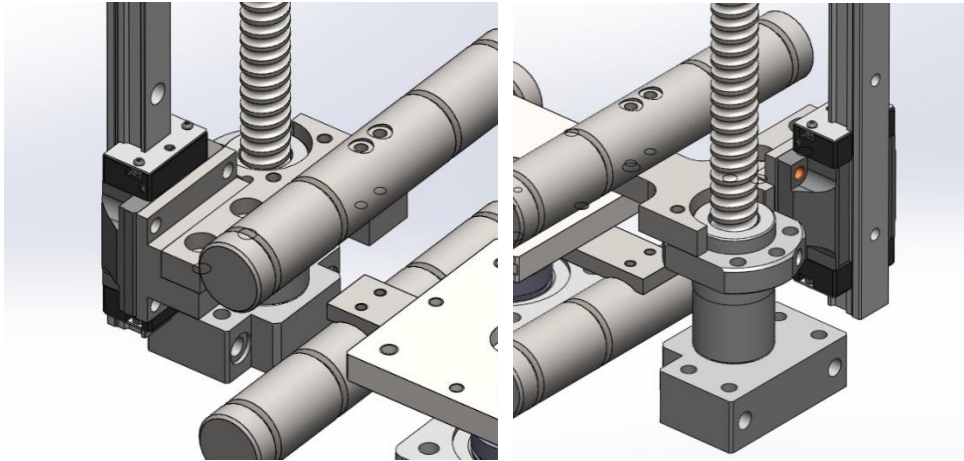


Figure 3.7. Detailed view of the preload mechanism

Since it is not desired to transmit the moment load due to preloading force, profile linear guidance bearings are utilized to maintain that moment load. A Finite Element based stress analysis is performed in Solidworks Simulation Software Package. Stress analysis is performed in order to ensure not to load ball-screws with bending moment. The bearing and the screw are treated as fixed mounts. The stress distribution is given in Figure 3.8. According to this study there are some load transmitted to the bearing. However, analysis results may be misleading because nut is supported by ball screw in reality, then it creates some flexibility on that mount. Therefore, higher load may be distributed on the linear bearing, which is more rigidly mounted on the fixture.

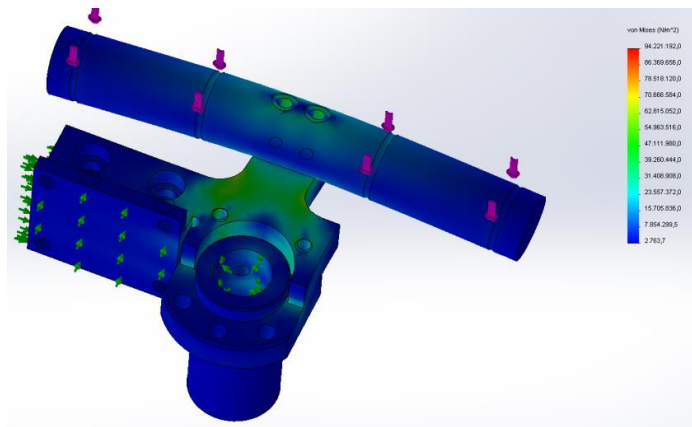


Figure 3.8. Stress distribution on the preload mechanism

For linear guidance of the force plate a shaft-guidance linear bearing is used. The reason why the shaft bearings are used is they provide little friction compared to profile bearings.

The assembled system with coil springs is shown in Figure 3.9.

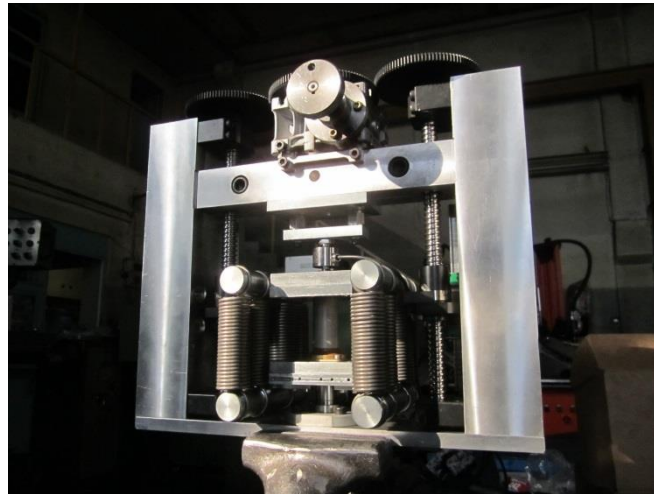


Figure 3.9. System with coil springs

3.5. Design Evaluation

The first attempt for dynamic stiffness measurements with preload mechanism is in which coil springs are used. In order to validate the design, a 30x30x60 elastomeric specimen with unknown content was used. This study focuses on dynamic stiffness measurements, since the modulus of elastomer material can be obtained by using dynamic stiffness measurements and geometric properties. Real stiffness and loss factor values will be obtained from the relations in Section 2.3.2.2.

The results for real stiffness and loss factor measurements obtained in this test are plotted in Figure 3.10 and Figure 3.11. It is obviously seen that erroneous measurements are obtained for both real stiffness and loss factor beyond a specific frequency. It is thought that this frequency may correspond to the internal resonance frequency of the springs.

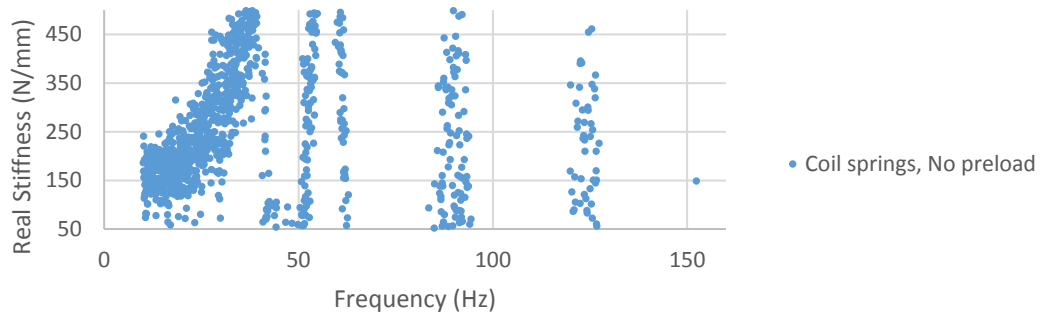


Figure 3.10. Real stiffness measurements vs frequency at the first attempt

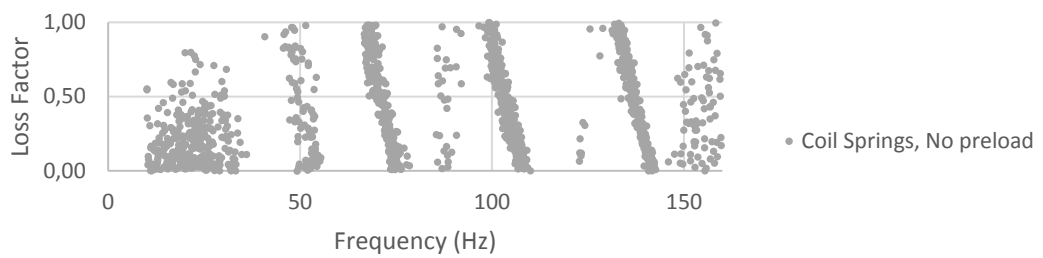


Figure 3.11. Loss factor measurements vs frequency at the first attempt

The reason why the results are deteriorated in that way could be internal resonance of the springs or improper connection between the coil springs and the fixture. It is thought that use of a flexible material with a tighter connection would solve both problems. For a quick solution the coil springs are replaced by elastomeric bands. Design details are presented in the next section.

3.6. Design Revision

3.6.1. Design of a Preloading Mechanism with Elastomeric Bands

Silicone bands are utilized as resilient elements because the glass-transition temperature is beyond the operation range and elastic modulus is relatively insensitive to the temperature.

The force exerted by the elastic bands under preload is determined by assuming silicone rubber as neo-hookean solid. The engineering stress-stretch relationship for

an incompressible neo-hookean rectangular solid under uniaxial tension is given in Eq(3-3) (Ogden, 2013)

$$\sigma_{11}^{eng} = 2C_1 \left(\lambda - \frac{1}{\lambda^2} \right) \quad (3-3)$$

For incompressible material the value $2C_1$ is equal to $E/3$. λ is the stretch and the relationship with the strain is $\lambda = 1 + \epsilon$. Due to limited test capabilities for that study, the elastic modulus is estimated from the hardness of the material. The hardness of the material used in this study is measured by a hand durometer as 70 Shore A. The elastic modulus of the silicone bands used in this system are obtained as $E = 8.8 \text{ MPa}$ by relationship given in Eq(3-4) (Kunz & Studer, 2006), where $\mu = 0.5$, $R = 0.395 \text{ mm}$, $C_1 = 0.549 \text{ N}$, $C_2 = 0.07516 \text{ N}$ and $C_3 = 0.025 \text{ mm}$.

$$E = \frac{1 - \mu^2}{2RC_3} \frac{C_1 + C_2 Sh_A}{100 - Sh_A} (2.6 - 0.02 Sh_A) \left[\frac{N}{\text{mm}^2} \right] \quad (3-4)$$

For a rubber band with 4x50mm rectangular cross-section the amount of force expected is given in Table 3.1. With these bands the max preloading force is expected to be 700N.

Table 3.1. *Estimated force vs stroke for elastomeric bands*

Stretch	Stress (MPa)	Stroke (mm)	Force (N)
1.00	0.00	0	0
1.05	0.42	5	67
1.10	0.80	10	128
1.20	1.48	20	237
1.50	3.10	50	495
1.70	3.97	70	635
1.85	4.57	85	731

The system with decoupling springs made of elastomeric bands is shown in Figure 3.12. The bands are mounted on the fixture by clamping by screws through the holes opened on rubber bands.

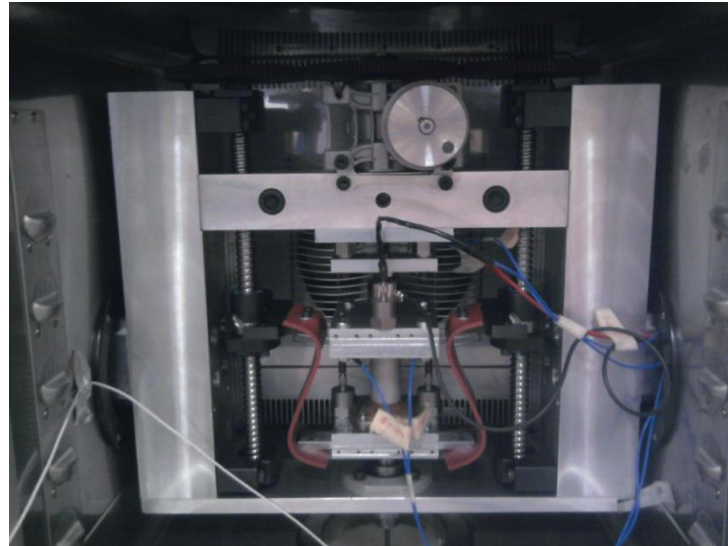


Figure 3.12. Preloading mechanism with elastomeric bands

3.6.2. Calculation of Internal Resonance Frequency of Preloading Mechanism

In this section internal frequencies of the preloading mechanism with decoupling springs will be evaluated. In this case decoupling spring is treated as continuous media and longitudinal vibrations are considered. For adequately stiff fixture the preload mechanism is represented as in Figure 3.13.

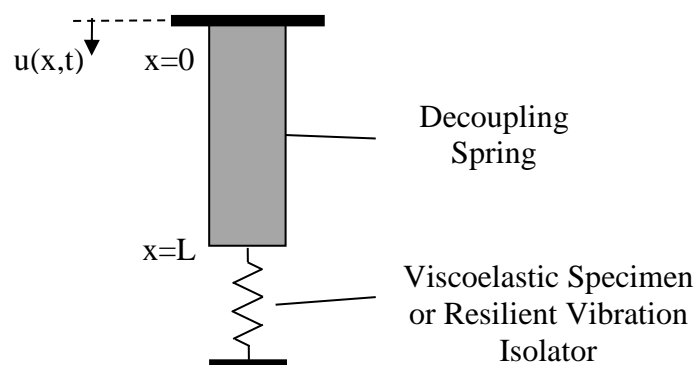


Figure 3.13. Mechanical representation of the preloading mechanism

By neglecting the gravitational effect on the body, the governing equation for that system is written in Eq (3-5) (Da Silva (ed), 2005). This model also neglects the mass connected to the specimen. Solution is proceeded by assuming displacement variable as separable into space and time functions as Eq (3-6). For a fixed time function, deformation gets a specific shape space function becomes fixed. These are mode shape functions and corresponding frequencies that satisfies that condition are natural frequencies. The solution of space equation, i.e. mode shape equation (eq) is provided in Eq (3-7). One end is fixed to the ground then no displacement occurs; therefore, first boundary condition of the problem is given in Eq (3-8). At the other end a spring is coupled then force relationship gives the other boundary condition, which is given in Eq (3-9). Specimen is considered as linear elastic spring for brevity.

$$\frac{\partial^2 u(x, t)}{\partial t^2} = c^2 \frac{\partial^2 u(x, t)}{\partial x^2} \quad (3-5)$$

$$u(x, t) = X(x)T(t) \quad (3-6)$$

$$\frac{d^2 X(x)}{dx^2} + \lambda^2 X(x) = 0 \quad (3-7)$$

$$X(0) = 0 \quad (3-8)$$

$$EA \frac{dX(l)}{dx} + kX(l) = 0 \quad (3-9)$$

Applying BC's to the problem and for non-trivial solutions the relationship in Eq (3-10) is obtained, which is called *transcendental equation* (Da Silva (ed), 2005). The smallest non-zero value of lambda gives the first natural frequency of the system (Eq (3-11)). In Eq (3-11) c is the wave speed in the media.

$$\tan \lambda_i l + \frac{EA}{k} \lambda_i = 0 \quad (3-10)$$

$$\omega_i = \lambda_i c \quad (3-11)$$

For small values of the specimen stiffness the boundary condition converges to a free end then internal resonance frequency is obtained from the relationship in Eq (3-12).

$$\omega_i = \frac{\pi}{2L} c \quad (3-12)$$

3.6.2.1. Internal Resonance Frequency of System with Coil Springs

The wave speed in a coil spring is calculated from the relationship given in Eq (3-13). (Semat & Katz, 1958) In this equation L is the solid length of the spring and μ is the weight of the spring and calculated for a wire coil spring by Eq (3-14) (Budynas & Nisbett, 2006).

$$c = \sqrt{\frac{k_d L}{\mu}} \quad (3-13)$$

$$\mu = \frac{W}{L} = \rho A = \rho \frac{\pi d^2}{4} \frac{\pi D N_a}{L} \quad (3-14)$$

Assuming that coil spring is a continuous media with relationship $k = EA/L$, then Eq (3-10) is modified as in Eq (3-15).

$$\tan \lambda_i l + \frac{k_d L}{k} \lambda_i = 0 \quad (3-15)$$

Decoupling spring stiffness k_d used in this study is 1.18 N/mm . For different real stiffness values between $0.01 - 1000 \text{ N/mm}$ for specimen, calculated internal resonance frequency values for decoupling springs are given in Table 3.2.

Table 3.2. *Internal resonance frequency calculations for decoupling springs with coil spring*

SPECIMEN STIFFNESS (N/MM)	λ	Ω (HZ)
0.01	0.02510	24.0
0.1	0.02595	24.8
1	0.03153	30.1
10	0.04505	43.1
100	0.04967	47.5
1000	0.05021	48.0

Although it is desired to increase the internal resonance frequency value by changing the coil spring parameters, it is not possible to obtain internal resonance frequency beyond 200Hz, which is the maximum frequency of interest. Therefore, use of elastomeric materials has been evaluated in order to go beyond that frequency.

3.6.2.2. Internal Resonance Frequency of System with Elastomeric Bands

The internal resonance frequencies of the system with elastomeric bands are calculated by using Eq (3-11) and the results are given in Table 3.3 for different specimen stiffness values. It is clearly seen that a decoupling spring with elastomeric material with coil spring has greater internal resonance frequency than coil springs with similar stiffness.

Table 3.3. *Internal resonance frequency calculations for decoupling springs with elastomeric bands*

Specimen stiffness (N/mm)	λ	ω (Hz)
0.01	0.01571	235
0.1	0.01574	235
1	0.01606	240
10	0.01866	279
100	0.02698	403
1000	0.03087	461

3.7. Re-Evaluation of the Design

The real stiffness and loss factor measurements from a 30x30x60 EPDM specimen with original test setup by Erol and modified test setup without preload are plotted in Figure 3.14. In this study, only the results from elastomeric material specimen can be compared because the original test setup is designed only for the characterization of the materials. The results are given in real stiffness and loss factor, calculated by using the relations in Section 2.3.2.2. The material storage modulus and loss factor could be obtained by using geometrical properties. These relations are provided in Section 2.3.2.3.

The results for 125N preload are also represented in Figure 3.14. The preload value of 125N is an estimated value since we could not make the signal conditioner work for the load cell we have used. Therefore, we have to estimate the preload using the deflection in the decoupling bands and their total estimate for effective stiffness.

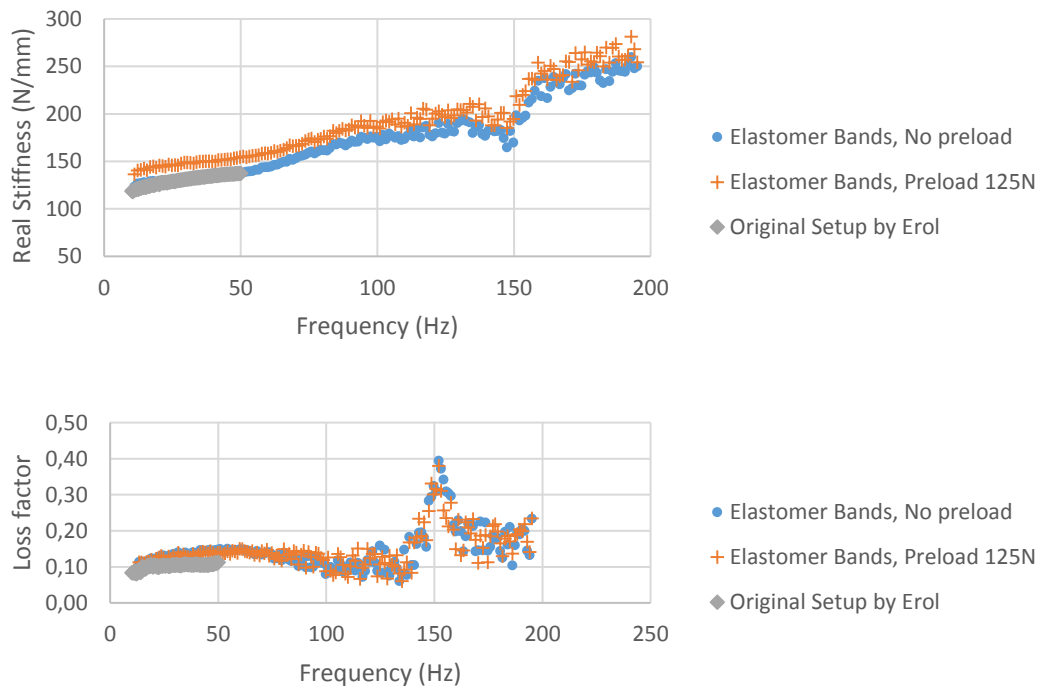


Figure 3.14. Real stiffness and loss factor measurements for the system with elastomeric bands

Figure 3.14. shows that the original and modified setup for tests without preload give consistent results. Under preload, there is an increase in the material's stiffness and loss factor in the entire frequency range, which indicates that material is preloaded.

Measured stiffness of the specimen is in range between 120-250 N/mm. According to Table 3.3 which lists internal resonance frequency versus specimen stiffness, internal resonance frequencies for elastomeric bands should be out of the frequency range of interest. Therefore, it is not expected to encounter same kind of distortion in measurements. A deviation observed in results at 150 Hz. The reason of that deviation may be presence of other structural modes or errors in determination of the dynamic stiffness of the decoupling springs.

In addition, test results with some elastomer specimens are provided in Appendix A. The stiffness values of the specimen used in these measurements are not known prior to testing, so they will only be compared with the results obtained with the setup designed in Chapter 4.

3.8. Conclusions

In the context of this study, two different concepts for decoupling spring is designed and demonstrated then measurements are taken over a frequency range. As a result, it could be stated that if decoupling springs are used the internal natural frequencies of the decoupling springs should be avoided within the frequency range of interest. It has been evaluated that elastomeric materials can be utilized in this regard since they have high natural frequency compared to coil springs.

CHAPTER 4

DESIGN EFFORTS FOR A NEW TEST SETUP

4.1. Introduction

In this section design efforts for a new test setup are presented. This test setup is intended for both viscoelastic material characterization and dynamic characterization of elastomer components under preload. Direct methods are used in this setup, discussed in Section 2.3.2.2. Specimen will be excited by an electrodynamic shaker. The setup has temperature and preload control, as well as software amplitude control capabilities. A mechanism with coil spring is designed for preload.

The new test system will be used to measure the frequency and temperature-dependent dynamic resistance of elastomer vibration isolators, which will be designed in the scope of a project. It can also be used to measure the complex modulus of viscoelastic materials from material specimen if desired. This test system has been planned as an alternative to the revised test system in Chapter 3.

The test system is manufactured and assembled and then validation tests were performed on a specimen. The spring mechanism did not work properly in this setup; therefore, it was planned to use elastomer elements for the preloading mechanism where the proposed revision is left as a future study and not studied in this thesis work. The test setup is not properly validated possibly due to some unexpected structural behaviors observed in this test setup.

Error analysis was carried out to investigate the possible causes of the problem and to determine what could be done for design revision. Within the scope of error analysis, reduced-order analytical models and Finite-Element-based harmonic analyzes were utilized. The FE model is associated with the modal test. The results obtained with the frequency-sweep simulations were compared.

Metallic calibration spring and rectangular elastomeric specimen were used in the tests. As a result of the study, some ideas about the revisions that should be made in the apparatus are obtained, and some structural features that an ideal elastomer test apparatus should have are determined.

4.2. Design Objectives, Requirements and Constraints

The test setup will be used for measurement of complex modulus of viscoelastic materials, as well as dynamic characterization of vibration isolators. These measurements will be performed with respect to temperature, frequency, static preload and dynamic amplitude. Test setup is designed in accordance with Direct Method discussed in Section 2.3.2.2.

Temperature control will be performed by ESPEC SU-662 bench-top temperature chamber with 400x400x400mm control volume. That chamber is custom-built for this study with two 120mm-diameter holes at the top and bottom walls and two 40mm-diameter holes at the side walls. These holes allow the transmission rods to enter the temperature control volume from above and below. Temperature range is set as -65/+150°C.

APS 400 electrodynamic shaker is utilized with APS 145 amplifier combination. The frequency range is limited by the actuator with max frequency value is 200 Hz.

Harmonic force measurement will be performed by IEPE force sensor. Static preloading force will be measured by strain-gage based force transducer. Lower frequency is limited by IEPE force sensor as 5Hz, which is the determined by high-pass filter of the data acquisition device used for IEPE transducers.

Preloading will be performed with a software-controlled mechanism. EXLAR Tritex Linear servo actuators will be utilized for controlling the position of the preloading mechanism. Coil springs will be used as flexible elements for decoupling springs.

Presence of bending modes of the fixture within the frequency range of interest is not allowed. However, there is no objective for the other possible modes since the influence of that modes is not clearly estimated at the beginning of the study.

4.3. Design Efforts

4.3.1. Conceptual Design

The design is a stand-alone system with a heavy fixture in order to conduct dynamic tests of oversized specimens with preload, controlled strain and temperature. Overview of the test system is given in Figure 4.1.

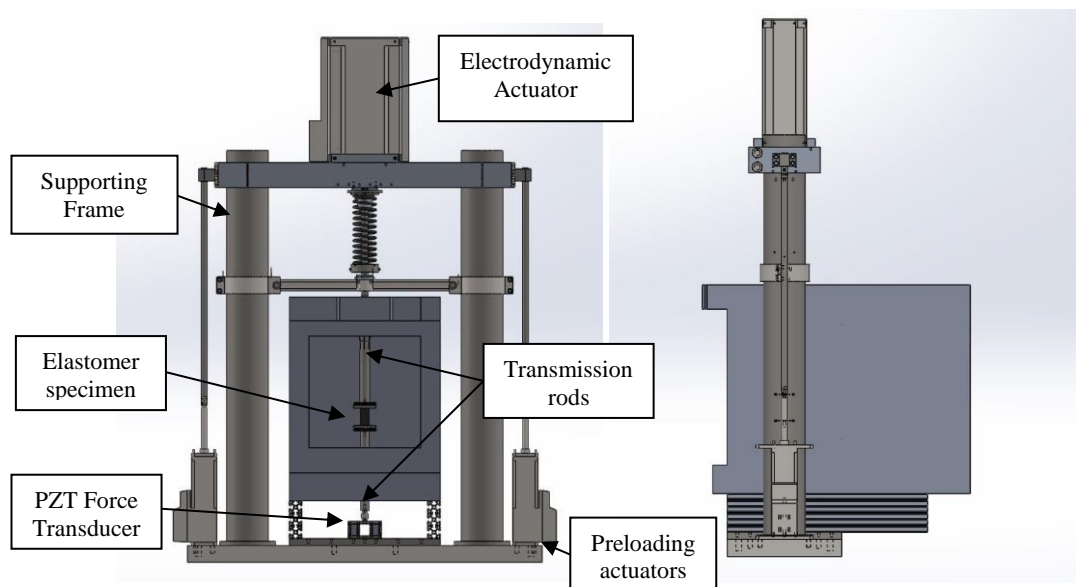


Figure 4.1. Overview of the test setup

Test system is a heavy structure made of steel in order to assure minimum modal response and avoid modal coupling. Large clearance between horizontal elements and columns exists to have a space for a temperature chamber to control temperature. Whole structure is supported on rubber layers. The foundation of the system is concrete structure covered by soft floor cover.

A large temperature chamber is located to the central section of the assembly in order to provide temperature control. The geometric dimensions of the chamber have a significant limitation on the test fix size and therefore the transfer rods must have a certain length. At the top, the electrodynamic shaker is mounted which is guided by linear bearings following grounded shafts. The flexibility of this part also affects the character of the structure. Transmitted force to supporting frame is measured by a piezoelectric force transducer and deformations are measured by accelerometers located on transmission rods.

4.3.2. Investigation of the Validity of the Structural Design using Finite Element Based Simulations

The test system is designed to be as rigid as possible under the specified geometric constraints. Therefore, geometrical parameters and materials are determined in order to keep the resonance frequencies of the fixture as high as possible. Resonance frequencies are investigated by extraction of natural frequencies and corresponding mode shapes using Finite Element (FE) method.

The performance of the test setup is evaluated by determination of force capacity using FE method. In this FE model linear harmonic analysis procedures are used which based on the same model in modal analysis.

4.3.2.1. Modal Analysis

A Finite Element (FE) model is built to simulate modal behavior and harmonic response of the system with a software package, Abaqus/CAE. Previous studies have shown that fixture bending modes have negative effects on results (Ozgen, Design and Development of a Complex Shear Modulus Measurement Setup For Viscoelastic Materials, 2005) (Ozgen, Erol, & Batihan, Dynamic Stiffness-Based Test Systems for Viscoelastic Material Characterization: Design Considerations, 2012). Therefore, this study will calculate the natural frequencies and the corresponding mode shapes of the system. The analysis model is shown in Figure 4.2.

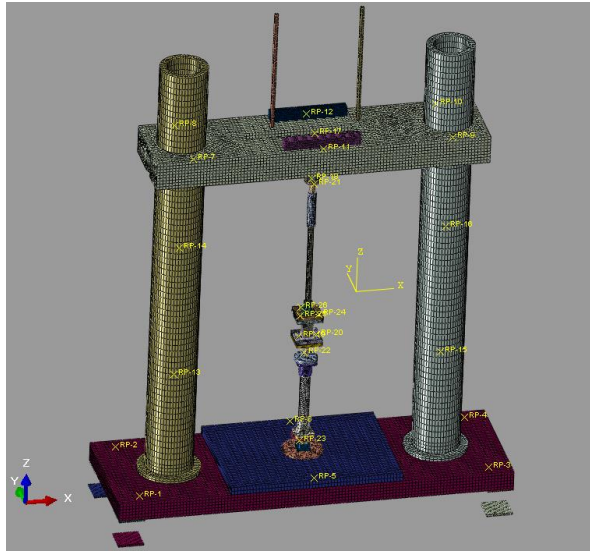


Figure 4.2. FE model of test system

Frame blocks are modelled with C3D8I –fully integrated linear hexagonal element with incompatible modes in order to model bending behavior more correctly with smaller number of elements. Incompatible elements have additional shape functions in order to prevent shear locking encountered in fully integrated linear elements. Columns are assembled to mount plate by threaded fasteners while upper horizontal column is fixed to the columns by flexible clamps. Joint between the columns and the bottom frame are modelled with mesh-independent fasteners (keyword: *FASTENER) in order to achieve approximate dynamic behavior of bolted joint.

For upper frame two bolts are used at each flexible clamp in order to assure a tight assembly. Tightening of these bolts bends the body such that inner surfaces are in contact with the vertical columns. These regions are modelled with tie definition (keyword: *TIE) since it is expected that clamping action will disable the movement between the column and the frame.

Specimen is assumed to be linear elastic with frequency-dependent viscoelastic properties. Long-term modulus –modulus at zero frequency is assumed as 5 MPa with Poisson’s ratio as 0.47. These regions are modelled with C3D20H – quadratic

hexagonal continuum elements with hybrid formulation- in order to prevent volumetric locking due to high Poisson's ratio. Elastic rubber pads are also modelled with same material properties.

Electrodynamic actuator is a bulky and complex structure with coils and permanent magnets; however, armature (moving part of the actuator) is guided by 12mm-diameter solid shafts supported with circulating-type linear guideways. Actuator body and armature is assumed to be rigid parts, so that point mass elements are used to model them, whereas guidance shafts are modelled with C3D8I solid elements. The interaction between guideways and shaft is assumed to be a cylindrical joint –only axial displacement along and rotation around shaft axis is allowed - with no friction; therefore, connector elements are defined between shaft and armature (keyword: *CONNECTOR).

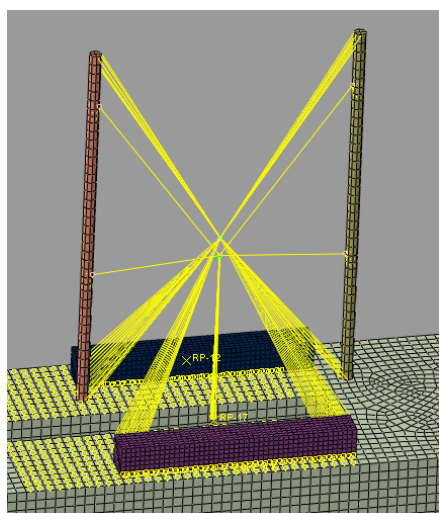


Figure 4.3. Modelling electrodynamic-actuator

Piezoelectric (PE) force transducer is modelled with C3D8I solid elements. Although inner structure is unknown strain-gage type force transducer is modelled with a solid bar with circular cross-section. Temperature chamber is not included in the model since it is decoupled from the test system.

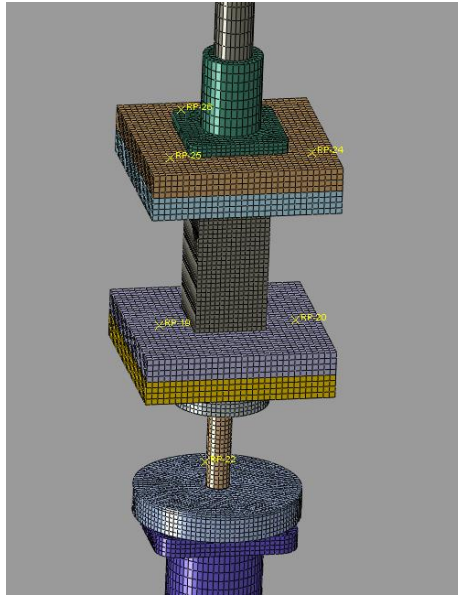


Figure 4.4. Region where specimen is mounted

Mode shapes obtained as results of FE analysis are shown in Figure 4.5-Figure 4.21 and listed in Table 4.1.

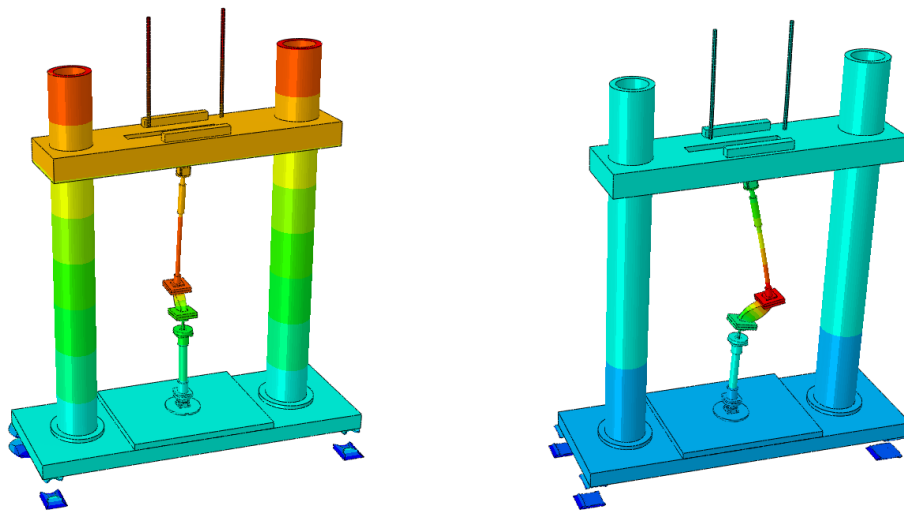


Figure 4.5. Analysis results, 1st-(left) and 2nd (right) mode shapes, 12.3 Hz, 16.5 Hz

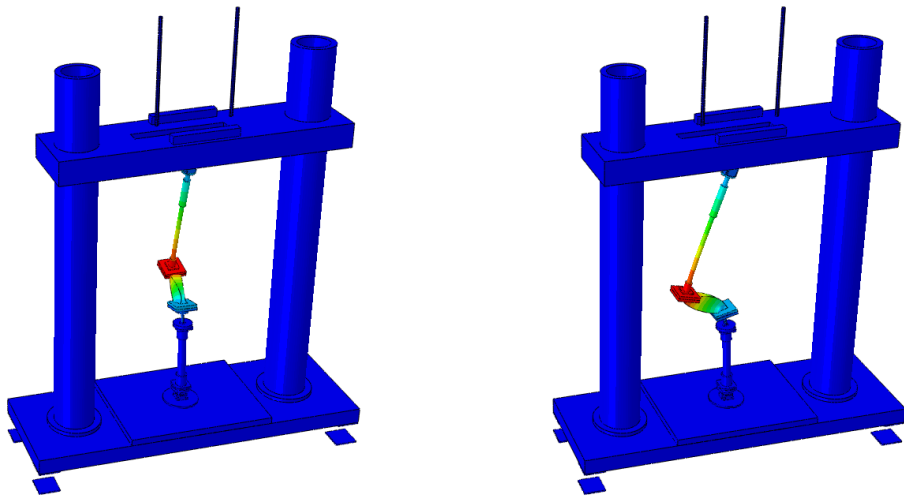


Figure 4.6. Analysis results, 3rd-(left) and 4th (right) mode shapes, 19.8 Hz, 19.9 Hz

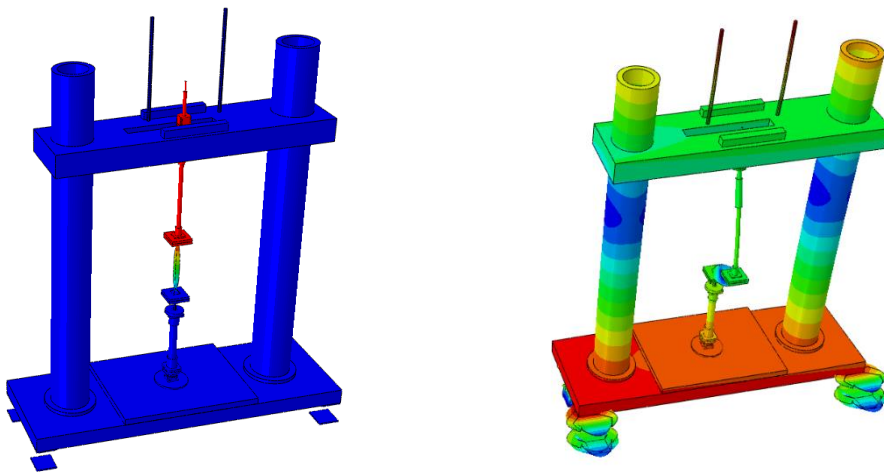


Figure 4.7. Analysis results, 5th-(left) and 6th (right) mode shapes, 27.1 Hz, 28.4 Hz

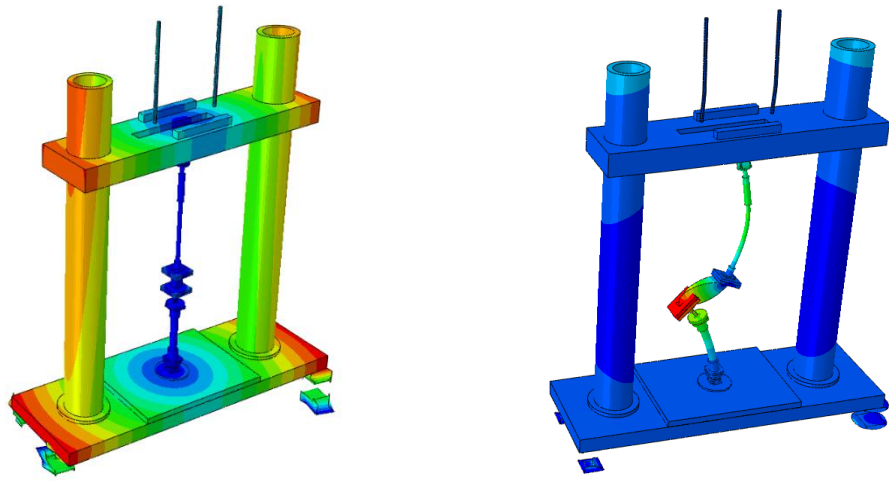


Figure 4.8. Analysis results, 7th-(left) and 8th (right) mode shapes, 28.9 Hz, 57.1 Hz

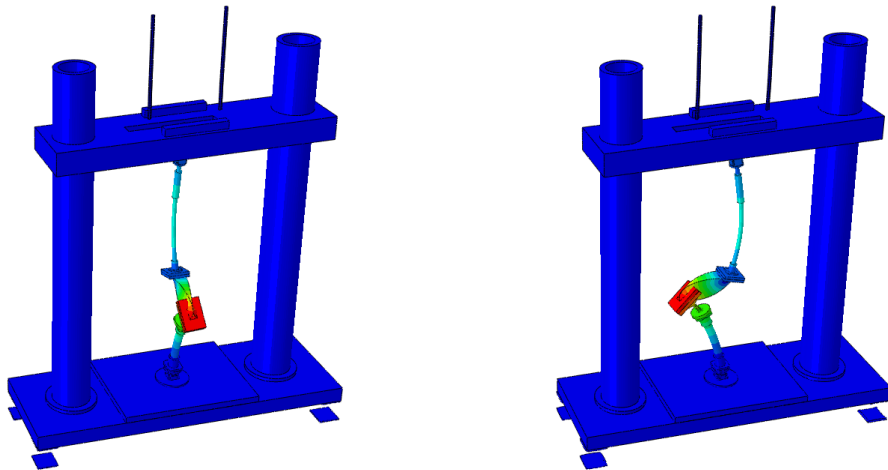


Figure 4.9. Analysis results, 9th-(left) and 10th (right) mode shapes, 59.8 Hz, 59.9 Hz

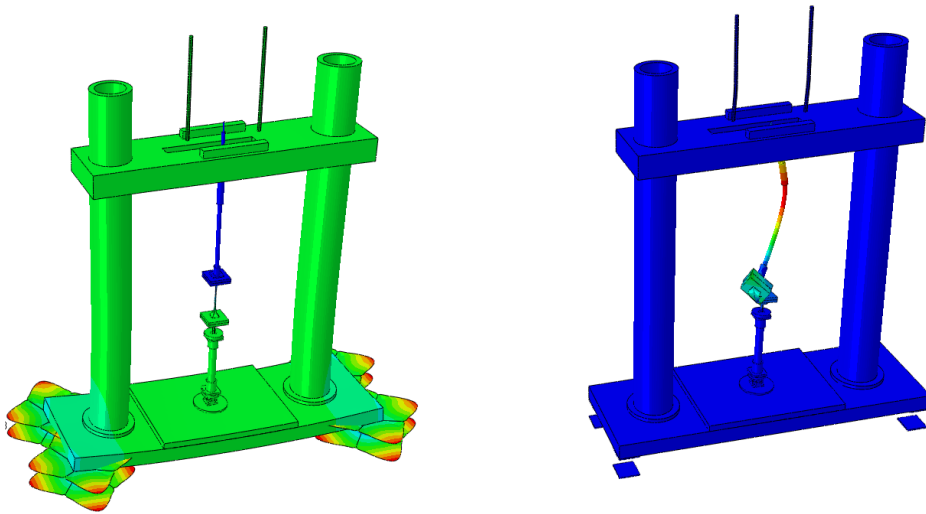


Figure 4.10. Analysis results, 11th-(left) and 12th (right) mode shapes, 74.2 Hz, 75.8 Hz

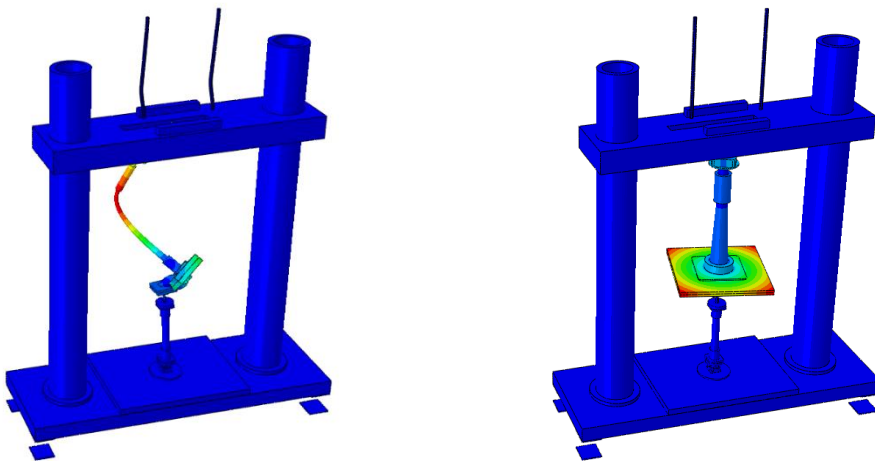


Figure 4.11. Analysis results, 13th-(left) and 14th (right) mode shapes, 75.9 Hz, 82.9 Hz

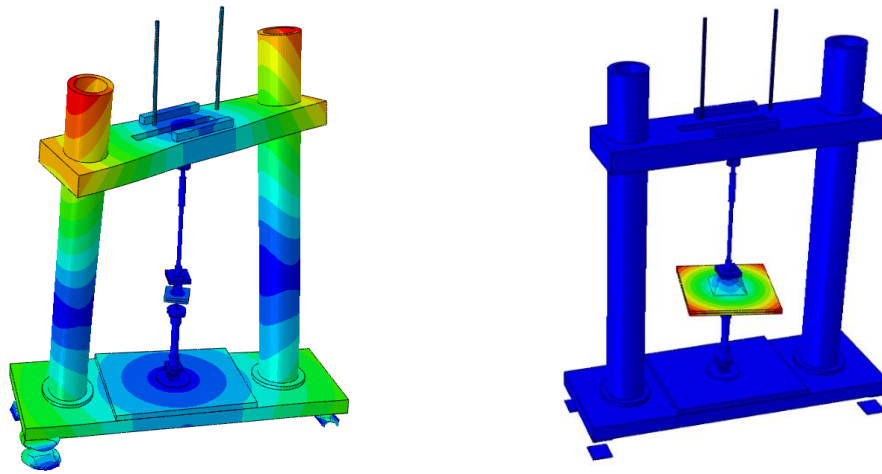


Figure 4.12. Analysis results, 15th-(left) and 16th (right) mode shapes, 121.9 Hz, 152.3 Hz

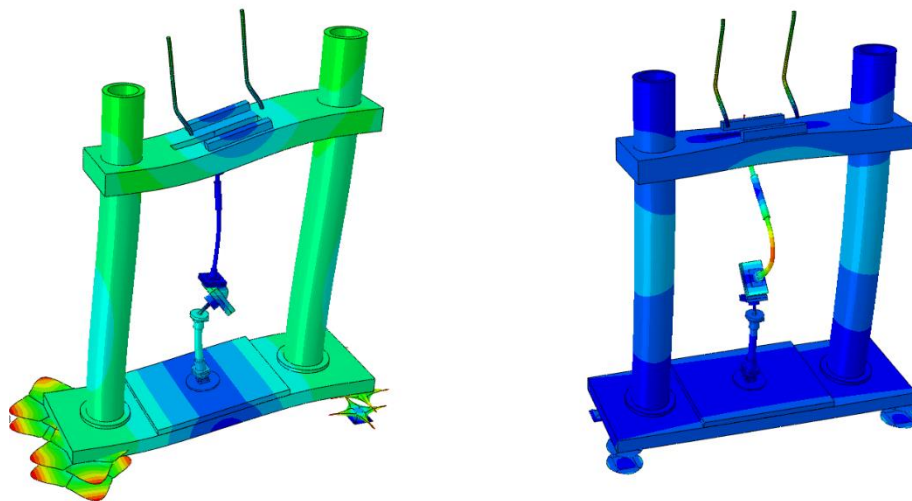


Figure 4.13. Analysis results, 17th-(left) and 18th (right) mode shapes, 155.3 Hz, 166.6 Hz

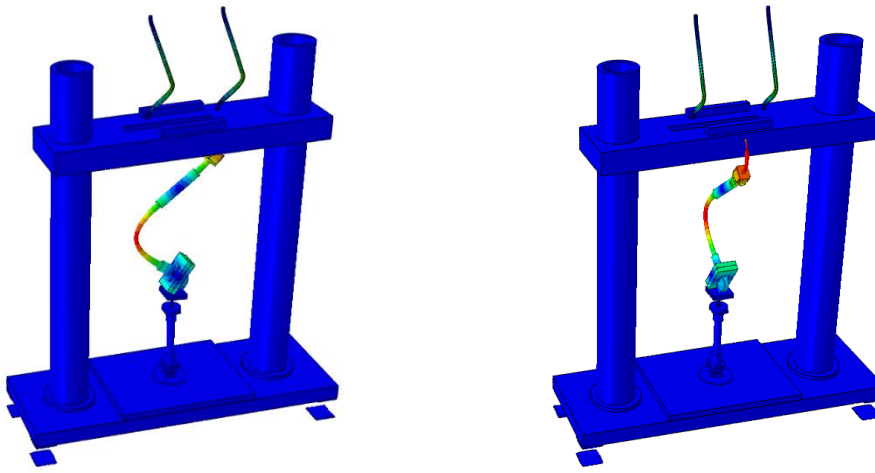


Figure 4.14. Analysis results, 19th-(left) and 20th (right) mode shapes, 184.5 Hz, 187.8 Hz

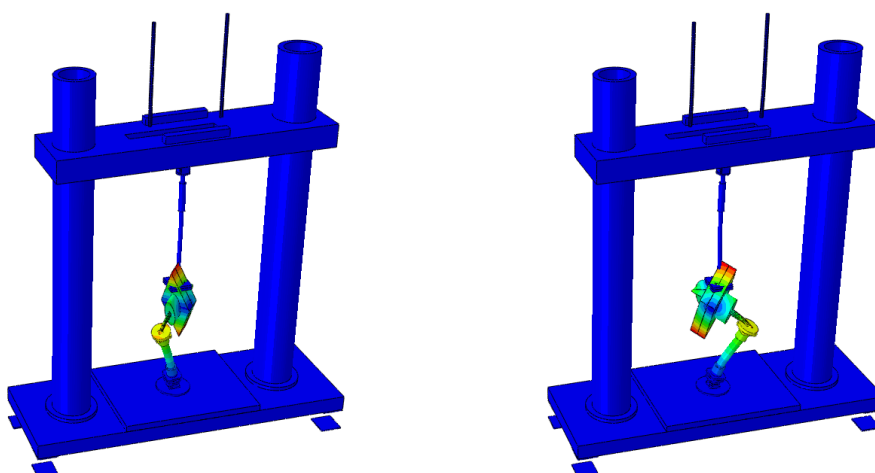


Figure 4.15. Analysis results, 21st-(left) and 22nd (right) mode shapes, 216.9 Hz, 217.5 Hz

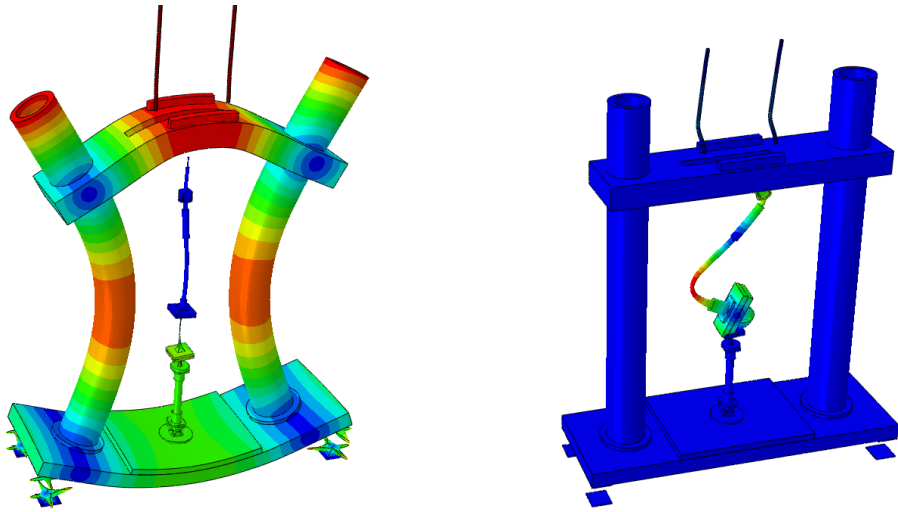


Figure 4.16. Analysis results, 23rd-(left) and 24th (right) mode shapes, 235.4 Hz, 288.9 Hz

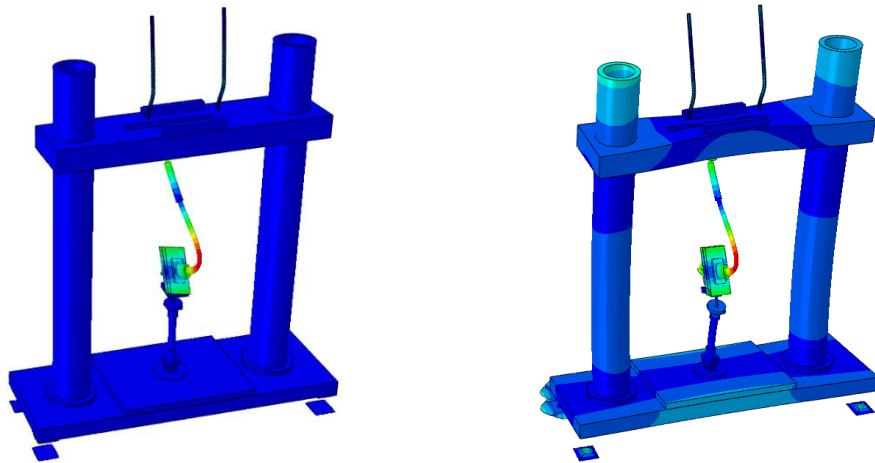


Figure 4.17. Analysis results, 25th-(left) and 26th (right) mode shapes, 290.6 Hz, 305.4 Hz

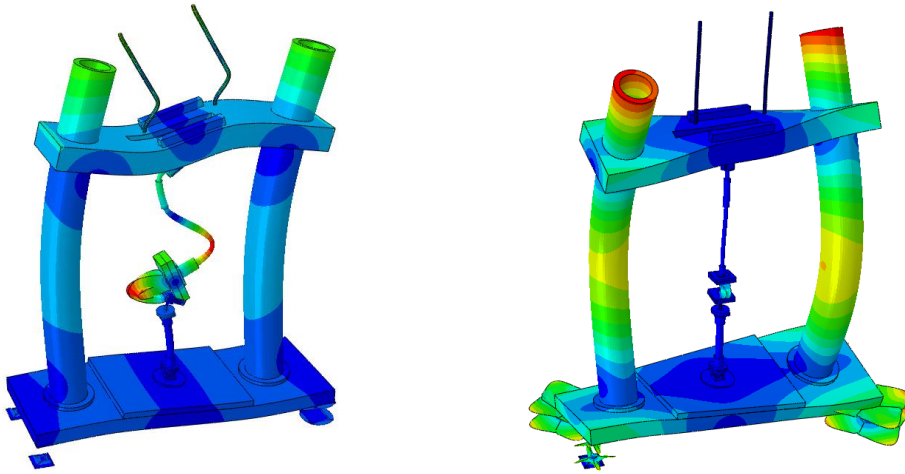


Figure 4.18. Analysis results, 27th-(left) and 28th (right) mode shapes, 343.8 Hz, 370.1 Hz

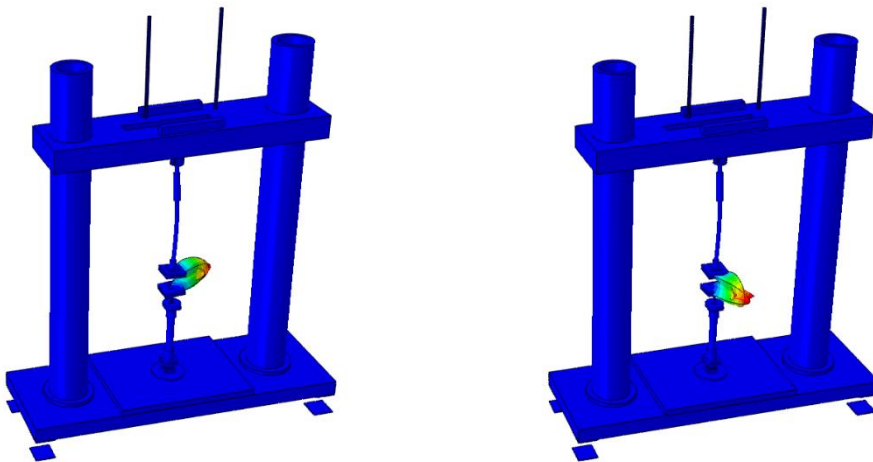


Figure 4.19. Analysis results, 29th-(left) and 30th (right) mode shapes, 380.5 Hz, 380.5 Hz

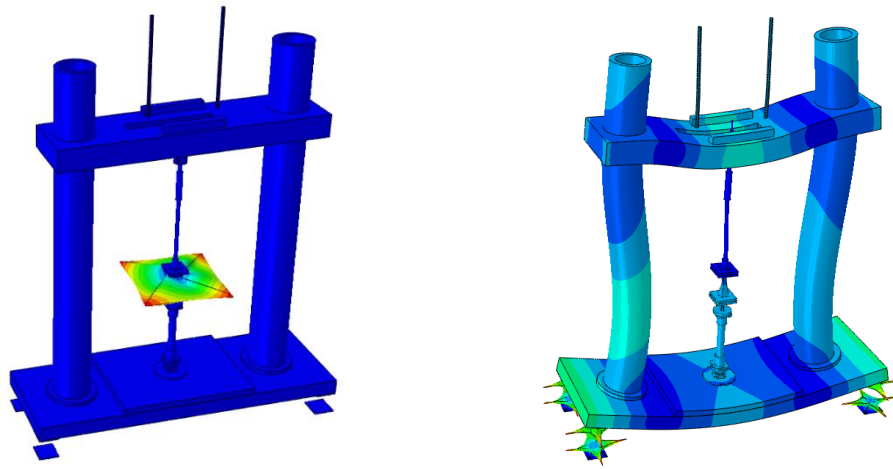


Figure 4.20. Analysis results, 31st-(left) and 32nd (right) mode shapes, 411.3 Hz, 437.1 Hz

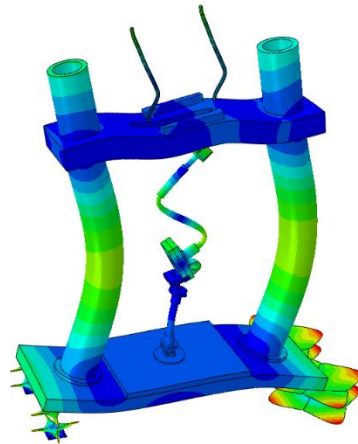


Figure 4.21. Analysis results, 33rd mode shape, 449.5 Hz

Table 4.1. *Mode frequencies and shapes obtained by FE analysis*

Mode shape #	Freq (Hz)	Label
1	12.353	Frame sway, upper TR 1st bending coupled
2	16.525	Frame sway, upper TR 1st bending coupled
3	19.83	Upper TR 1st bending
4	19.897	Upper TR 1st bending
5	27.127	Upper TR axial
6	28.396	Frame sway side-to-side, upper TR 1st bending coupled
7	28.914	Frame SDOF torsion on elastic mounts
8	57.058	Upper TR 2nd and lower TR 1st bending coupled
9	59.631	Upper TR 2nd and lower TR 1st bending coupled
10	59.978	Upper TR 2nd and lower TR 1st bending coupled
11	74.237	Frame SDOF axial on elastic mounts
12	75.813	Upper TR 2nd bending
13	75.864	Upper TR 2nd bending
14	82.861	Upper TR 1st torsion
15	121.9	Frame 1st bending+torsion
16	152.25	Lower TR 1st torsion
17	155.26	Frame bending quadrilateral mode
18	166.63	Upper TR 2nd and guidance shafts bending coupled
19	184.53	Upper TR 2nd and guidance shafts bending coupled
20	187.78	Upper TR 2nd and guidance shafts bending coupled
21	216.93	Lower TR 2nd bending
22	217.5	Lower TR 2nd bending
23	235.39	Frame bending opposite sides
24	288.9	Upper TR 3rd bending
25	290.06	Upper TR 3rd bending
26	305.38	Upper TR 3rd and frame bending coupled
27	343.75	Upper TR 3rd and frame bending coupled
28	370.09	Frame 2nd bending+torsion
29	380.5	Specimen bending
30	380.52	Specimen bending
31	411.26	Specimen torsion
32	437.05	Frame bending
33	449.43	Frame bending and upper TR 4th bending coupled

The frequency range of interest is 1-200Hz. The bending modes of the fixture are above 200 Hz; therefore, it is ensured that they are out of the frequency range of

interest. The modes below 200 Hz are commonly of transmission rods. These modes may be excited in frequency sweeps; however, it is not known at this step whether excitation of these modes influences the measurements. The mode #11 which is SDOF like motion of the whole fixture is another mode that is in the frequency range of interest. Whether excitation of those modes influences the results or not will be seen in validation studies.

4.3.2.2. Determination of Maximum Deformation Force Transmitted to the Specimen and Corresponding Deflections

Elastomer mechanical properties are dependent on strain amplitude and frequency. Test specifications are determined according to the application. Capacity of the test system should satisfy the application requirements. For that purpose, the limits of the test system will be evaluated.

The force generated by the actuator both deforms the sample and moves the force transmission components. The greater the force transferred to the sample, the more deformed the sample. As the frequency increases, more force is needed to move the force transmission components, which reduces the force to be transferred to the specimen. For tests depending on the deformation amplitude, it is important to determine the maximum deflection of specimens with certain stiffness. Therefore, the capacity of the setup should be determined by determining the maximum force that can be transferred to the specimen with respect to the frequency.

In this study, the deformation amplitude and the corresponding deformation amplitudes of the samples with three different stiffness values will be determined. For this purpose, 2 DOF mass & spring model is utilized. This model is based on Direct Method, explained in Section 2.3.2.2. The model consists of two mass moving in same type of coordinate connected with springs (See Figure 4.22) These masses represent the mounting blocks of the specimen. The spring between two mass represents the specimen, the other one is the sensor.

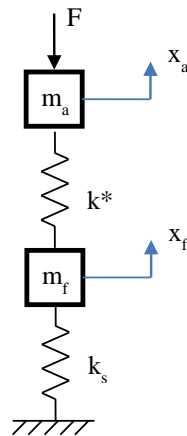


Figure 4.22. 2 DOF model used for determination of force capacity

Equation of motion in frequency domain is provided in Eq (4-1). F represents the force generated by the actuator. APS 400 electrodynamic shaker is utilized with APS 145 amplifier combination. The force profile of the actuator is given in Figure 4.23. (APS 400 ELCTRO-SEIS Long Stroke Shaker with Linear Ball Bearings Datasheet, 2013).

$$\begin{bmatrix} -\omega^2 M_a + k^* & -k^* \\ -k^* & -\omega^2 M_f + (k_f + k^*) \end{bmatrix} \begin{Bmatrix} X_a \\ X_f \end{Bmatrix} = \begin{Bmatrix} F \\ 0 \end{Bmatrix} \quad (4-1)$$

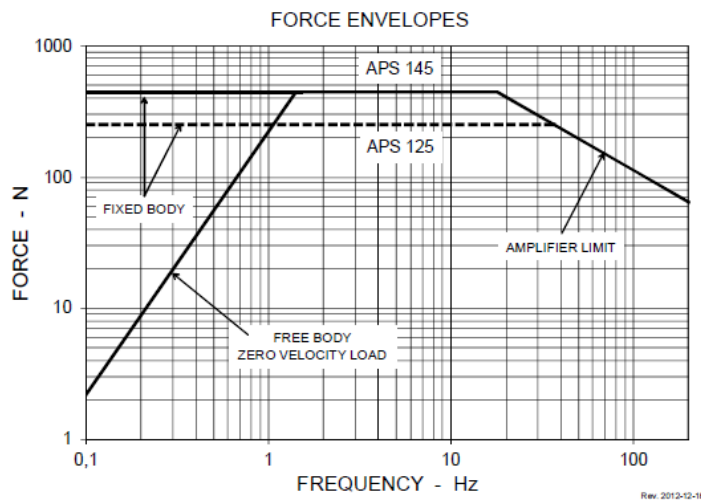


Figure 4.23. Force profile of APS 400 Shaker

The specimen used in the analysis model is modelled with a stiffness element, labeled as k^* . Three different specimen stiffness values, 5, 50 and 500 N/mm are used in the model. Force measured by the sensor is calculated by the deformation of spring represents the sensor (See Eq. (4-2)) Resilience of that spring is selected as $1 \cdot 10^9$ N/mm, which is considerably high compared to specimen stiffness.

$$F_s = k_s x_b \quad (4-2)$$

Max frequency of the actuator is specified as 200 Hz; therefore, the calculations are performed up to that frequency. Maximum achievable deflection and measured force is plot in Figure 4.24 and Figure 4.25.

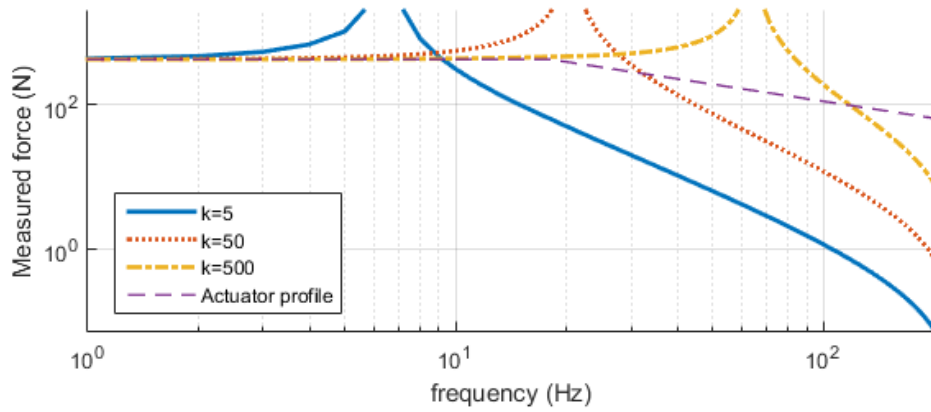


Figure 4.24. Transmitted force vs frequency for three stiffness configurations

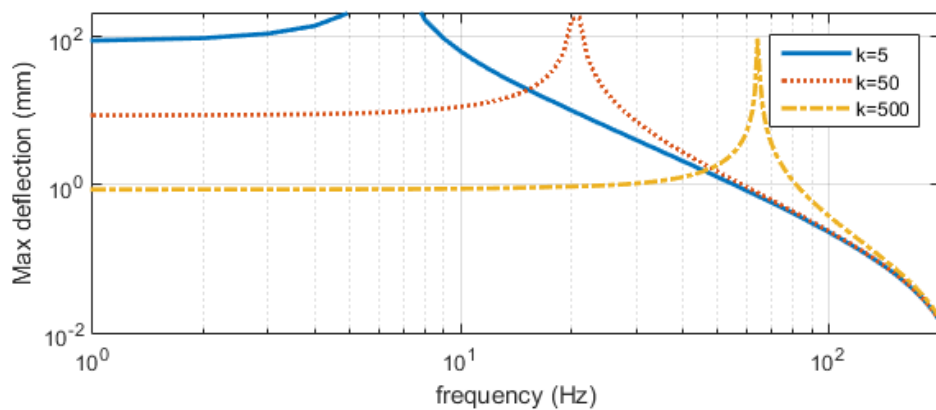


Figure 4.25. Maximum deflection for three stiffness configurations

The force and deflection levels obtained in minimum and maximum frequency in the calculation range is shown in Table 4.2 and Table 4.3.

Table 4.2. *Transmitted force values at frequency limits*

Specimen	Transmitted Force (N)	
	w>0	w=200Hz
k=5 N/mm	440	0.073
k=50 N/mm	431	0.735
k=500 N/mm	430	7.934

Table 4.3. *Maximum deflection values at frequency limits*

Specimen	Max deflection (mm)	
	w>0	w=200Hz
k=5 N/mm	88.1	0.014
k=50 N/mm	8.82	0.015
k=500 N/mm	0.86	0.016

By looking at that results it is concluded that transmitted force and corresponding maximum deflection amplitude drops severely after the specific frequency for each specimen. This frequency corresponds to axial mode of single-DOF-like system consist of transmission rods and specimen. The frequency increases with the stiffness of the specimen while mass of the rods does not change. The range below that frequency may be designated as “effective range” because the maximum achievable deformation drops after that frequency.

In order to estimate the maximum deformation that can be obtained from a specimen with a certain stiffness, the method described in this section can be used. If it is desired to extend the effective range, then efforts can be made to decrease the mass of the transmission elements.

4.3.3. Instrumentation and Measurement

The instrumentation layout of the test system is given in Figure 4.26. For measuring the preloading force a strain-gage based force transducer is utilized, whereas dynamic force is to be measured by PZT force transducers. PZT sensor with IEPE acquired with a high-pass filter then they could not be used below 5Hz. Deflection measurement is derived from acceleration and in order to measure acceleration data PZT accelerometers are utilized.

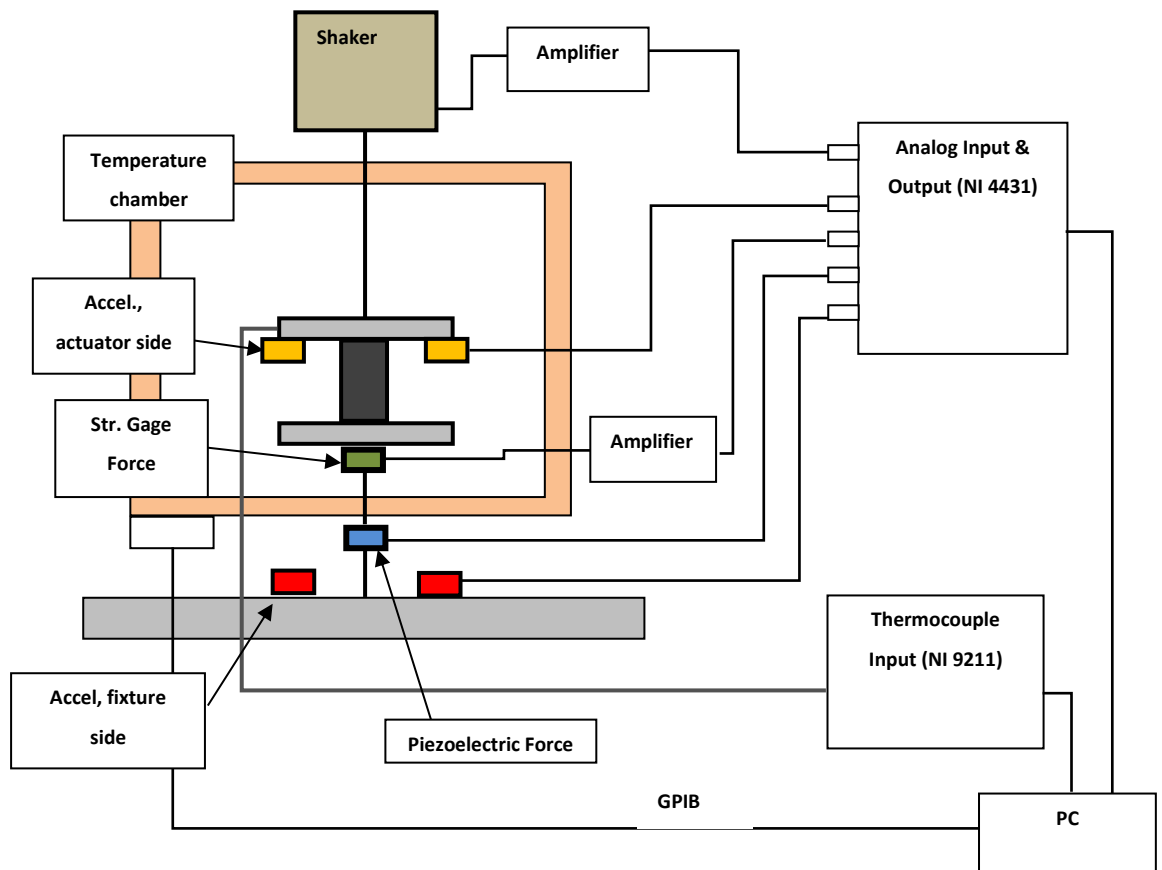


Figure 4.26. Instrumentation layout for test setup

Harmonic force measurement is performed by single IEPE force sensor. The deformation of the specimen is measured by MEMS accelerometers, one is mounted

on actuator side, the other one is mounted on the foundation side. All data is collected by NI-4431 Data Acquisition device with software controlled IEPE excitation. Therefore, data from IEPE and non-IEPE transducers could be collected with same device. Control signal for electrodynamic shaker is generated by NI-4431 and fed to APS 145 amplifier. Software of the test setup is based on the setup discussed in Section 3.4.3. In addition, same control algorithm is used in this setup.

4.4. Design Evaluation

The setup is manufactured and assembled as shown in Figure 4.27. The test fixture, temperature chamber, PC and data acquisition hardware is shown in this figure.

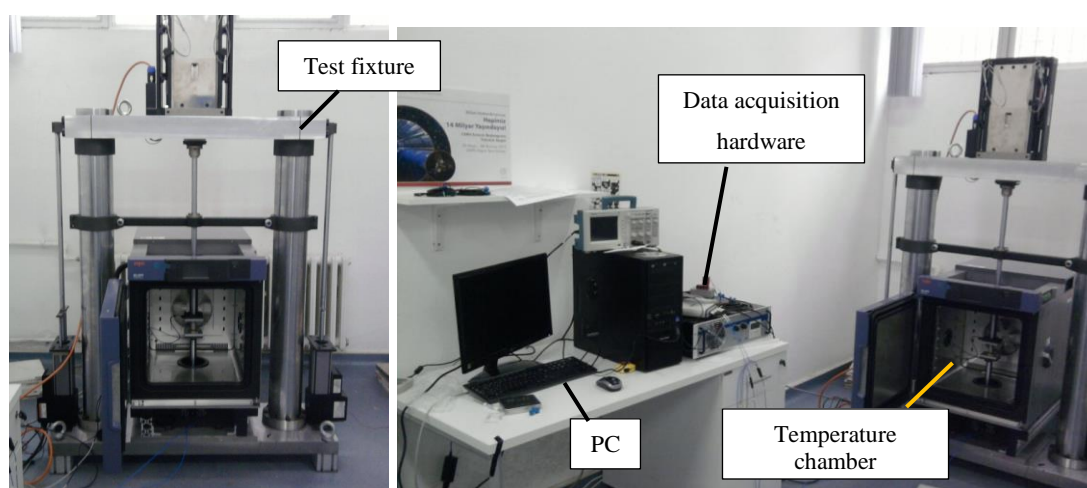


Figure 4.27. Assembled test setup and its components

Trial test are performed on a commercial vibration isolator, LORD AM 009-14 to measure real stiffness and loss factor. Real stiffness and loss factor values will be obtained from the relations in Section 2.3.2.2. The first results obtained with this setup are completely distorted. These results are not represented in the thesis. As a result, coil springs are removed from the setup.

For second trial frequency sweep test are performed. The results are plotted in Figure 4.28 for real stiffness and Figure 4.29 for loss factor. To check the consistency of the measurements, frequency sweep test results measured by MTS 831.50 test setup for the same specimen are used for comparison. The results obtained by MTS setup is at

room temperature and 0.1mm peak-to-peak displacement amplitude, whereas the tests performed with designed setup is not amplitude-controlled. Deformation amplitude is not provided in these tests since measured amplitudes has not been recorded during tests unintentionally.

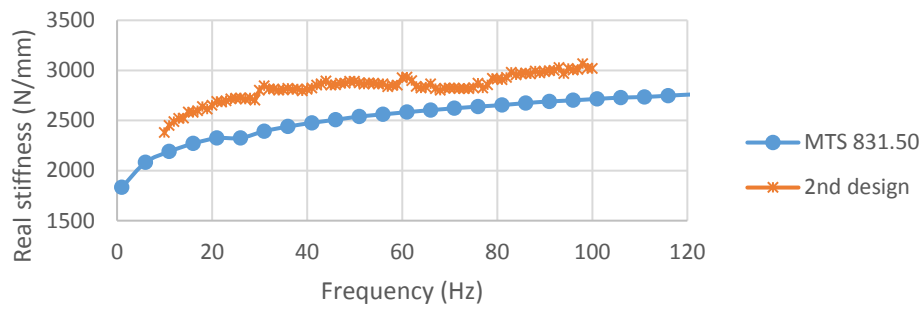


Figure 4.28. Real stiffness measurements for AM 009-14, compared with MTS 831.50

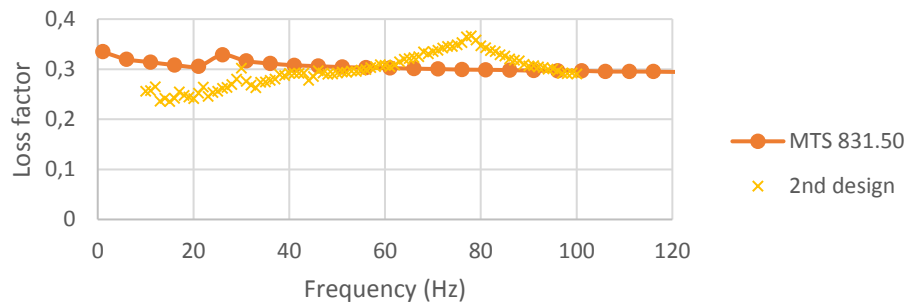


Figure 4.29. Loss factor measurements for AM-009-14, compared with MTS 831.50

In these results, a significant shift in real stiffness measurements is observed. The reason of that shift could be that tests are performed in different displacement amplitudes. In addition, there are some distortions observed at several frequencies. It is thought that the sensor location could affect measurements. In order to check this, the accelerometer at the actuator side is located on three different locations in order to

observe whether the locations of the sensor are effective on measurements or not. These locations are shown in Figure 4.30.

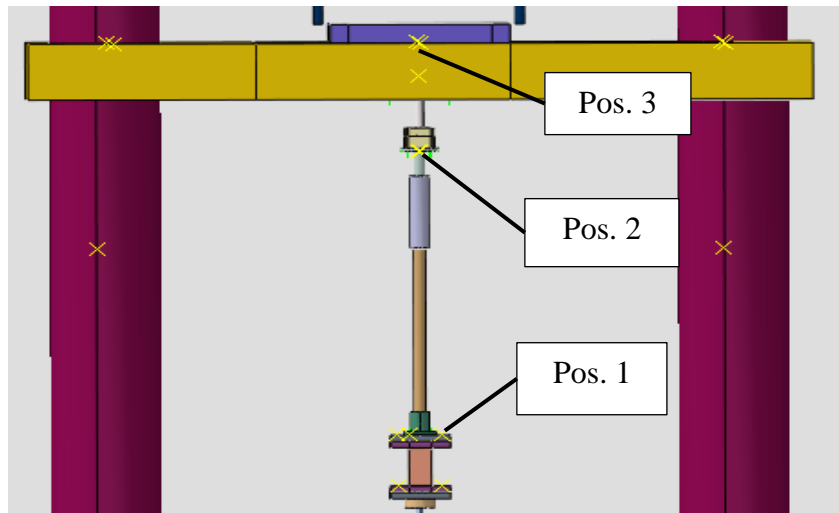


Figure 4.30. Accelerometer locations

For the first one, accelerometer is located close to the specimen, same as the second trial (labeled as Pos. 1), second one is located in the middle of the transmission rod (labeled as Pos. 2) and last one is located close to the actuator (Pos. 3). The measurements are shown in Figure 4.31 for real stiffness and Figure 4.32 for loss factor.

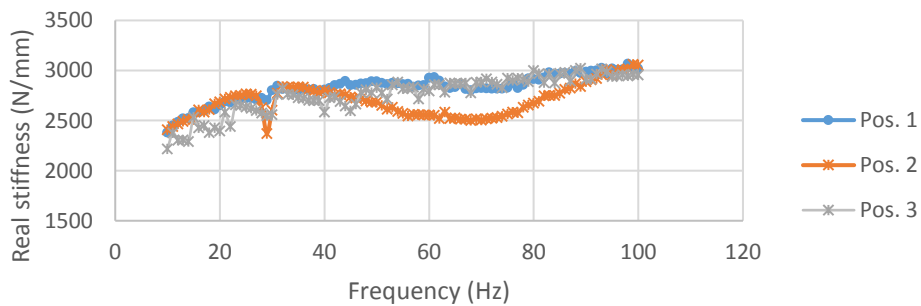


Figure 4.31. Dynamic stiffness measurements for LORD AM-009

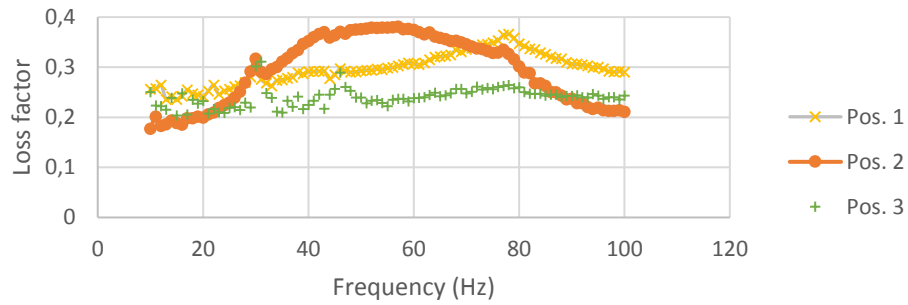


Figure 4.32. Loss factor measurements for LORD AM-009

Distortions in measurements are observed depending on sensor location, which could be sign of some influence of structural characteristics to the measurements. Therefore, an error analysis study is established in order to determine the effects of the structural characteristics of the test system features. The organization and the details are discussed in following sections.

4.5. Determination of the Dynamic Effects of Structural Features on Accuracy of Dynamic Stiffness Measurements

An error analysis study is made in order to answer some questions regarding the dynamic stiffness measurement accuracy of the test setup and its vibratory characteristics as a mechanical structure. There are some questions to be answered, which are stated below:

- 1- Fixture is supported on a flexible surface. Is it required to be fixed?
- 2- Alignment of transmission rods is not perfect. Is it required to be perfect?
- 3- Sensors could not be placed on the center. Does placing with an offset matter?
If occurs, can using multiple sensors solve the problem?
- 4- Correction mass may not be correct. Is the influence of correction mass significant?

These questions are aimed to be answered at the end of this study.

The flow of the error study is given as follows:

- 1- Reduced-order models are built in order to observe effects of some structural features on the accuracy of measurements (Section 4.5.1.).
- 2- Modal test and correlation study are performed in order to validate and update the modal analysis results (Section 4.5.2).
- 3- Linear frequency-domain FE analysis is performed in order to simulate the frequency-sweep tests (Section 4.5.3). It is also expected to validate the observations in reduced-order models (discussed in Section 4.5.1.)
- 4- A metallic calibration spring is designed with a known stiffness for frequency sweep tests in order to validate the analysis models discussed in Section 4.5.3. The reason why a metallic spring is used is that that gives same stiffness within all frequency range with little structural damping.
- 5- Frequency-sweep tests are performed with calibration springs and results are compared with the analysis results. If tests and analysis results are obtained in with correlation, then it means the setup is also validated.

4.5.1. Simulation of Dynamic Stiffness Measurements using Reduced-Order Models Developed to Represent Dynamics of the Test Setup

The conceptual form of the test system consists of a resilient spring with two coaxial degree-of-freedom (DOF). However, due to functional requirements and geometrical constraints the system becomes more complex and undesired effects of this complexity may deteriorate the measurements. Reduced-order models are built to investigate the behavior of features of the test system. General behavior of the structure and coupling effects are expected to be observed. Some decisions regarding constructional details and sensor locations could be made after this analysis.

At each step a new feature is added then the effect of the modification is aimed to be seen. Each model is a test system and a generic resilient element is fictionally mounted on these systems. Then using the formula in Eq (4-6) the stiffness of the resilient element is calculated. It is expected to get the same value as the initialized value if the

system works correctly. If any undesired behavior occurs, it could be related with new feature.

The titles of the models used in the study are listed as below:

- 1- Two Axial DOF Point Mass Model (Section 4.5.1.1)
- 2- Four Axial DOF Point Mass Model (Section 4.5.1.2)
- 3- Model with Two Beam Elements (Section 4.5.1.3)
- 4- Model with Two Beam Elements Supported by Transverse Beam (Section 4.5.1.4)
- 5- Model with Two Beam Elements Supported by Transverse Beam, with Sensor offset (Section 4.5.1.5)
- 6- Model with Two Beam Elements Supported by Transverse Beam, Constrained Actuator (Section 4.5.1.6)
- 7- Model with Two Beam Elements Supported by Transverse Beam, Constrained Actuator and Sensor Offset (Section 4.5.1.7)

The details of each model are explained in advance. However, all models use same procedure and explained as follows:

- 1- Using system parameters mass (M) and stiffness (K) matrices are built to establish equation of motion for undamped forced response. (Eq (4-3))
- 2- By eigenvalue analysis natural frequencies and mode shapes are calculated. (Eq (4-4))
- 3- Damped response is calculated by direct inverse of Equation of Motion obtained in frequency domain (Eq (4-5)).
- 4- Stiffness is calculated according to the Eq (4-6). If displacement is measured from acceleration conversion in Eq.(4-7) must be performed.
- 5- Results are compared with the initialized value.

$$\mathbf{M}\ddot{\mathbf{x}} + \mathbf{K}\mathbf{x} = \mathbf{F} \quad (4-3)$$

$$\omega, \phi = eig(\mathbf{K}, \mathbf{M}) \quad (4-4)$$

$$x_i(\omega) = [-\omega^2 \mathbf{M} + \mathbf{K}^*]^{-1} F \quad (4-5)$$

$$k = \frac{F - m_f a_f}{x_a - x_f} \quad (4-6)$$

$$a_{a,f} = -\omega^2 x_{a,f} \quad (4-7)$$

In the following sections numerical calculations have been performed for each model. Details and differences of the models are discussed in later sections.

A physical system consists of a specimen, a flexible sensor and two transmission elements. Transmission rods are hollow cylinders made of aluminum. Specimen is mounted on mounting blocks with mass, each connected to one side of transmission rods. Sensor is considered as a flexible structural member. System parameters are listed in Table 4.4. These parameters are selected in agreement with the order of magnitude of a real system. In some models there are additional features, details of these have considered in each model. Unit force is applied to one of the transmission elements at all frequencies as actuator force.

Table 4.4. System Parameters

Parameter	Notation	Value	Unit
Specimen stiffness, x,y direction	k^*	2000	N/mm
Torsional stiffness	k_t^*	$2.0 \cdot 10^4$	N.mm
Sensor stiffness	k_s	$1.0 \cdot 10^9$	N/mm
Mass of mounting block at actuator side	m_a	$1.2 \cdot 10^{-3}$	Tonne
Mass of mounting block at fixed side	m_f	$1.2 \cdot 10^{-3}$	Tonne
Outer diameter of transmission rod at actuator side	D_{o1}	16	mm
Inner diameter of transmission rod at fixed side	D_{i1}	8	mm
Length of transmission rod at actuator side	L_1	700	mm
Outer diameter of transmission rod at fixed side	D_{o2}	30	mm
Inner diameter of transmission rod at fixed side	D_{o1}	0	mm
Length of transmission rod at fixed side	L_2	250	mm
Elastic modulus of the rods	E_1, E_2	$7 \cdot 10^4$	MPa
Specific gravity of the rods	ρ_1, ρ_2	2.85	

4.5.1.1. Two-Axial DOF Point Mass Model and Dynamic Stiffness Measurement Simulations

This model is basic form of the Direct Method, explained in Section 2.3.2.2. The model consists of two mass moving in same type of coordinate connected with springs. These masses represent the mounting blocks of the specimen (See Figure 4.33). The spring between two mass represents the specimen, the other one is the sensor. Force measured by the sensor is calculated by the deformation of latter spring (Eq. (4-8)). Resilience of that spring is considerably high compared to specimen.

$$F_s = k_s x_b \quad (4-8)$$

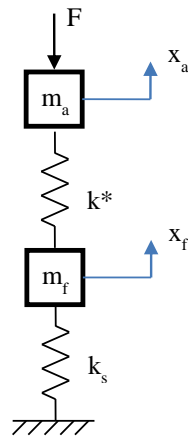


Figure 4.33. Two-Axial DOF Point Mass Model

The list of natural frequencies calculated for this model is given in Table 4.5 and corresponding mode shapes are illustrated in Figure 4.34.

Table 4.5. Calculated natural frequencies for Two-Axial DOF Point Mass Model

Mode #	Frequency (Hz)
1	355.9
2	2.05×10^5

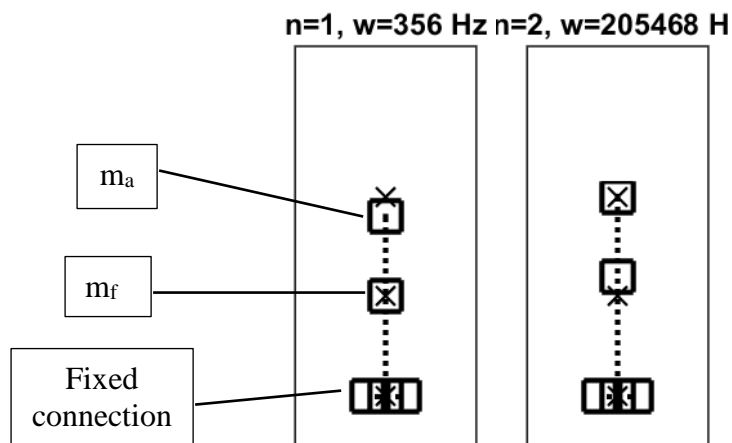


Figure 4.34. Mode shapes for Two-Axial DOF Point Mass Model

Calculated stiffness vs frequency plots are provided in Figure 4.35. In addition, deviation percentage from reference value is given in Figure 4.36, titled as “error %”. In Figure 4.35-Figure 4.36, the natural frequencies listed in Table 4.5 is shown with cross mark symbols (x) and labeled as “modes in the legend of the plots. The frequency range is set as 0-2000Hz.

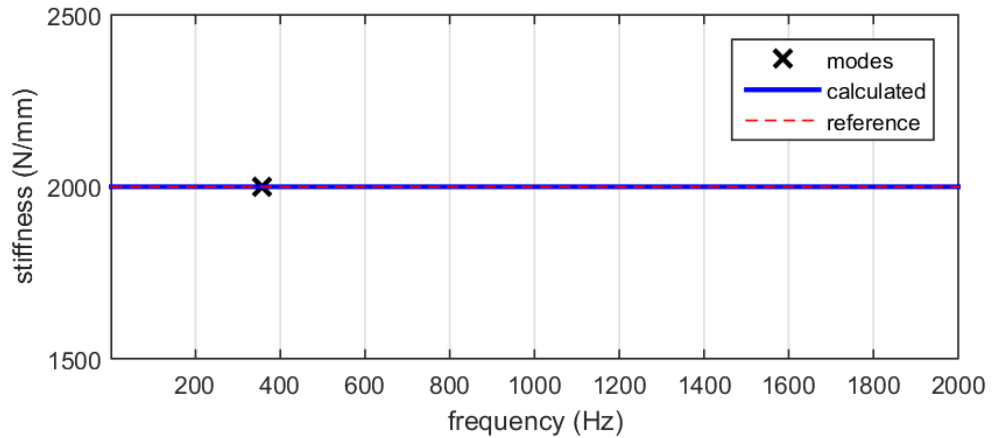


Figure 4.35. Stiffness calculation for Two-Axial DOF Point Mass Model

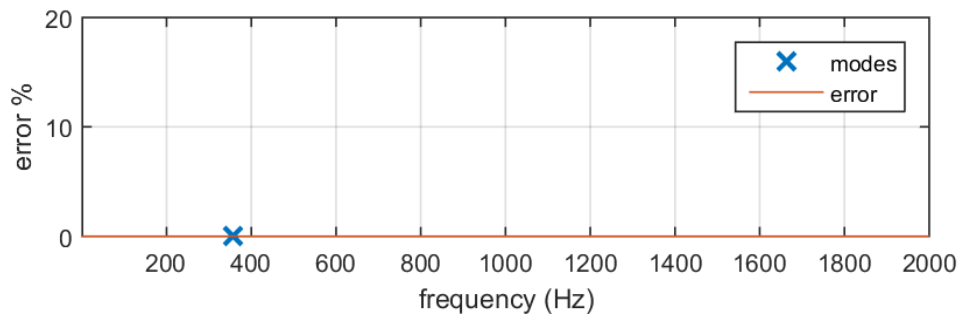


Figure 4.36. Deviation of calculated stiffness from reference for Two-Axial DOF Point Mass Model

Result obtained by this model gives same as the initial value –no divergence or discrepancy is occurred. It is clear that first mode is of mass at the actuator side(m_a) and sensor mode is very high then it falls out of range.

4.5.1.2. Four-Axial DOF Point Mass Model and Dynamic Stiffness Measurement Simulations

The model in 4.5.1.1 is modified by adding longitudinal stiffness of the transmission rods. The connection points of the transmission rods are the DOF's of the model. Force sensor is modelled as a flexible element like previous model located between base and transmission element at the bottom. The force measurement is obtained by deformation of this stiffness element (Eq. (4-8)). The model is represented in Figure 4.37.

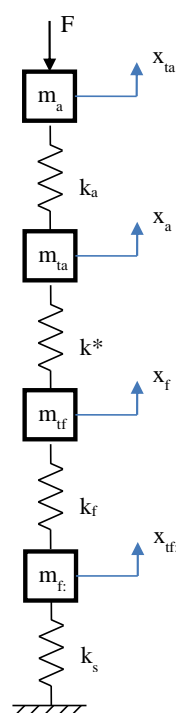


Figure 4.37. Four-Axial DOF Point Mass Model

Equation of motion of this model is given in Eq. (4-9). In Eq (4-9), m_a, m_f are effective mass of the transmission rods at the connection point, m_{ta}, m_{tf} are the mass of the mounting blocks, k_a, k_f are the equivalent axial stiffness of the transmission rods and k_s is the sensor stiffness.

$$\begin{aligned}
& \left(-\omega^2 \begin{bmatrix} m_a & 0 & 0 & 0 \\ & m_a + m_{ta} & 0 & 0 \\ & & m_f + m_{tf} & 0 \\ \text{sym} & & & m_f \end{bmatrix} \right. \\
& \quad \left. + \begin{bmatrix} k_a & -k_a & 0 & 0 \\ & k_a + k^* & -k^* & 0 \\ & & k_f + k^* & -k_f \\ \text{sym} & & & k_f + k_s \end{bmatrix} \right) \begin{Bmatrix} x_a \\ x_{ta} \\ x_{tf} \\ x_f \end{Bmatrix} \\
& = \begin{Bmatrix} F \\ 0 \\ 0 \\ 0 \end{Bmatrix}
\end{aligned} \tag{4-9}$$

The list of natural frequencies calculated for this model are given in Table 4.6 and corresponding mode shapes are illustrated in Figure 4.38

Table 4.6. Calculated natural frequencies for Four-Axial DOF Point Mass Model

Mode #	Frequency (Hz)
1	189.2
2	$1.92 \cdot 10^3$
3	$2.03 \cdot 10^3$
4	$3.88 \cdot 10^5$

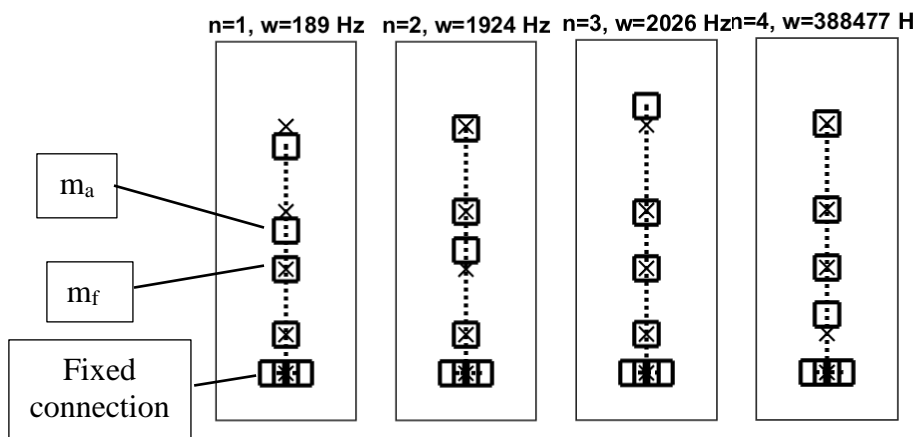


Figure 4.38. Mode shapes for Four-Axial DOF Point Mass Model

Calculated stiffness vs frequency plots are provided in Figure 4.39. In addition, deviation percentage from reference value is given in Figure 4.40, titled as “error %”. In Figure 4.39-Figure 4.40, the natural frequencies listed in Table 4.6 are shown with cross mark symbols (x) and labeled as “modes” in the legend of the plots. The frequency range is set as 0-2000Hz.

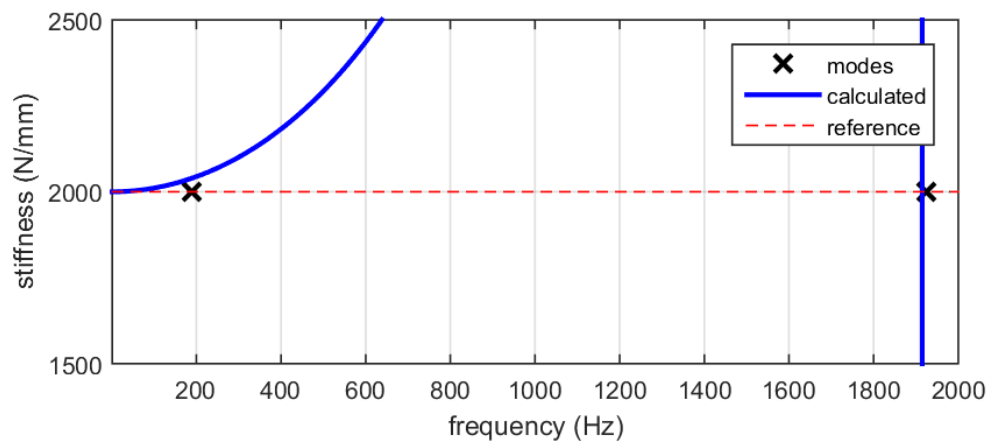


Figure 4.39. Stiffness calculation for Four-Axial DOF Point Mass Model

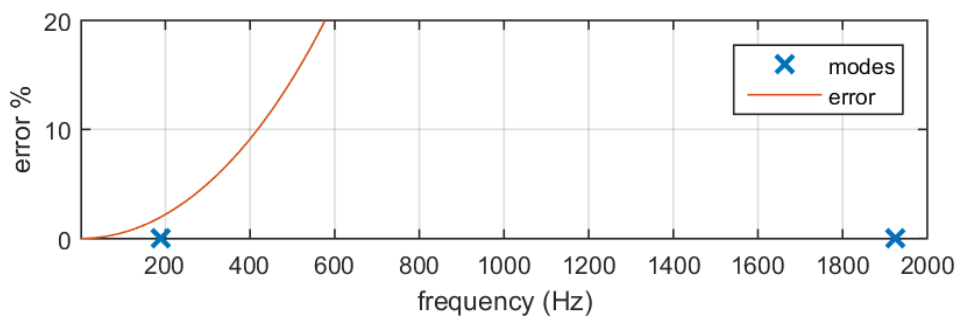


Figure 4.40. Deviation of calculated stiffness from reference for Four-Axial DOF Point Mass Model

The calculated stiffness values are close to the reference value for low frequencies, whereas the frequency corresponds to second mode ($f_2=1924$ Hz) results diverge,

which corresponds to axial compression mode of the transmission rod. This is because deformation amplitude of the transmission rod is very high compared to of specimen then displacement of the specimen becomes insignificant –results in ill-conditioned state. Therefore, if axial compression modes of the transmission rods are avoided the method would give close results to the stiffness of the specimen.

4.5.1.3. Model with Two Beam Elements and Dynamic Stiffness Measurement Simulations

The aim of this model is to observe any coupling effect between transverse deflection of the transmission elements and the results. Therefore, axially-compressible transmission elements are replaced with beam elements with transverse and longitudinal flexibility in this model. Schematic of the model is illustrated in Figure 4.41. In this figure X_i is a vector represents the displacements of i'th DOF, w (Eq.(4-10)): Translation in two axes lying on the page (x,y) and rotation about perpendicular axis to the page (θ). In addition, while not represented on the figure, there are lumped mass at X_2 and X_3 .

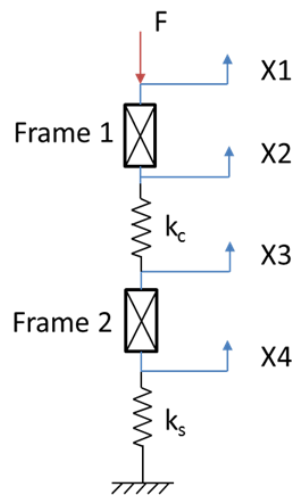


Figure 4.41. Model with Two Beam Elements

$$X_i = \begin{Bmatrix} x \\ y \\ \theta \end{Bmatrix} \quad (4-10)$$

Beam elements used to model transmission rods are called as general beam element (Abaqus 2016 Documentation Guide) or frame element (Liu & Quek, 2003). An element can deform both axial and perpendicular to the axis of the bar.

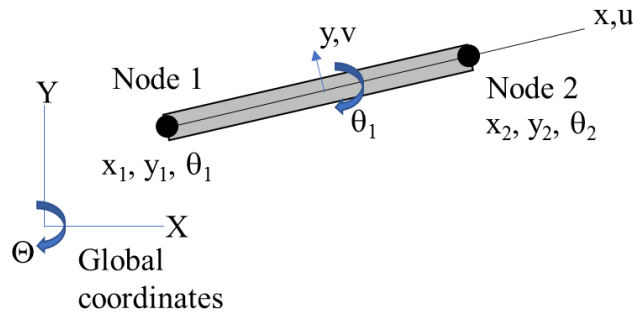


Figure 4.42. Schematic representation of frame element or generalized beam element

For 2-dimensional case space general beam element has two nodes each with 3 DOF, two translation and one rotation (see Figure 4.42). First DOF, labeled as x_i is the axial tension-compression. y_i and θ_i are transverse deflection and rotation. Mass and stiffness matrices are given in Eq (4-11)-(4-15) and Eq (4-16)-(4-20) respectively (Liu & Quek, 2003). a_i values are half-length of the beam, $L_i/2$.

$$K_{beam} = \begin{bmatrix} K_{11} & K_{12} \\ K_{21} & K_{22} \end{bmatrix} \quad (4-11)$$

$$K_{11} = \begin{bmatrix} \frac{A_1 E_1}{2a_1} & 0 & 0 \\ 0 & \frac{3E_1 I_1}{2a_1^3} & \frac{3E_1 I_1}{2a_1^2} \\ sym & \frac{2E_1 I_1}{a_1} & \end{bmatrix} \quad (4-12)$$

$$K_{12} = \begin{bmatrix} -\frac{A_1 E_1}{2a_1} & 0 & 0 \\ 0 & \frac{3E_1 I_1}{2a_1^3} & \frac{3E_1 I_1}{2a_1^2} \\ 0 & -\frac{3E_1 I_1}{2a_1^2} & \frac{E_1 I_1}{a_1} \end{bmatrix} \quad (4-13)$$

$$K_{22} = \begin{bmatrix} \frac{A_1 E_1}{2a_1} & 0 & 0 \\ & \frac{3E_1 I_1}{2a_1^3} & -\frac{3E_1 I_1}{2a_1^2} \\ sym & & \frac{2E_1 I_1}{a_1} \end{bmatrix} \quad (4-14)$$

$$K_{21} = sym(K_{12}) \quad (4-15)$$

$$M_{beam} = \begin{bmatrix} M_{11} & M_{12} \\ M_{21} & M_{22} \end{bmatrix} \quad (4-16)$$

$$M_{11}, M_{22} = \frac{\rho A_1 a_1}{105} \begin{bmatrix} 70 & 0 & 0 \\ & 78 & 22a_1 \\ sym & & 8a_1^2 \end{bmatrix} \quad (4-17)$$

$$M_{12} = \frac{\rho A_1 a_1}{105} \begin{bmatrix} 35 & 0 & 0 \\ 0 & 27 & -13a_1 \\ 0 & 13a_1 & -6a_1^2 \end{bmatrix} \quad (4-18)$$

$$M_{21} = sym(M_{12}) \quad (4-19)$$

System parameters are obtained by using physical properties given in Table 4.4. Equation of motion of the system is given in Eq (4-20). There are two beam elements in this system, which are labeled with superscript “i” as K^i, M^i . System matrices of these elements are built using Equations (4-11)-(4-19). Also, sensor and specimen are treated as 2-D elements with three DOF. Their stiffness matrices are given in Eq (4-21) & (4-22) with parameters given in Table 4.4.

$$\left(-\omega^2 \begin{bmatrix} M_{11}^1 & M_{12}^1 & 0 & 0 \\ & M_{22}^1 & 0 & 0 \\ & & M_{11}^2 & M_{12}^2 \\ & & & M_{22}^2 \end{bmatrix} + \begin{bmatrix} K_{11}^1 & K_{12}^1 & 0 & 0 \\ & K_{22}^1 + K_c & -K_c & 0 \\ & & K_{11}^2 + K_c & K_{12}^2 \\ & & & K_{22}^2 + K_s \end{bmatrix} \right) \begin{Bmatrix} x_1 \\ x_2 \\ x_3 \\ x_4 \end{Bmatrix} = \begin{Bmatrix} F \\ 0 \\ 0 \\ 0 \end{Bmatrix} \quad (4-20)$$

$$K_s = \begin{bmatrix} k_s & 0 & 0 \\ 0 & k_s & 0 \\ 0 & 0 & k_s \end{bmatrix} \quad (4-21)$$

$$K_c = \begin{bmatrix} k_{cx} & 0 & 0 \\ 0 & k_{cy} & 0 \\ 0 & 0 & k_{c\theta} \end{bmatrix} \quad (4-22)$$

The list of natural frequencies calculated for this model are given in Table 4.7 and corresponding mode shapes for first nine modes are illustrated in Figure 4.43.

Table 4.7. *Calculated natural frequencies for Model with Two Beam Elements*

Mode #	Frequency (Hz)
1	3.2
2	68.6
3	128.6
4	182.7
5	291.0
6	508.5
7	1.92*10 ³
8	1.93*10 ³
9	2.12*10 ³
10	1.47*10 ⁴
11	3.95*10 ⁵
12	8.70*10 ⁵

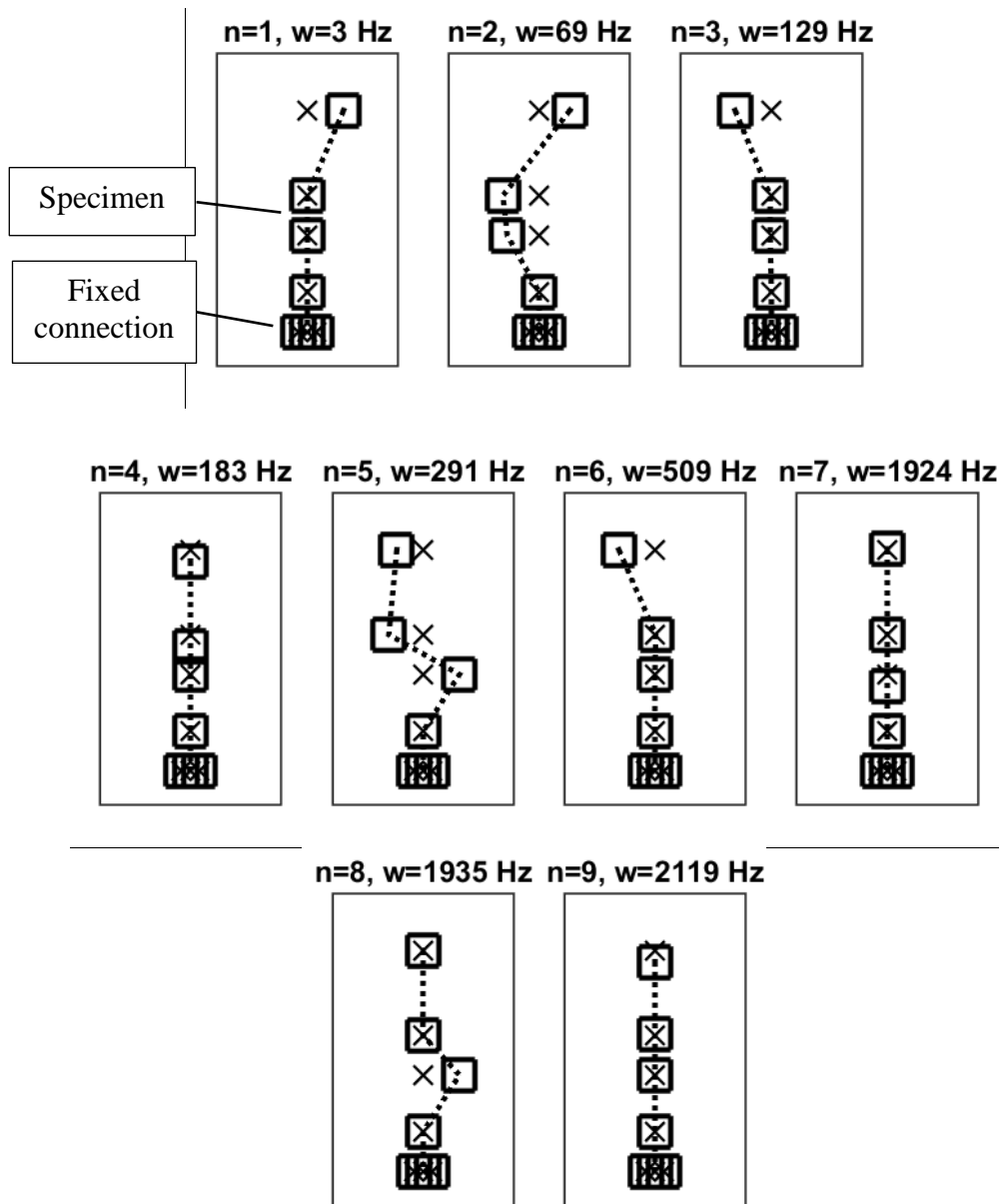


Figure 4.43. First nine modes, 1-4,6-7th modes are bending and 5,8,9th are axial

Calculated stiffness vs frequency plots are provided in Figure 4.44. In addition, deviation percentage form reference value is given in Figure 4.45, titled as “error %”.

In Figure 4.44-Figure 4.45, the natural frequencies listed in Table 4.7Table 4.5 are shown with cross mark symbols (x) and labeled as “modes” in the legend of the plots. The frequency range is set as 0-2000Hz.

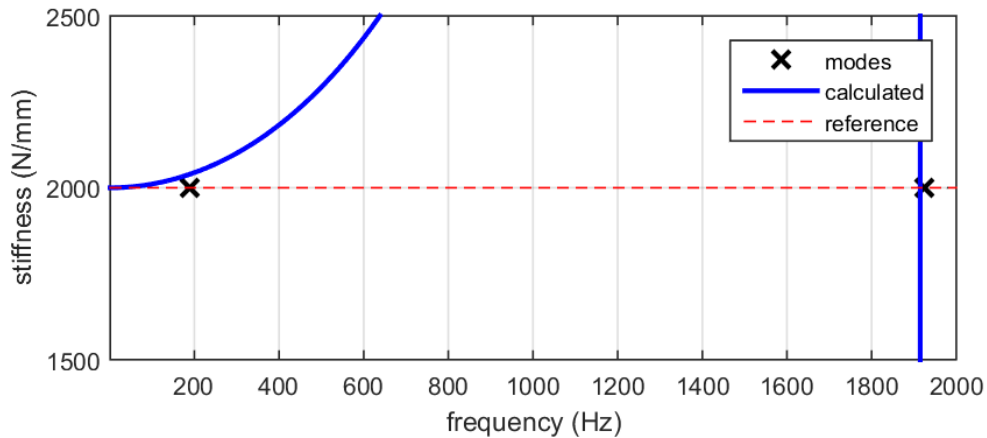


Figure 4.44. Stiffness calculation for Model with Two Beam Elements

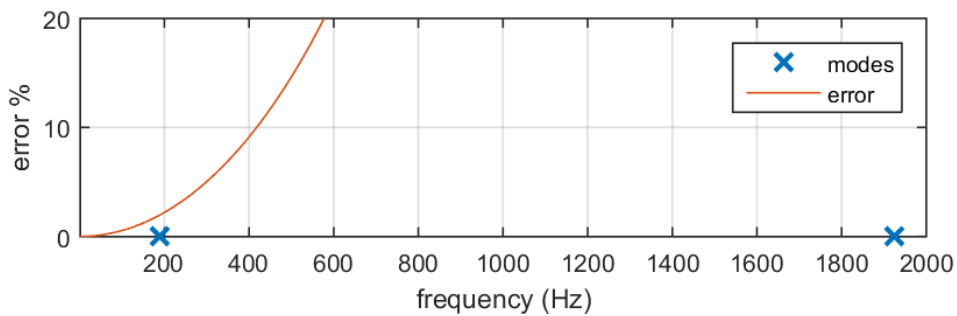


Figure 4.45. Deviation of calculated stiffness from reference for Model with Two Beam Elements

Stiffness calculations and error values have similarities with the previous model – stiffness diverges while going to the frequency for axial flexion mode of upper transmission rod. For this model it can be concluded that here is no coupling effect observed between bending and axial motion. The reason is that, by looking into the system matrices of general beam elements one can see that axial and transverse

deflections are completely decoupled. Therefore, for deflections in this model same results will be eventually obtained as the previous section.

In next model some modifications will be made in order to facilitate coupling between transverse and axial motion.

4.5.1.4. Model with Two Beam Elements Supported by Transverse Beam and Dynamic Stiffness Measurement Simulations

In previous models bending flexibility of fixture has not been concerned. If system is supported by a fixture it may need to be considered. This model is aimed to observe the effects of a flexible fixture on specimen stiffness calculations such as bending or divergence. In this model a flexible fixture is modeled as a general beam element rotated 90° about off-page axis. It is treated as whole system is supported by a cantilever-beam type fixture. This modification will create coupling terms in system matrices thus coupling effect between axial and transverse motion of transmission elements is occurred.

Transverse element is connected to ground. The equation of motion of remaining part is given in Eq (4-23) and (4-24).

$$K_{11}^3 = \begin{bmatrix} \frac{A_3 E_3}{2a_3} & 0 & 0 \\ \frac{3E_3 I_3}{2a_3^3} & \frac{3E_3 I_3}{2a_3^2} & \frac{2E_3 I_3}{a_3} \\ sym & & \end{bmatrix} \quad (4-23)$$

$$M_{11}^3 = \frac{\rho A_3 a_3}{105} \begin{bmatrix} 70 & 0 & 0 \\ 78 & 22a_3 & \\ sym & & 8a_3^2 \end{bmatrix} \quad (4-24)$$

Rotation is performed by transforming the system matrices by direction cosines matrix. For 90° rotation matrix is given in Eq (4-26).

$$K'_{11}{}^3 = \Phi^T K_{11}{}^3 \Phi \quad (4-25)$$

$$M'_{11}{}^3 = \Phi^T M_{11}{}^3 \Phi$$

$$\Phi = \begin{bmatrix} 0 & -1 & 0 \\ 1 & 0 & 0 \\ 0 & 0 & 1 \end{bmatrix} \quad (4-26)$$

Equation of motion of the system in frequency domain is given in Eq (4-27). Unit force is applied on all directions on DOF X_1 .

$$\left(-\omega^2 \begin{bmatrix} M_{11}^1 & M_{12}^1 & 0 & 0 & 0 \\ & M_{22}^1 & 0 & 0 & 0 \\ & & M_{11}^2 & M_{12}^2 & 0 \\ & & & M_{22}^2 & 0 \\ \text{sym} & & & & M_{11}^3 \end{bmatrix} + \begin{bmatrix} K_{11}^1 & K_{12}^1 & 0 & 0 & 0 \\ & K_{22}^1 + k & -k & 0 & 0 \\ & & K_{11}^2 + k_c & K_{12}^2 & 0 \\ & & & K_{22}^2 + k_s & -k_s \\ \text{sym} & & & & K_{11}^3 \end{bmatrix} \right) = \begin{Bmatrix} F \\ 0 \\ 0 \\ 0 \\ 0 \end{Bmatrix} \quad (4-27)$$

The list of natural frequencies calculated for this model is given in Table 4.7 and corresponding mode shapes are illustrated in Figure 4.45.

Table 4.8. *Calculated natural frequencies for Model with Two Beam Elements Supported by Transverse Beam*

Mode #	Frequency (Hz)	Mode #	Frequency (Hz)
1	3.2	9	1.83*10 ³
2	51.5	10	1.94*10 ³
3	68.7	11	1.97*10 ³
4	128.6	12	2.12*10 ³
5	183.7	13	1.47*10 ⁴
6	290.9	14	3.95*10 ⁵
7	508.5	15	8.70*10 ⁵
8	511.5		

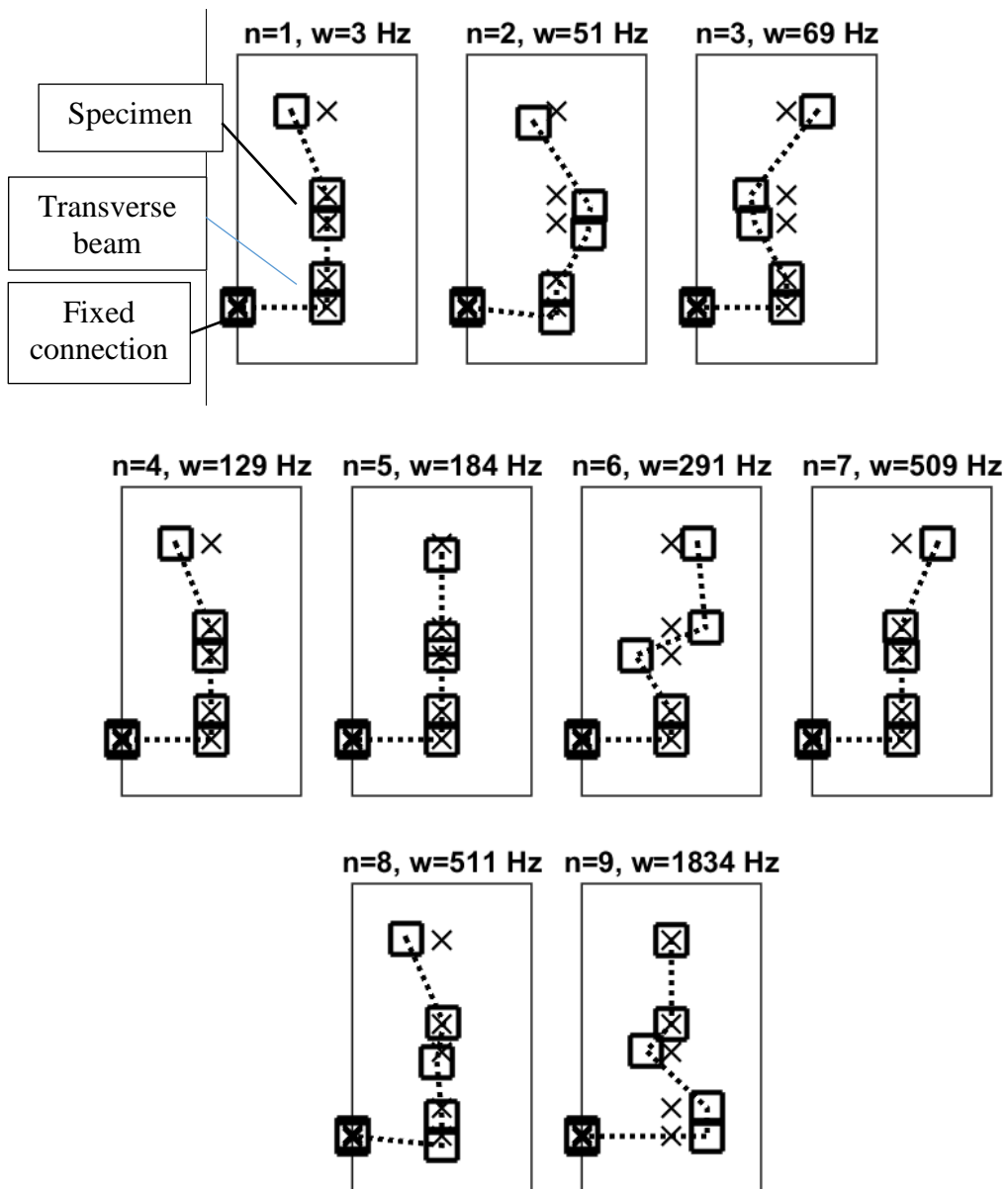


Figure 4.46. First nine modes for Model with Two Beam Elements

Calculated stiffness vs frequency plots are provided in Figure 4.47 for frequency range 0-2000Hz. Stiffness vs frequency plots for 0-400Hz is given in Figure 4.48. In addition, deviation percentage form reference value is given in Figure 4.49, titled as “error %”.

In all figures, the natural frequencies listed in Table 4.7 are shown with cross mark symbols (x) and labeled as “modes” in the legend of the plots.

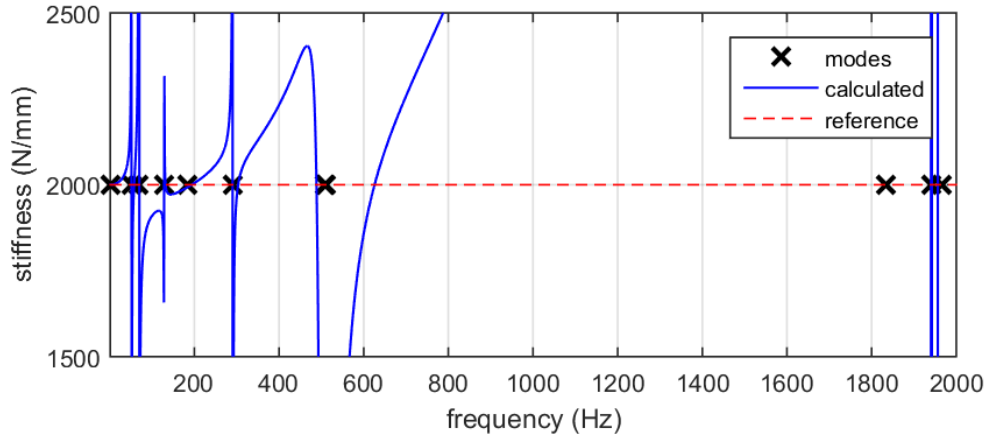


Figure 4.47. Stiffness calculation for Model with Two Beam Elements Supported by Transverse Beam, 0-2000 Hz

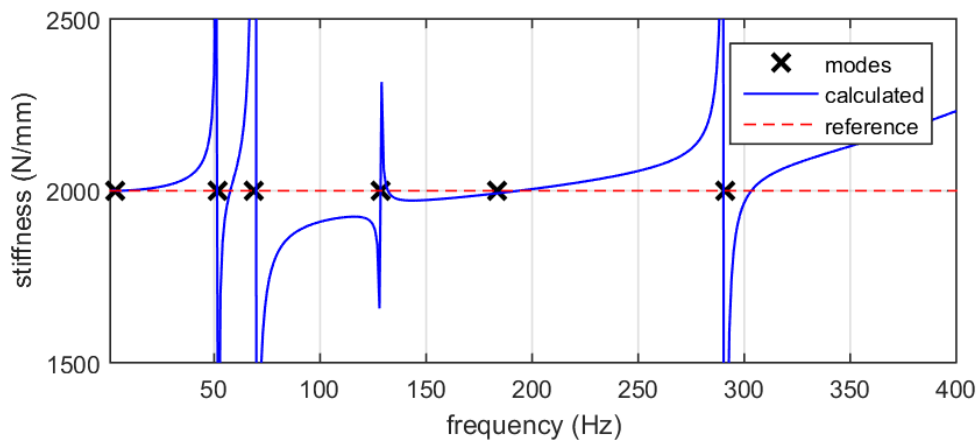


Figure 4.48. Stiffness calculation for Model with Two Beam Elements Supported by Transverse Beam, 0-400 Hz

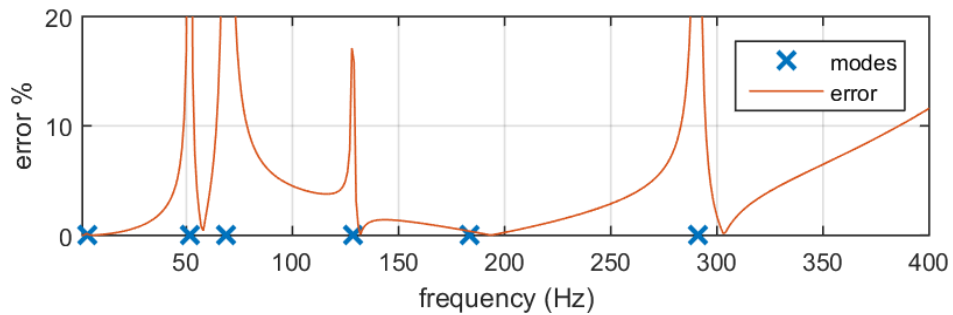


Figure 4.49. Deviation of calculated stiffness from reference between 0-400 Hz for Model with Two Beam Elements Supported by Transverse Beam

Figure 4.47- Figure 4.48 shows that stiffness calculations diverge when bending modes are present. Compared to the model in Section 4.5.1.3 coupling effect is created between bending and axial motion by introducing a transverse beam. Therefore, it could be stated that if the supporting fixture is flexible along the axis other than the axis along the deformation of the specimen, the bending characteristics of the transmission rods should be taken into account.

4.5.1.5. Model with Two Beam Elements Supported by Transverse Beam, with Sensor Offset and Dynamic Stiffness Measurement Simulations

Sensor axes may not be aligned with the specimen line of action. If it occurs results may deviate because offset may exaggerate the contribution of bending modes. In this model the effect of offset from line of action is demonstrated. The model in Section 4.5.1.5 is used without modification except so-called measurements.

Recall that line of action is along x-axis, y is transverse direction and θ is the rotation along axis at perpendicular to page. Consider a location rigidly coupled to the default sensor location. By small angle assumption displacements measured at a location are modified by relations in Eq (4-23) and Eq (4-24).

$$y_{offset} = y_{ideal} \quad (4-28)$$

$$x_{offset} = x_{ideal} + \theta d \quad (4-29)$$

Calculated stiffness vs frequency plots are provided in Figure 4.50. Calculations are performed for ideal case and two different offset values, 0.1 and 0.5 mm. In addition, deviation percentage from reference value is given in Figure 4.51, titled as “error %”. In these figures the natural frequencies listed in Table 4.8, same as in Section 4.5.1.4, Table 4.5 are shown with cross mark symbols (x) and labeled as “modes” in the legend of the plots. The frequency range is set as 0-400Hz.

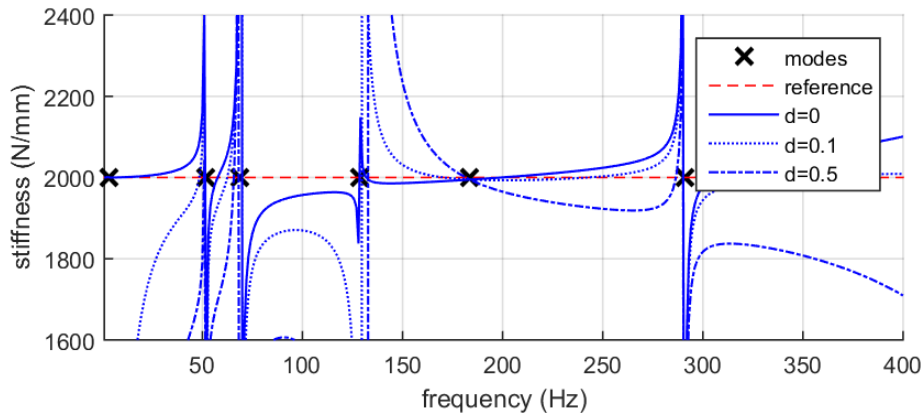


Figure 4.50. Stiffness calculation for Model with Two Beam Elements Supported by Transverse Beam, with Sensor offset

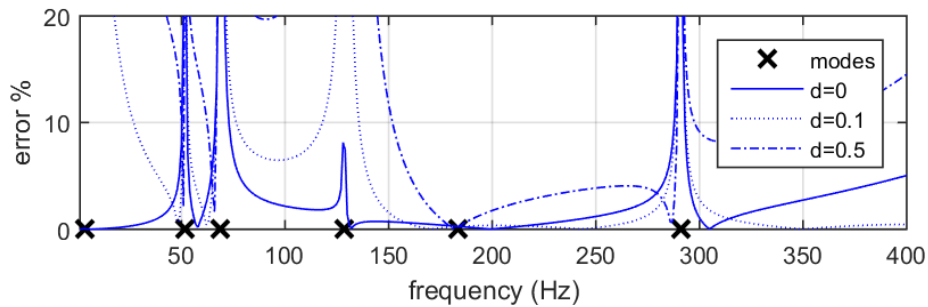


Figure 4.51. Deviation of calculated stiffness from reference for Model with Two Beam Elements Supported by Transverse Beam, with Sensor offset

It is clear that for even small offset values results corrupt significantly. Therefore, sensor offset is an important issue if the bending and axial motion is coupled and actuator is not constrained.

4.5.1.6. Model with Two Beam Elements Supported by Transverse Beam, Constrained Actuator and Dynamic Stiffness Measurement Simulations

In previous models it is shown that bending motion interferes the results of stiffness calculations. It is evaluated that since transverse motion is not constrained on vibrating side (transmission rod between actuator and specimen) transverse motion becomes comparable to axial motion. As seen in Sections 4.5.1.4 and 4.5.1.5, measurements are strongly affected from that motion, especially if there is offset at sensing location. Therefore it is decided to modify the model in Section 4.5.1.4 by constraining transverse motion (at y and θ -direction) but remaining free at axial direction – a cylindrical connection between ground and actuator. Equation of motion is same as Eq (4-27) with modified system matrices as given in Equations (4-30)-(4-39).

$$K^1 = \begin{bmatrix} K_{11} & K_{12} \\ K_{21} & K_{22} \end{bmatrix} \quad (4-30)$$

$$K_{11} = \begin{bmatrix} \frac{A_1 E_1}{2a_1} \end{bmatrix} \quad (4-31)$$

$$K_{12} = \begin{bmatrix} -\frac{A_1 E_1}{2a_1} & 0 & 0 \end{bmatrix} \quad (4-32)$$

$$K_{22} = \begin{bmatrix} \frac{A_1 E_1}{2a_1} & 0 & 0 \\ & \frac{3E_1 I_1}{2a_1^3} & -\frac{3E_1 I_1}{2a_1^2} \\ sym & & \frac{2E_1 I_1}{a_1} \end{bmatrix} \quad (4-33)$$

$$K_{21} = K_{12}^T \quad (4-34)$$

$$M^1 = \begin{bmatrix} M_{11} & M_{12} \\ M_{21} & M_{22} \end{bmatrix} \quad (4-35)$$

$$M_{11} = \frac{70\rho A_1 a_1}{105} \quad (4-36)$$

$$M_{22} = \frac{\rho A_1 a_1}{105} \begin{bmatrix} 70 & 0 & 0 \\ \text{sym} & 78 & 22a_1 \\ & & 8a_1^2 \end{bmatrix} \quad (4-37)$$

$$M_{12} = \frac{\rho A_1 a_1}{105} [35 \quad 0 \quad 0] \quad (4-38)$$

$$M_{21} = M_{12}^T \quad (4-39)$$

The list of natural frequencies calculated for this model is given in Table 4.9 and corresponding mode shapes are illustrated in Figure 4.52.

Table 4.9. *Calculated natural frequencies for Model with Two Beam Elements Supported by Transverse Beam, Constrained Actuator*

Mode #	Frequency (Hz)	Mode #	Frequency (Hz)
1	51.5	8	1.94*10 ³
2	69.0	9	1.97*10 ³
3	150.3	10	2.12*10 ³
4	183.7	11	1.47*10 ⁴
5	291.9	12	3.95*10 ⁵
6	511.5	13	8.70*10 ⁵
7	1.83*10 ³		

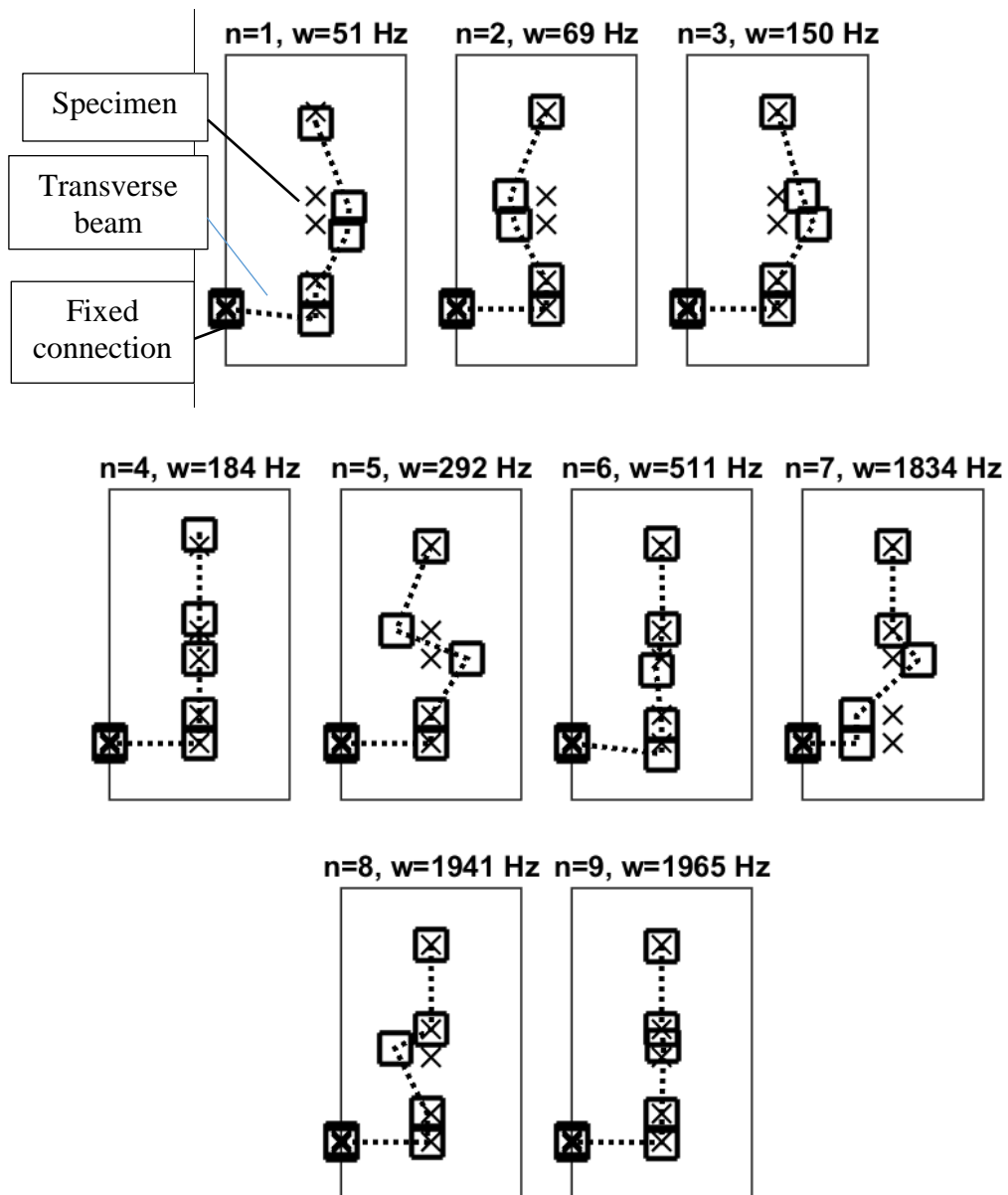


Figure 4.52. First nine modes for Model with Two Beam Elements Supported by Transverse Beam, Constrained Actuator

Calculated stiffness vs frequency plots are provided in Figure 4.53 for frequency range 0-400Hz. In addition, deviation percentage from reference value is given in Figure 4.54, titled as “error %”. In all figures, the natural frequencies listed in Table 4.9 are shown with cross mark symbols (x) and labeled as “modes” in the legend of the plots.

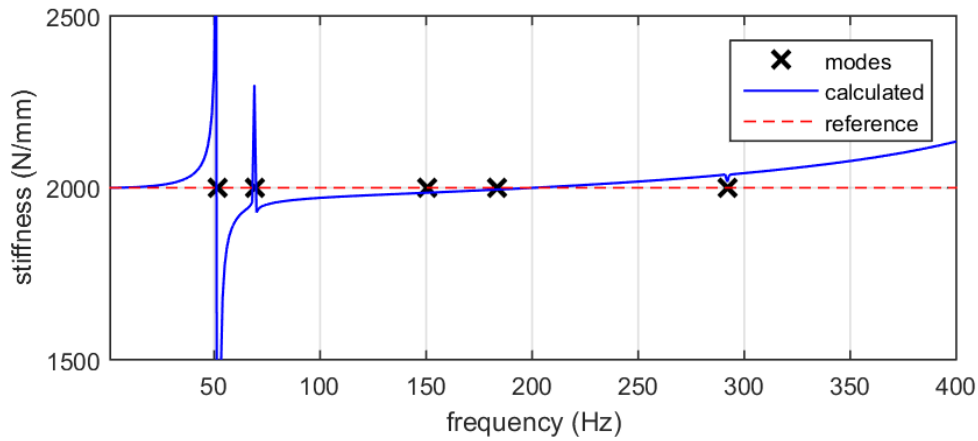


Figure 4.53. Stiffness calculation for Model with Two Beam Elements Supported by Transverse Beam, Constrained Actuator

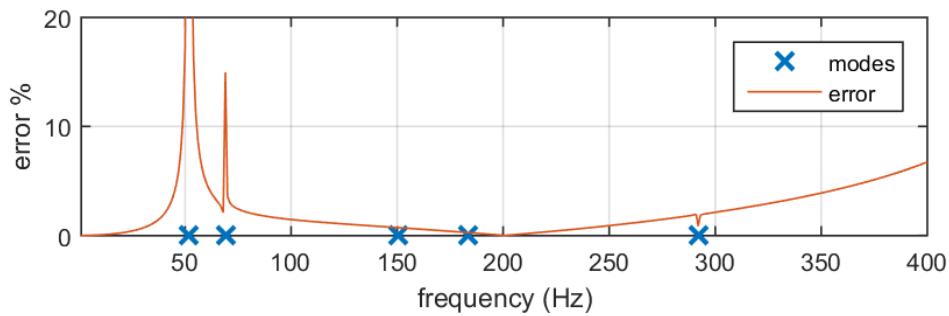


Figure 4.54. Deviation of calculated stiffness from reference for Model with Two Beam Elements Supported by Transverse Beam, Constrained Actuator

Results for new system are provided in Figure 4.53. Coupling with bending motion is still present but not as violent as previous model. Calculated stiffness diverges at the frequency in which rotated beam bends, but other members move like rigid body (Mode #1) - this mode is same as the mode calculated in the model in Section 4.5.1.4, Mode #2. Therefore, bending motion of the fixture is only important factor if actuator is fully constrained and no sensor offset is present.

4.5.1.7. Model with Two Beam Elements and Rotated Beam, Constrained Transverse Motion for Vibrating Side with Sensor Offset and Dynamic Stiffness Measurement Simulations

In this model the effect of sensor offset is investigated when transverse motion is constrained. Model in previous section is evaluated with the method given in Section 4.5.1.5. Calculated stiffness vs frequency plots are provided in Figure 4.55 for sensor offset values 5 and 10mm between frequency range 0-400Hz. In addition, deviation percentage from reference value is given in Figure 4.56, titled as “error %”. In all figures, the natural frequencies listed in Table 4.9 are shown with cross mark symbols (x) and labeled as “modes” in the legend of the plots. Results deviate at bending modes, however not significantly as unconstrained case (Section 4.5.1.4.).

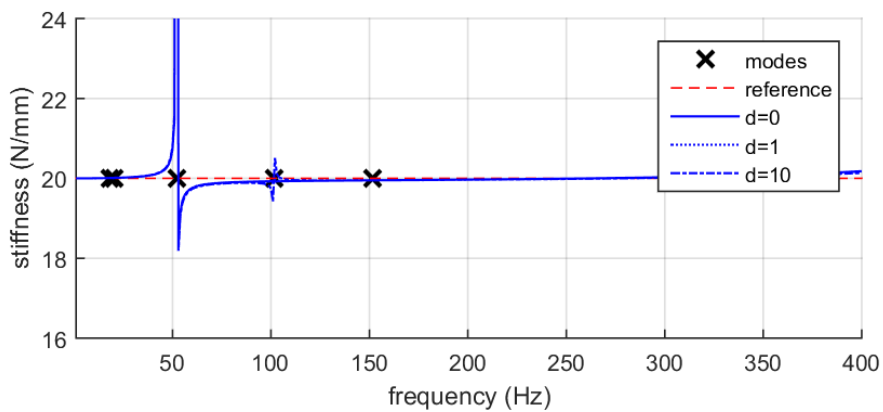


Figure 4.55. Stiffness calculation for Model with Two Beam Elements Supported by Transverse Beam, Constrained Actuator, Sensor Offset

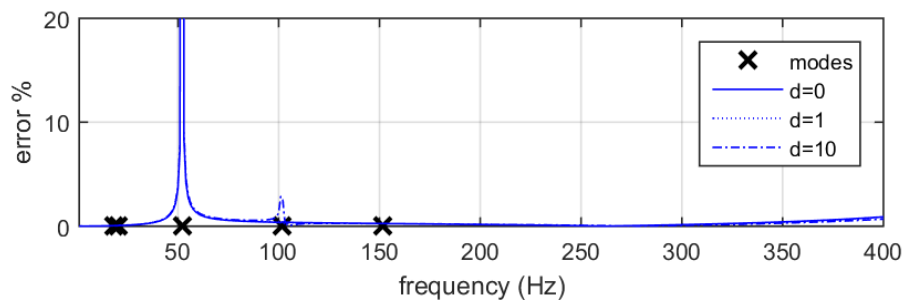


Figure 4.56. Deviation of calculated stiffness from reference for Model with Two Beam Elements Supported by Transverse Beam, Constrained Actuator, Sensor Offset

4.5.1.8. Conclusions

At the end of this section it can be concluded that:

- Method is applicable up to axial compression frequency of transmission elements.
- Axial and bending motion is completely decoupled for small displacements when fixture behaves as rigid.
- Bending motion of transmission elements is coupled with axial compression if fixture is resilient in transverse direction.
- Coupling effects are more significant if transverse motion is less constrained.
- If there is coupling between bending and axial motion sensor location should be placed as close to line of action as possible.
- Ideal test system has shortest transmission rods, is rigidly mounted to ground and the actuator is fully constrained.

4.5.2. Modal Characterization

In order to predict the modal characteristics of the test system modal analysis is performed. The results will be validated with modal test after manufacturing and assembling the test system. If analysis model is validated harmonic analysis will be performed further to simulate the tests performed by the test systems, i.e. place a specimen with known dynamic stiffness properties and simulate the dynamic stiffness test on the FE model of the test system using harmonic response analysis. The dynamic stiffness values of the specimen are extracted using the procedure defined for the test method used in the setup. Finally the simulated measurements of dynamic stiffness are compared with exact values (originally entered into the FE model).

4.5.2.1. Modal Test

Modal test is performed in order to validate the analysis results. It could also be used directly for validating the results obtained in section 4.5.1.

Structure is equipped with accelerometers with locations given in Figure 4.58. B&K modal hammer is used for excitation and PCB 3-axis piezoelectric accelerometers are used to measure response of the structure. Excitation force is applied to the point with label “26”. Data is recorded with LMS-SCADAS Data Acquisition System with 1024 Hz sampling rate. Test results are given in Figure 4.59-Figure 4.74 and listed in Table 4.10.



Figure 4.57. Overview of the test system

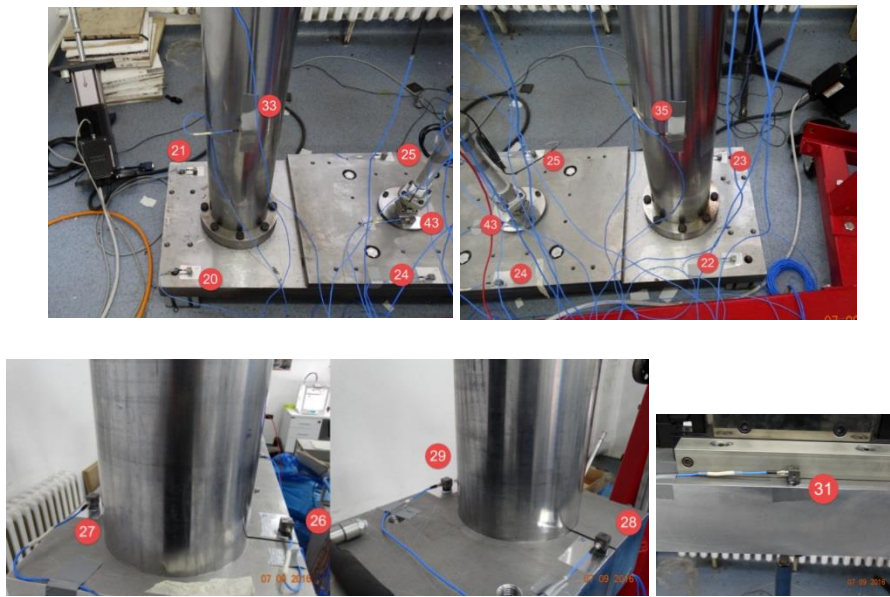


Figure 4.58. Locations of accelerometers to be used in modal tests

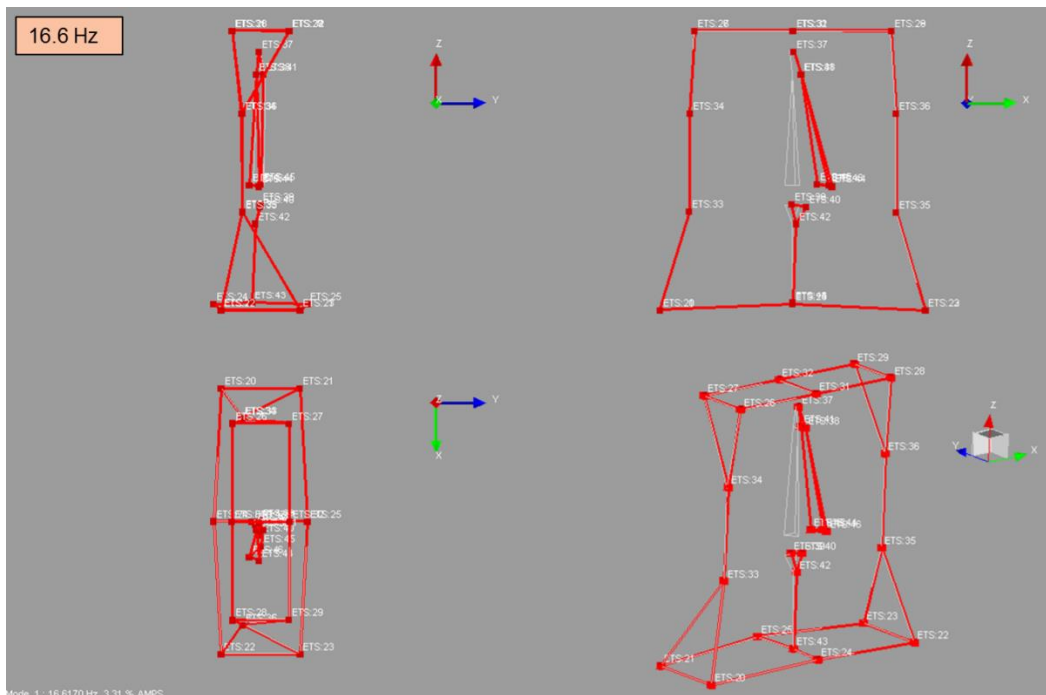


Figure 4.59. Test results, 1st mode shape, 16.6 Hz

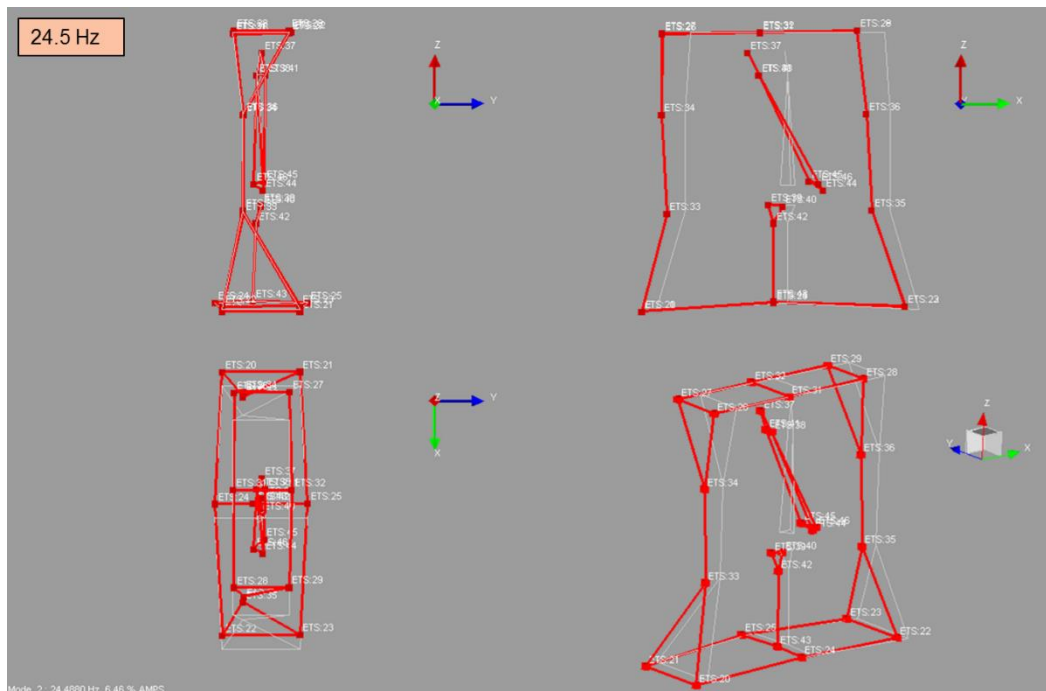


Figure 4.60. Test results, 2nd mode shape, 24.5 Hz

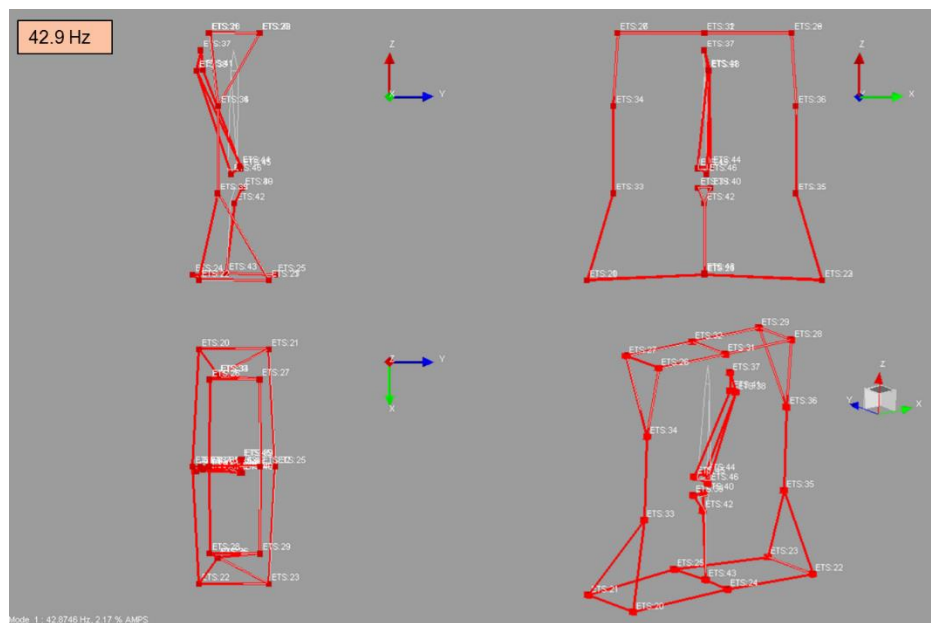


Figure 4.61. Test results, 3rd mode shape, 42.9 Hz

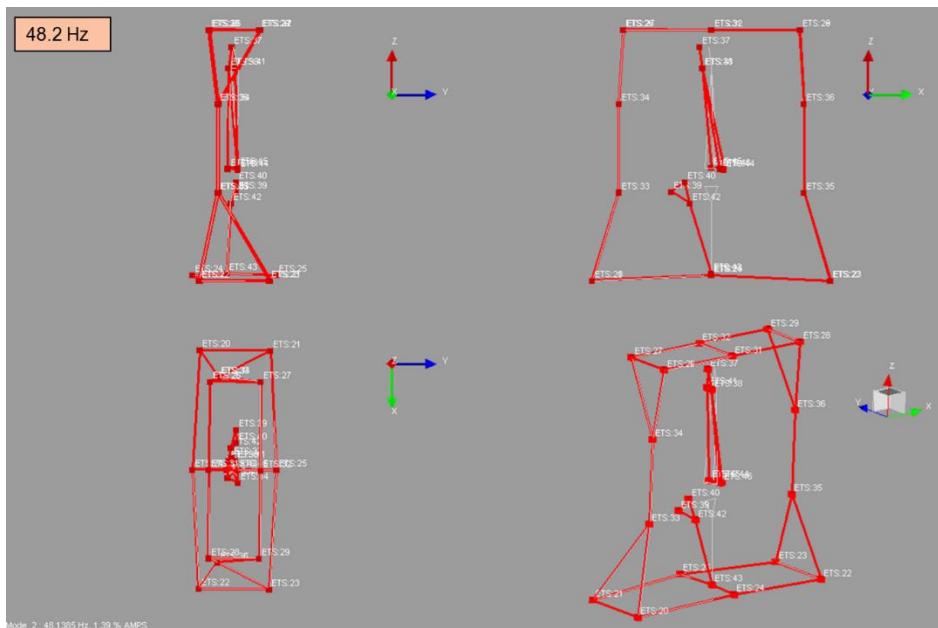


Figure 4.62. Test results, 4th mode shape, 48.2 Hz

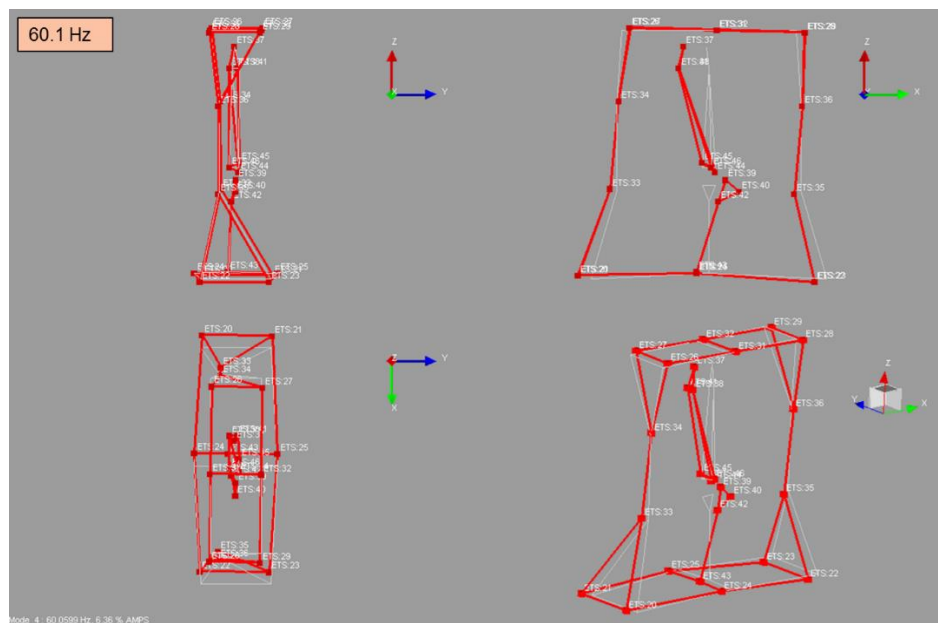


Figure 4.63. Test results, 5th mode shape, 60.1 Hz

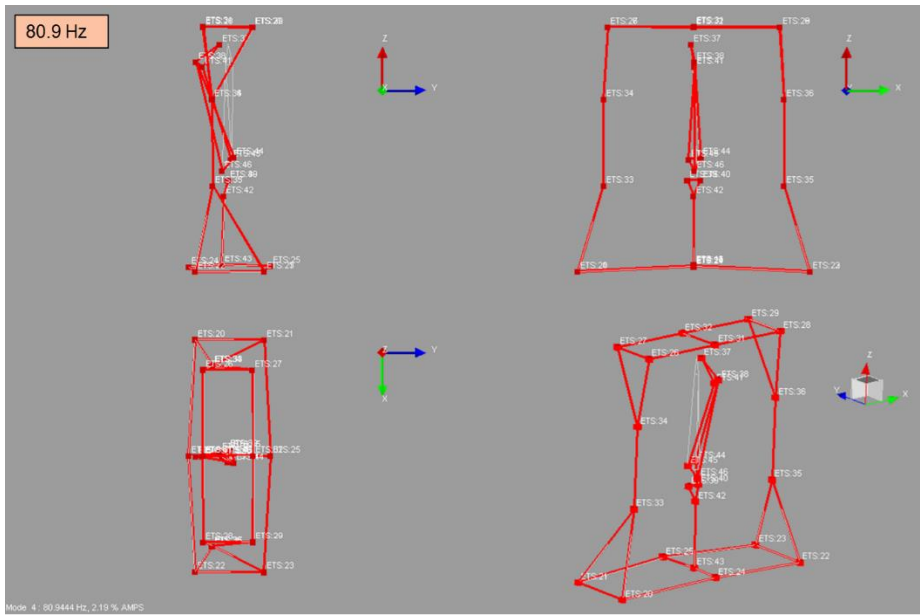


Figure 4.64. Test results, 6th mode shape, 80.9 Hz

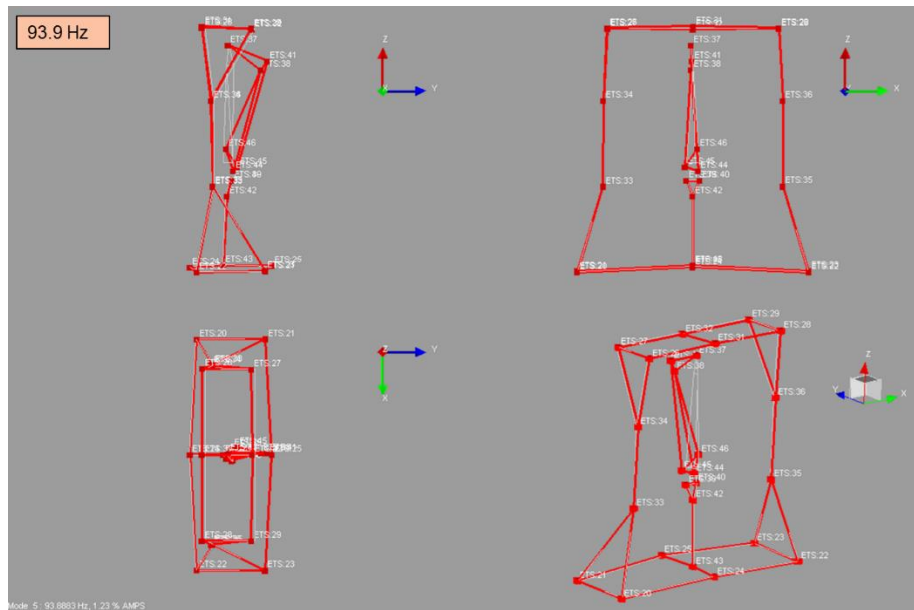


Figure 4.65. Test results, 7th mode shape, 93.9 Hz

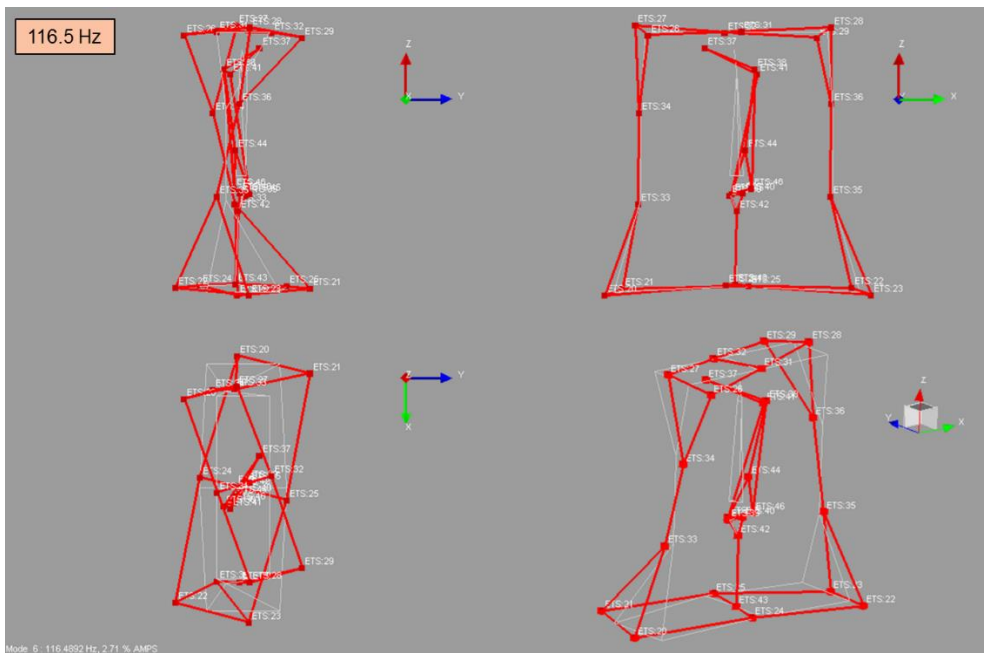


Figure 4.66. Test results, 8th mode shape, 116.5 Hz

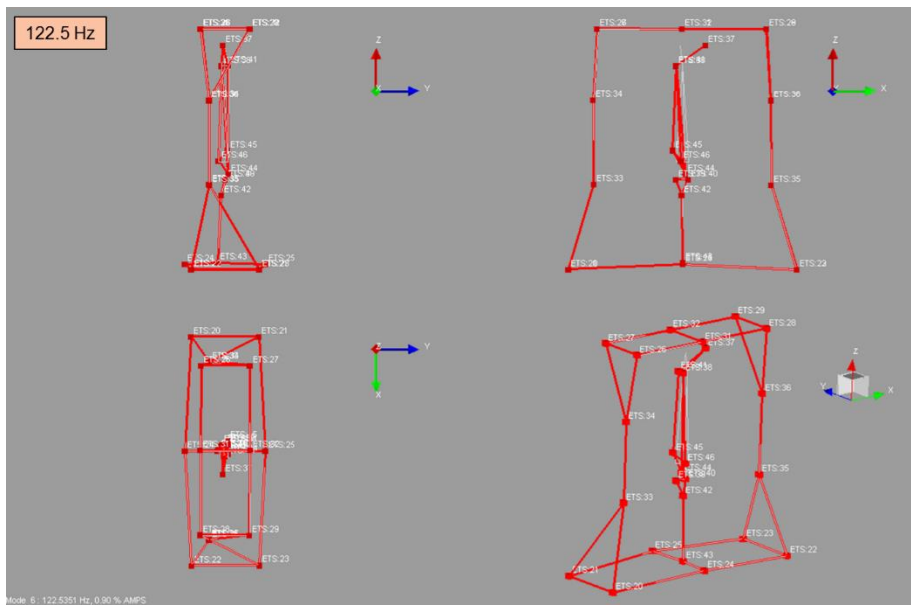


Figure 4.67. – Test results, 9th mode shape, 122.5 Hz

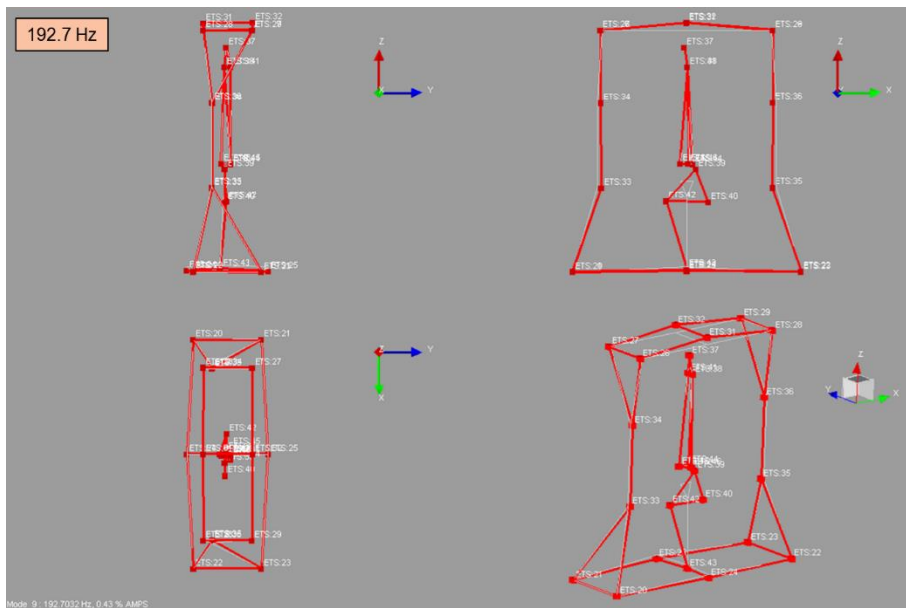


Figure 4.68. Test results, 10th mode shape, 192.7 Hz

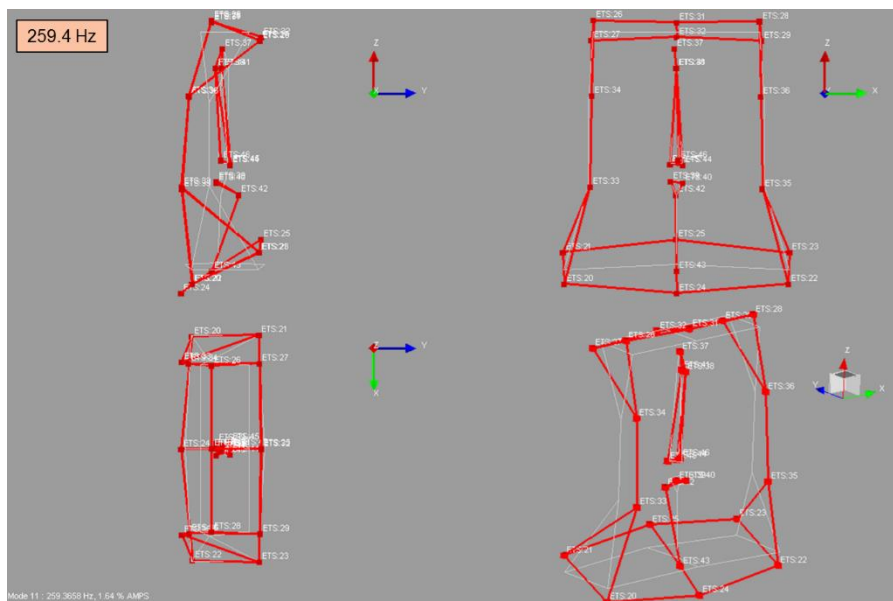


Figure 4.69. Test results, 11th mode shape, 259.4 Hz

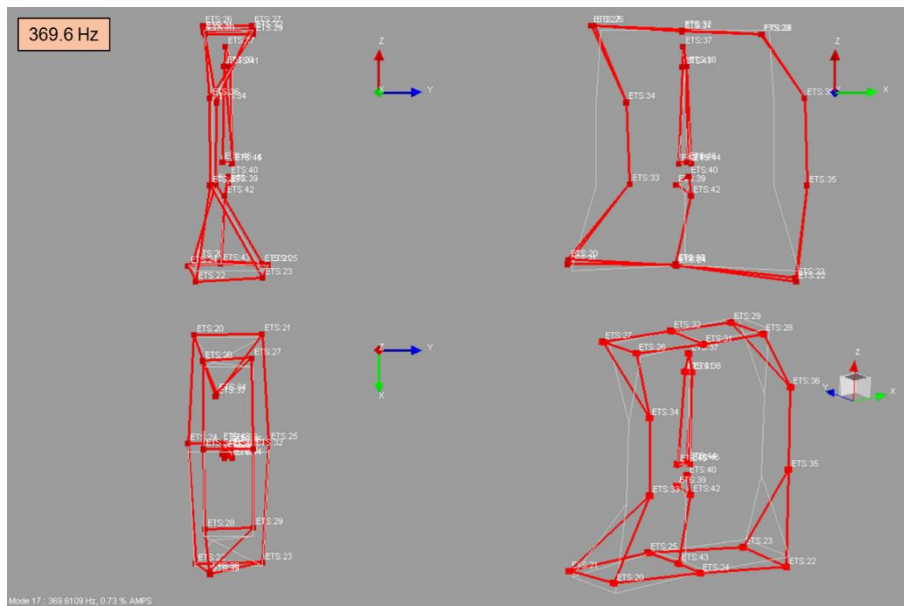


Figure 4.72. Test results, 14th mode shape, 369.6 Hz

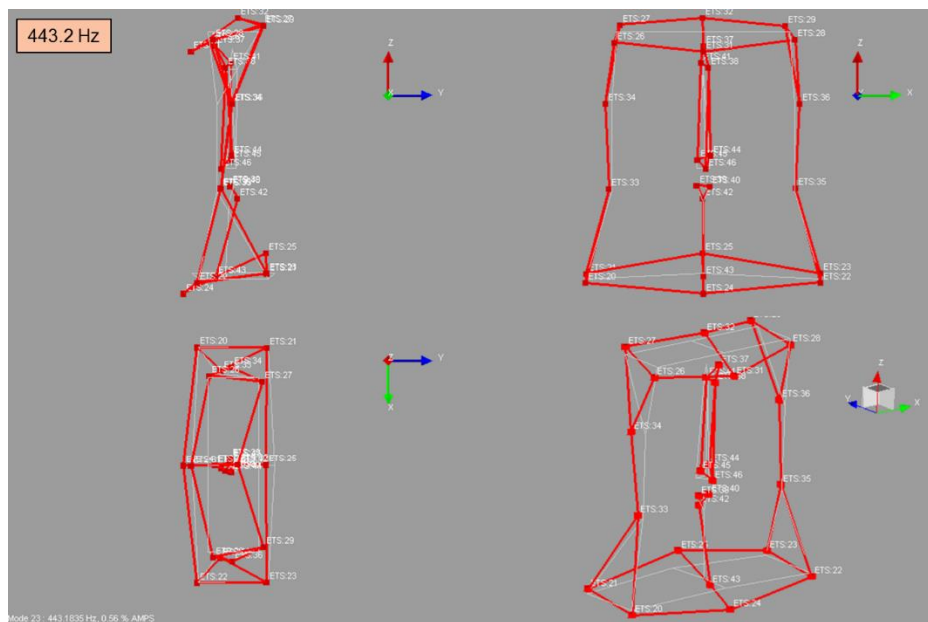


Figure 4.73. Test results, 15th mode shape, 443.2 Hz

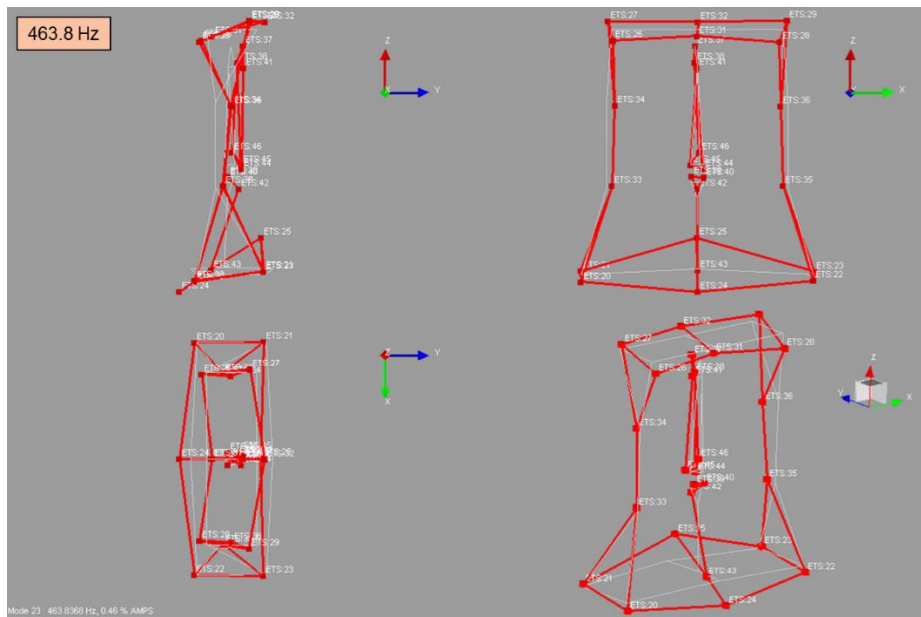


Figure 4.74. Test results, 16th mode shape, 463.8 Hz

Table 4.10. Mode frequencies and shapes obtained by modal test

Mode shape #	Freq (Hz)	Label
1	16.6	Upper TR 1st bending
2	24.5	Frame sway and Upper TR 2nd bending coupled
3	42.9	Upper TR 2nd and lower TR 1st bending coupled
4	48.2	Upper TR 2nd and lower TR 1st bending coupled
5	60.1	Frame rocking, upper TR 2nd and lower TR 1st bending coupled
6	80.9	Upper TR 2nd bending
7	93.9	Upper TR 2nd bending
8	116.5	Frame torsion and Upper TR 2nd bending coupled
9	122.5	Upper TR 3rd bending (aliased)
10	192.7	Lower TR 1st torsion
11	259.4	Frame column 1st and lower TR 1st bending coupled
12	328.5	Frame column + horizontal frame bending
13	343	Frame horizontal torsion
14	369.6	Frame two column bending
15	443.2	Frame column 2nd bending and lower TR 2nd bending coupled
16	463.8	Frame bending with undetermined mode shape

4.5.2.2. Analysis-Test Correlation

Correlation of FE analysis and test results are checked using Modal Assurance Criteria (MAC) in Eq (4-40).

$$MAC_{ij} = \frac{(U_{a,i}^T U_{x,i})^2}{(U_{x,i}^T)^2 (U_{a,j})^2} \quad (4-40)$$

In Eq (4-40) U_a and U_x are the eigenvectors which obtained from analysis and test respectively. For analysis and test correlation MAC numbers are shown in Figure 4.75.

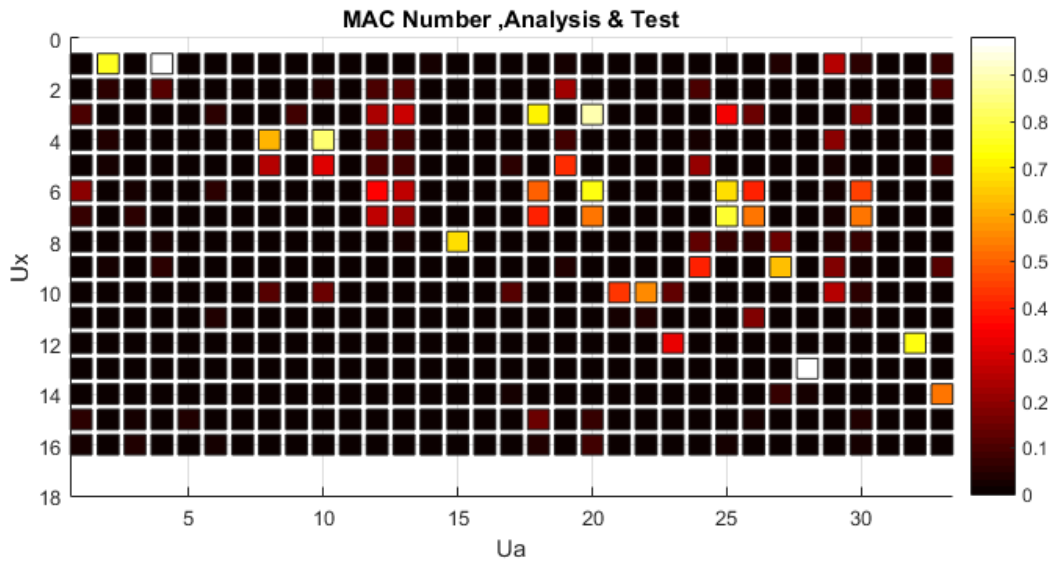


Figure 4.75. MAC numbers between analysis and test

From Figure 4.75 it is observed that there is no significant consistency between analysis and test results except for a few numbers of modes. List of eigenfrequencies corresponds to correlated modes is given in Table 4.2. The most significant observation made from this comparison is that results obtained from analysis are higher than test results. This is probably because elastic modulus value of the elastomer used in the analysis is higher than actual. Analysis model should be updated with a lower modulus for elastomer.

Table 4.11. *List of correlated modes*

Mode number		Freq (Hz)	
Analysis	Test	Analysis	Test
2	1	16.5	16.6
4	1	19.9	16.6
8	4	57.1	48.2
10	4	60.0	48.2
15	8	121.9	116.5
20	6	187.8	80.9
28	13	370.1	343.0

4.5.3. Simulation of Dynamic Stiffness Measurements in the Test Setup Using Finite Element Based Harmonic Response Analysis

Finite Element analysis is performed based on linear harmonic analysis procedures. Analysis model is constructed on the same model used in modal analysis, discussed in Section 4.3.2.1. Since harmonic displacement response due to harmonic forces is evaluated, Steady State Dynamics (SSD) procedures are used. ABAQUS offers three types of SSD procedures: Direct, Modal and Subspace-Based. Subspace-based method is the most computationally efficient method and allows including friction-induced and viscoelastic damping effects. (Abaqus 2016 Documentation Guide)

In these procedures, modal model is built with the modes obtained in frequency extraction analysis, then harmonic displacement values resulting from harmonic forces are calculated. For this reason, subspace-based methods must be preceded by a frequency extraction step. Solution is requested between 2-300 Hz. In frequency extraction step the modes from rigid body to 1000Hz are requested.

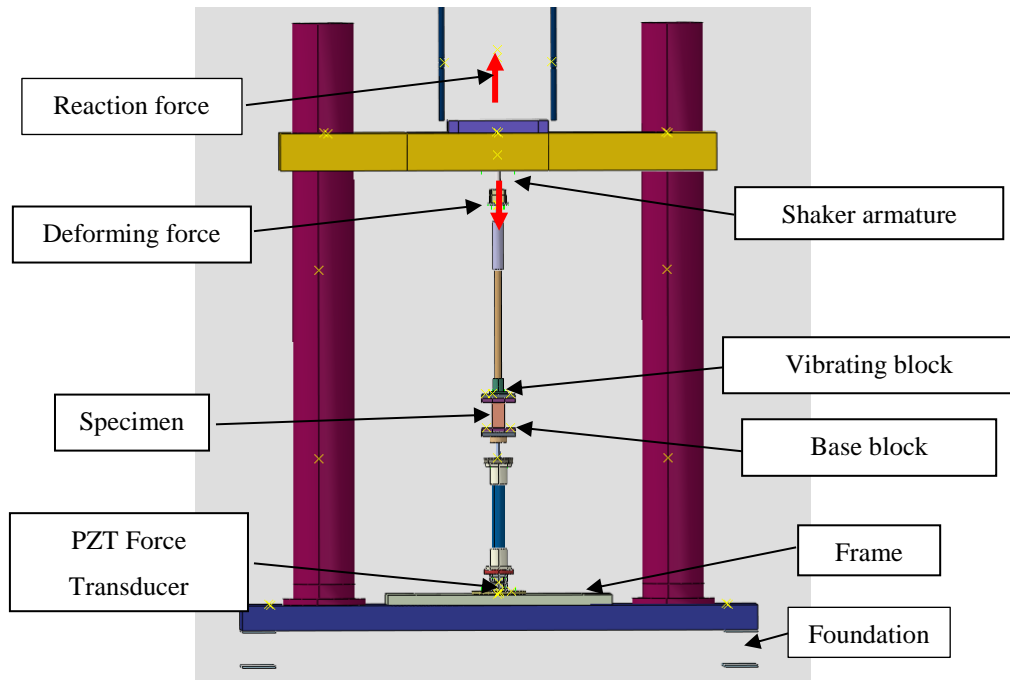


Figure 4.76. General configuration of the analysis model

Deformation force is applied on shaker armature and axial tension-compression is measured from Force Transducer (See Fig 1). Force has a unit magnitude since the procedure is linear. The force applied by the shaker is defined on Reference Point (RP) which represents the shaker armature. Since the force is created by electromagnetic induction and the shaker body is subjected to reaction force while induction force drives the armature, the same amount of force must be applied on the RP which represents the shaker body.

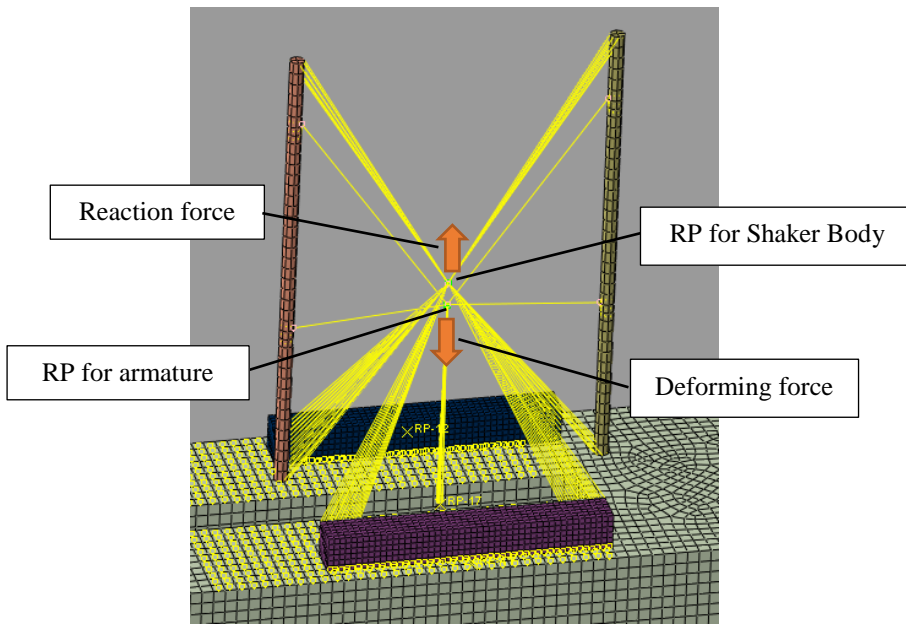


Figure 4.77. Electrodynamic actuator model

The specimen is modelled with three engineering elements that connected between mounting blocks (See Figure 4.78). These elements are along all three principal axis X,Y and Z. The properties of these elements are given in Table 4.12. Z-axis represents the direction of the applied force and X and Y directions are transverse directions. The stiffness values of the elements are obtained by modification of the correlated model while damping values are based on assumption. For simulations the frequency dependent properties of specimens are ignored.

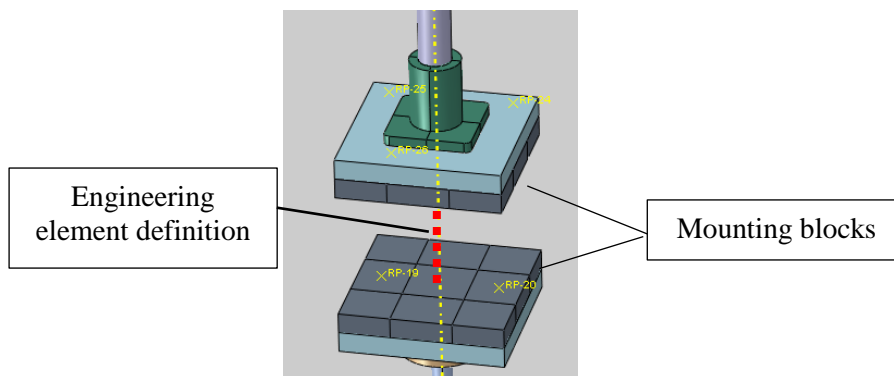


Figure 4.78. Engineering element definition between mounting blocks to represent resilient specimen

Table 4.12. *Specimen properties used in the test simulation model*

Axis	<i>Stiffness</i> (N/mm)	<i>Damping coefficient</i> (N.s/mm)
X	5	$1.0 \cdot 10^{-4}$
Y	5	$1.0 \cdot 10^{-4}$
Z	50	0.01

Dynamic stiffness is calculated by Eq (2-27) which discussed in detail in Section 2.3.2.2. It is known that transmission rods are nearly incompressible in axial direction about the frequency range of interest, then there should be no difference between measurements that is taken on the same body. Possible deviations would be occurred due to coupling effects form bending modes.

In this study, 3 different configurations have been created. The effects of base support and presence of offset between transmission rods on the results will be observed. Table-6.1 shows the details of each configuration. In the first configuration, the assembly is mounted on resilient foundation, and there is no offset between transmission rods. The resilient foundation represents the situation where the apparatus is not fixed to the ground but placed on an elastic interface. In the second configuration, the assembly is mounted on the resilient foundation and the transmission rods are not connected coaxially. This represents the possible error due to assembling. In the final configuration, the assembly is completely fixed to the ground from the base and the transmission rod is mounted with offset as in the previous case.

Table 4.13. Analysis configurations used in test simulation

Config.	Type of Base Support	Alignment of Transmission Rods (See Figure 4.79)
1	Resilient foundation	No offset
2	Resilient foundation	With offset
3	Fixed to ground	With offset

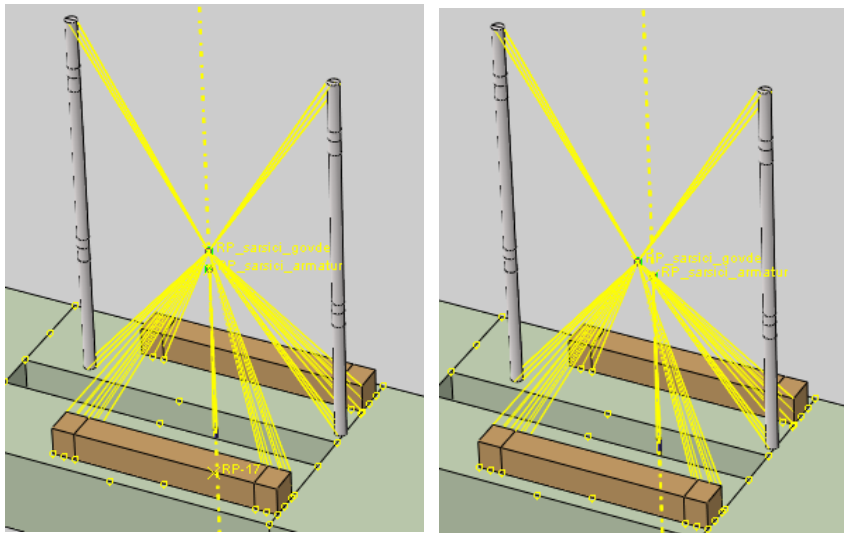


Figure 4.79. Configuration without offset between armature force axis and transmission rods (left) and with offset (right)

Acceleration response is taken on several points located on the structure. Measurement locations are illustrated in Figure 4.80. By selecting some of the points shown here, 5 different measurement methods are defined, and all methods are applied in each configuration. Details of each measurement method are given in Table 6.2. On the fixed and vibrating part, the measurement will be taken from one or several points from various positions of the system. The purpose of experimenting with different measurement methods is to see the effect of the location and number of the measurement point on the results and to see the structural interactions. In addition, it

is expected that whether the possible deviations are corrected by the measurement method or not.

Table 4.14. Measurement methods used in the analysis mode and their details

Case	Force	Acceleration, Vibrating side	Acceleration, Base side
1	IEPE	On vibrating block, single point, no averaging	On frame, single point, no averaging
2	IEPE	On vibrating block, single point, no averaging	On base block, one point, no averaging
3	IEPE	On vibrating block, three points with averaging	On base block, two points with averaging
4	IEPE	On armature, single point	On frame, single point
5	IEPE	On armature, single point	No measurement

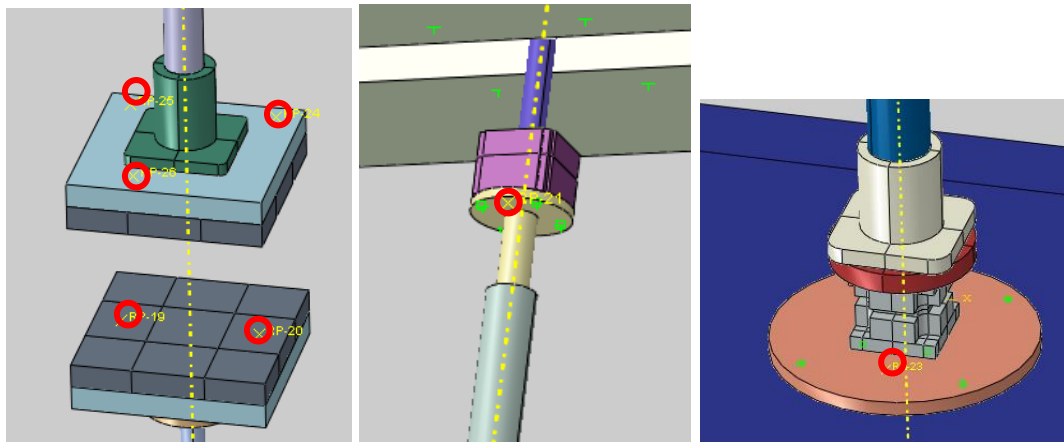


Figure 4.80. Measurement locations used in the analysis, vibrating blocks at left, armature on the middle and frame at right

4.5.3.1. Analysis Results

Firstly, real stiffness calculations and their deviation from the reference value will be represented for three configuration and 5 different measurement methods. After that same representation is done for damping coefficient calculations.

4.5.3.1.1. Real Stiffness Calculations

Real stiffness calculations for Configuration #1 are plot in Figure 4.81 and deviations from reference are given in Figure 4.82.

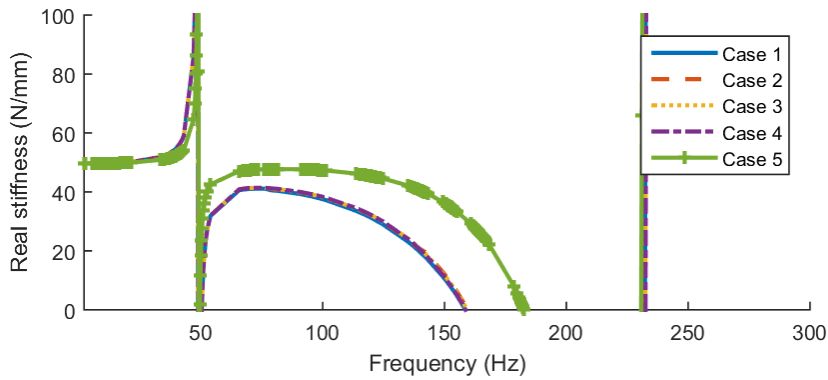


Figure 4.81. Real stiffness calculations for analysis configuration #1

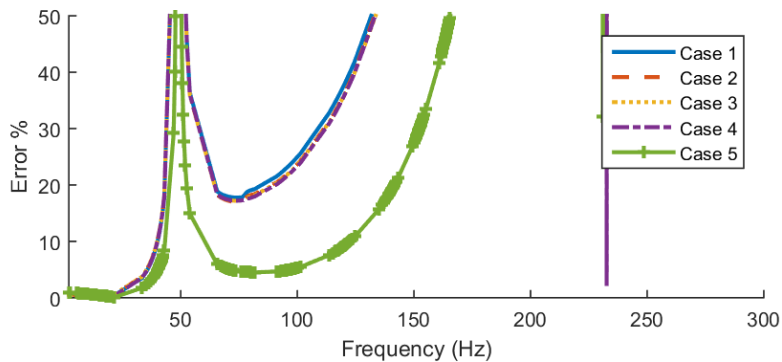


Figure 4.82. Deviations of real stiffness from reference for analysis configuration #1

It is observed that calculations are severely distorted at 48Hz and 230Hz. According to the mode shapes the interference of the modes with component along force axis is observed. At 48Hz there is rigid body-like motion on resilient mount and fixture has a bending mode along force axis at 230Hz. At those frequency values the applied force drives the fixture instead of deforming the test specimen. There is no distortion observed at the bending modes since they are not excited if there is no offset between specimen deformation and force axis.

For Configuration #2 real stiffness calculations are plot in Figure 4.83 and deviations from reference value is given in Figure 4.84. In addition to the previous case in this configuration distortions are observed at 12Hz, 75Hz and 180Hz. Offset between applied and the reaction force creates moment, which excites the modes in direction perpendicular to the force axis, which indicates the motion of the transmission rods. This results in measuring deformation different from the actual deformation of the test specimen.

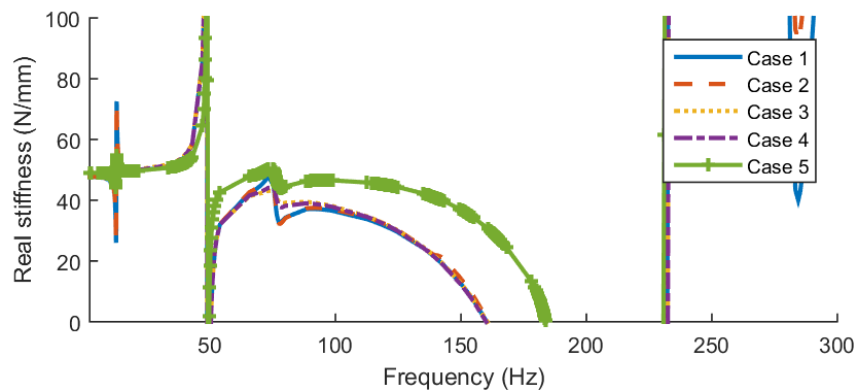


Figure 4.83. Real stiffness calculation for analysis configuration #2

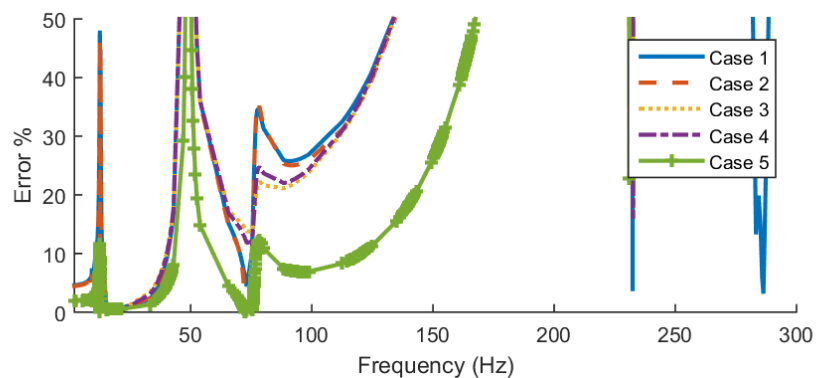


Figure 4.84. Deviation of real stiffness from reference for analysis configuration #2

In this model deviations are observed at frequencies where bending modes of the transmission rods are present. This effect is observed more significantly for Case 1&2 where accelerometers are placed close to the specimen, because acceleration due to bending of the rods are measured. It is also observed that averaging reduces distortions

if accelerometers are located close to the specimen. Placing accelerometers close to the actuator also reduces the distortions due to bending.

For Configuration #3 real stiffness calculations are plot in Figure 4.83 and deviations from reference value is given in Figure 4.84.

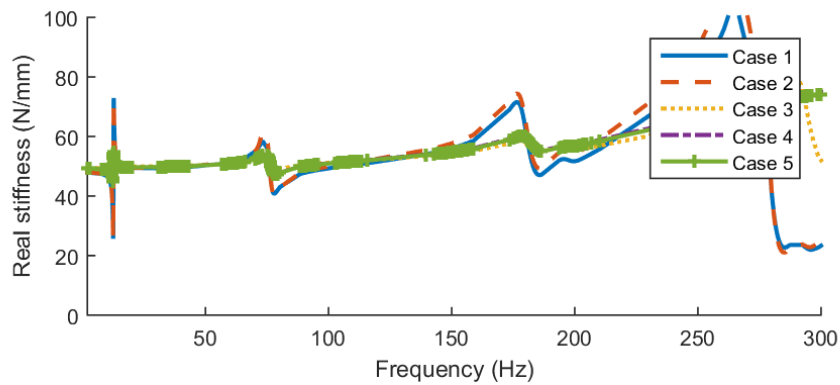


Figure 4.85. Real stiffness calculation for analysis configuration #2

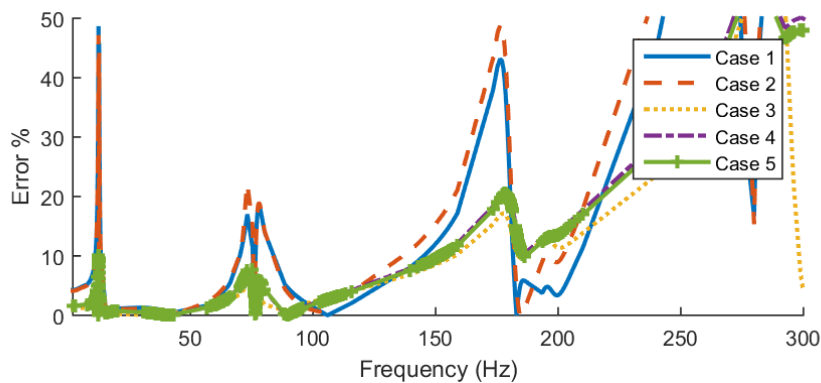


Figure 4.86. Deviation of real stiffness from reference for analysis configuration #2

Compared to the previous analysis configuration it is observed that only the distortions due to bending motion of the transmission rods are observed. Reduction of distortion is possible by averaging the acceleration measurements or placing the accelerometer close to the actuator, as observed in Configuration #2.

4.5.3.1.2. Damping Coefficient Calculations

Damping coefficient calculations for configuration #1,#2 and #3 are given in Figure 4.87, Figure 4.89 and Figure 4.91 respectively. Deviations of damping coefficient from reference value are given in Figure 4.88, Figure 4.90 and Figure 4.92 at the same respect. By these plots it is seen that calculations are distorted at the frequencies where dynamic stiffness are distorted as well.

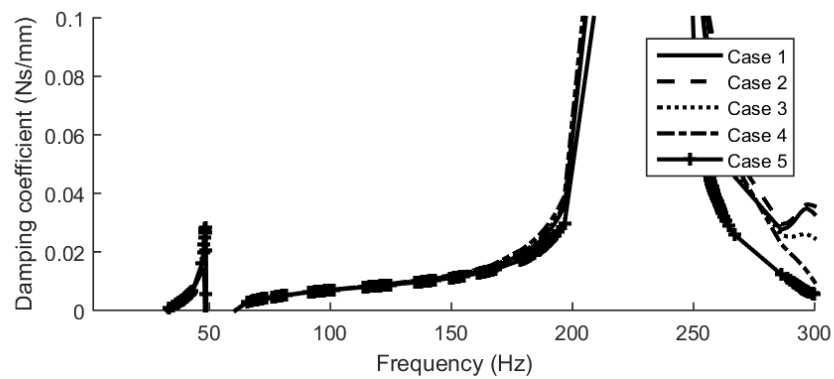


Figure 4.87. Damping coefficient calculations for analysis configuration #1

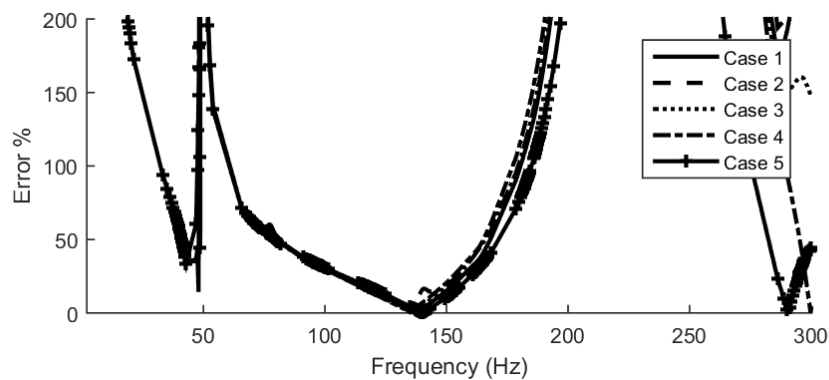


Figure 4.88. Deviations of damping coefficient from reference for analysis configuration #1

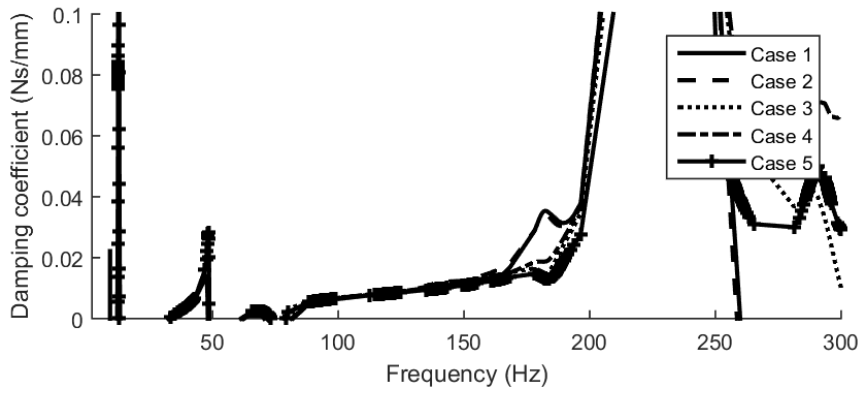


Figure 4.89. Damping coefficient calculations for analysis configuration #2

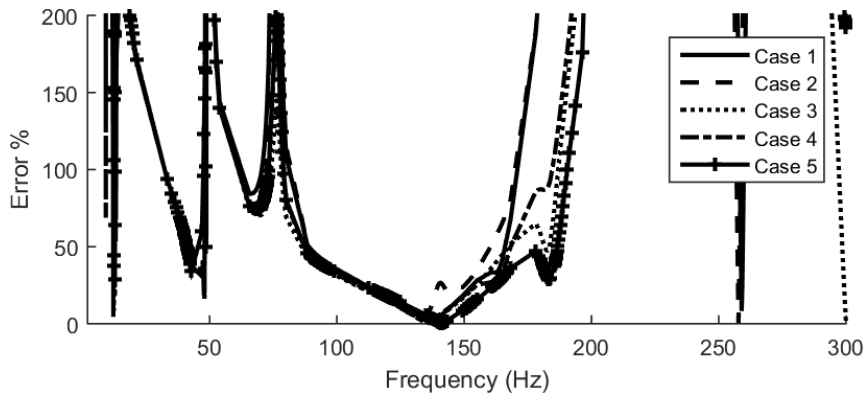


Figure 4.90. Deviations of damping coefficient from reference for analysis configuration #2

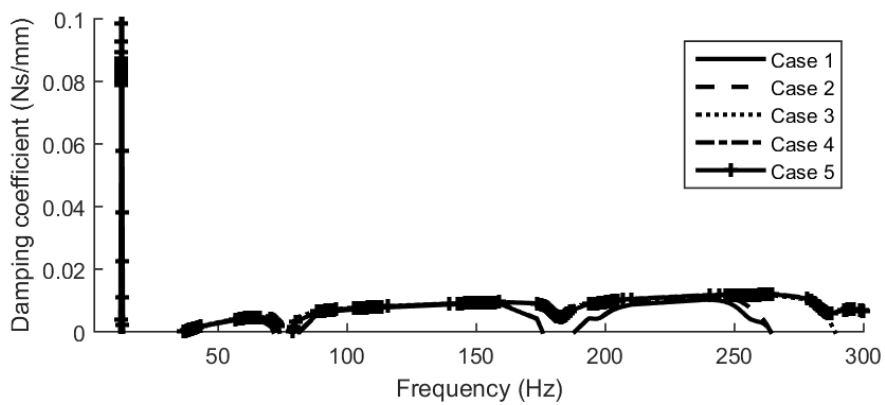


Figure 4.91. Damping coefficient calculations for analysis configuration #3

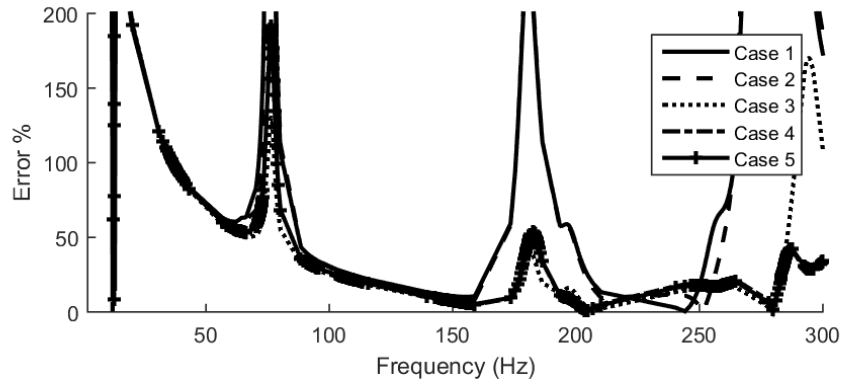


Figure 4.92. Deviations of damping coefficient from reference for analysis configuration #3

4.5.4. Comments on Analysis Results

As a result of this study, the effects of some structural features of the test fixture on the results are shown. If the fixture is rigid or the actuator is decoupled, the bending modes of the transmission rods do not influence on the results. However, bending motion of transmission rods is coupled with axial motion if fixture is resilient in transverse direction. Coupling effects are more significant if transverse motion is unconstrained.

In the case where the actuator is connected to the fixture and the force axis is offset, reaction forces excite the bending-induced modes of the transmission rods. To conclude, correct assembly of the actuator is important with respect to coupling of transverse motion. It is also important to prevent the movement of the fixture in the direction of the force application axis.

4.6. Design Re-Evaluation & Validation

In order to see the accuracy, performance and possible errors of the assembled test system in terms of dynamic stiffness measurements, it is necessary to test on the physical specimens that we know its dynamic stiffness. In order to do this, a metallic spring with a known stiffness is planned to use for validation study.

A metal spring is a good choice since metals show little internal damping when compared to elastomers. Real stiffness measured with the test setup must be close to static deflection coefficient. The phase difference between force and deflection should be close to zero.

Previous studies have been based on simulation, and an analysis-test comparison will be made to verify how the setup dynamic characteristics shown in the simulations affect dynamic stiffness measurements and whether has a negative effect on measurement accuracy.

4.6.1. Design of a Calibration Specimen

The size and shape of the spring depend on the required stiffness. Therefore, type of the validation specimen is selected according to: stiffness of the validation specimen should have similar value with the actual test specimen. It is also important that there must be no internal resonance of elastic member within the frequency range of interest (i.e self-ringing frequencies).

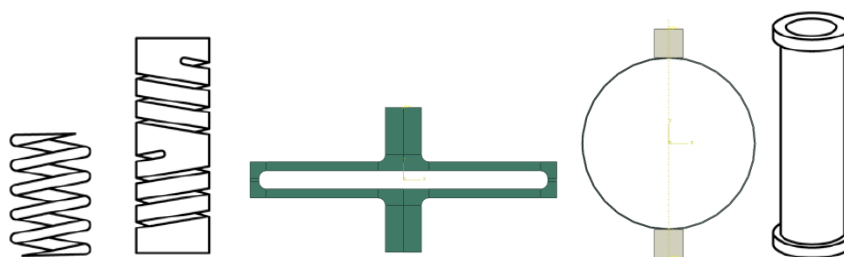


Figure 4.93. Spring types proposed for a calibration spring

The types of springs proposed for using as axial tension-compression are illustrated in Figure 4.93 (ASTM D5992 - Standard Guide for Dynamic Testing of Vulcanized Rubber and Rubber-Like Materials Using Vibratory Methods, 2011)

The specifications of these spring types are given below:

- Coil spring: Provides variety of stiffness with low cost. While compressing ends of the springs are rotate then friction at ends due to rotation is present but not significant at the practical point of view.
- Double opposed coil spring: eliminates rotation problem. Internal resonances are low.
- Ring spring: stated as an excellent option for a spring
- Quadruple beam spring: a compact form of ring spring and better linearity.
- Thin walled tube: most stiff option, highest self-ringing frequency. Care for yielding and buckling.

4.6.1.1. Detailed Design of Calibration Specimen

In this study design of quadruple beam spring and a ring spring is performed. Quadruple beam spring is aimed to represent stiff specimens while ring spring provides low stiffness values with high internal resonance frequency.

A parametric study is performed to select correct type for validation. For this application double-cantilever-beam and ring spring types will be evaluated.

The quadruple beam spring and its dimensions are represented in Figure 4.94 while ring spring is given in Figure 4.95. The thickness in the direction outside of the page is expressed by B for both springs.

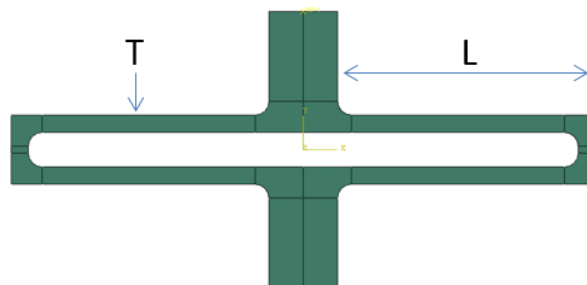


Figure 4.94. Quadruple beam spring with design dimensions

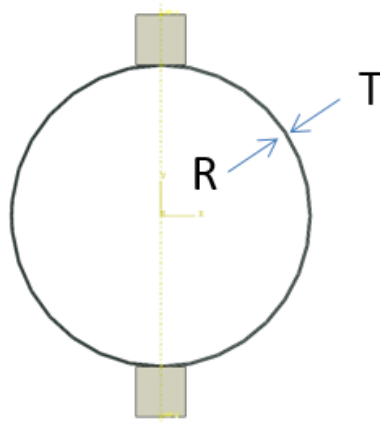


Figure 4.95. Ring spring with design dimensions

Finite element model is created for each specimen to determine the stiffness and maximum allowable load. The spring material is selected as Aluminum 6061 T6 for both springs with yield stress 276 MPa (Aluminum 6061-T6; 6061 T651). Each spring is fixed from one end and other and is constrained at all directions except along tension-compression axis. Reaction force is measured from the fixed location while deflection is measured from the other end. The force value corresponding to the point where it reaches the yield stress shall be determined as the maximum load. Internal resonances are determined by eigenvalue extraction analysis. The results and corresponding parameters are listed in Table 4.15 and Table 4.16.

Table 4.15. Parameters and results for quadruple beam spring

T (mm)	L (mm)	B (mm)	F (Hz)	Load at yield (N)	Deflection at yield (mm)	Calculated Stiffness (N/mm)
5	75	10	1042	1150	2.7	418
5	160	10	216	509	14.7	34.6
3	100	10	760	363	7.9	45.7
7	50	10	2388	2300	1.0	2258

Table 4.16. Parameters and results for ring spring

R (mm)	T (mm)	B (mm)	Internal resonance (Hz)	Calculated Stiffness (N/mm)
30	1	20	*	50
30	0.5	20	613	10.9
30	0.3	20	*	2.4
30	0.2	20	*	0.7
30	0.1	20	*	0.1

As a result of this study spring design is performed for range 30-2000N/mm with quadruple beam and 0.1-50N/mm with ring spring configuration. It is observed that for stiffness values below 40N/mm internal resonance frequency is reduced as much as to the frequency range of interest. Ring spring design is more convenient for lower stiffness values since it provides higher internal resonance.

4.6.1.2. Deflection Tests

Quasi-static deflection tests are applied on specimens to be used for validation cases are firstly. The aim of quasi-static tests is that the making force increment is adequately slow to avoid mass loading and possible damping effects.

The test specimen of which force vs deflection is measured is shown in Figure 4.96. This a ring spring made of aluminum with two steel blocks as fixture interfaces. Force-deflection tests are performed on Instron Uniaxial Tensile Test System. Since there is no fixture available for holding the plate interfaces, the tests are only performed on compression mode. *Since tests are performed in restricted area it is not allowed to take photo of the test system.*



Figure 4.96. Ring spring calibration specimen

Calibration spring is deformed to 0.6mm with 0.1 mm/s deflection rate then unloaded. This cycle is performed 5 times in total. The force-displacement curve is given in Figure 4.97. Spring coefficient of the ring spring is obtained as 50.5 N/mm. No significant hysteresis is observed. It is observed that linearity is preserved at least until 0.1mm of deflection.

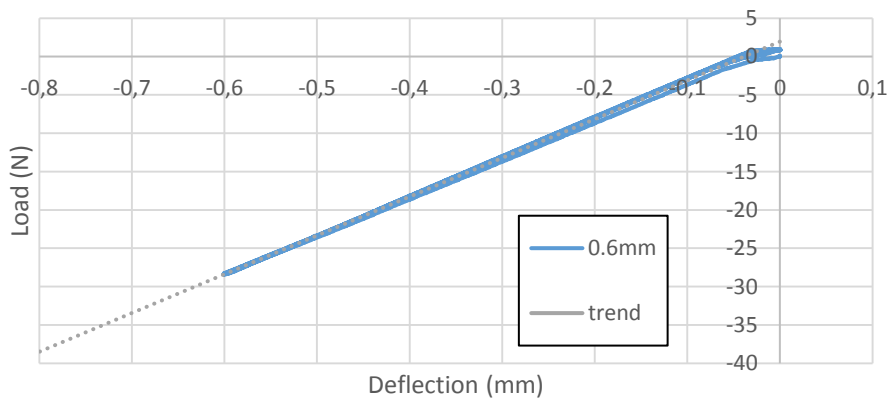


Figure 4.97. Force-deflection curve of the calibration spring

4.6.2. Dynamic Stiffness Validation Tests

This test system was developed for both isolators and viscoelastic material characterization. Therefore, the accuracy of the dynamic stiffness measurements is important for the characterization of the vibration isolators because these values are needed for the calculation of the vibration isolation performance. If complex modulus is to be obtained using the dimensions of the material specimen from the measured dynamic stiffness (as discussed in Section 2.3.2.3), the precise and accurate measurement of the dynamic stiffness is important for accurate and precise measurement of the material properties (complex modulus). For validation of the test system, the metallic specimen characterized in Section 4.6.1.1 is used. Test results are also compared with Finite Element (FE) model outputs to verify how the setup dynamic characteristics shown in the simulations affect dynamic stiffness measurements and whether has a negative effect on measurement accuracy.

In test model, force measurement is obtained from Piezoelectric transducer. Two accelerometers are utilized for displacement measurement. Analysis model evaluated in Section 4.5.3., Configuration #1 with measurement method labeled as “Case 4” is used for the comparison. Test is performed between 10-80Hz with 1Hz increments. Relative displacement is controlled with reference value 0.05mm. Displacements are obtained by from acceleration measurements with Eq (2-26).

Real stiffness measurements for metallic specimen are shown in Figure 4.98. Reference value used for the comparison is determined as 50N/mm according to the static deflection measurements discussed in Section 4.6.1.1. Damping coefficient of the specimen is also evaluated and results are shown in Figure 4.99. Since there is no reference value for evaluation of damping coefficient, the value used in the analysis model is used for the comparison, 0.01N.s/mm.

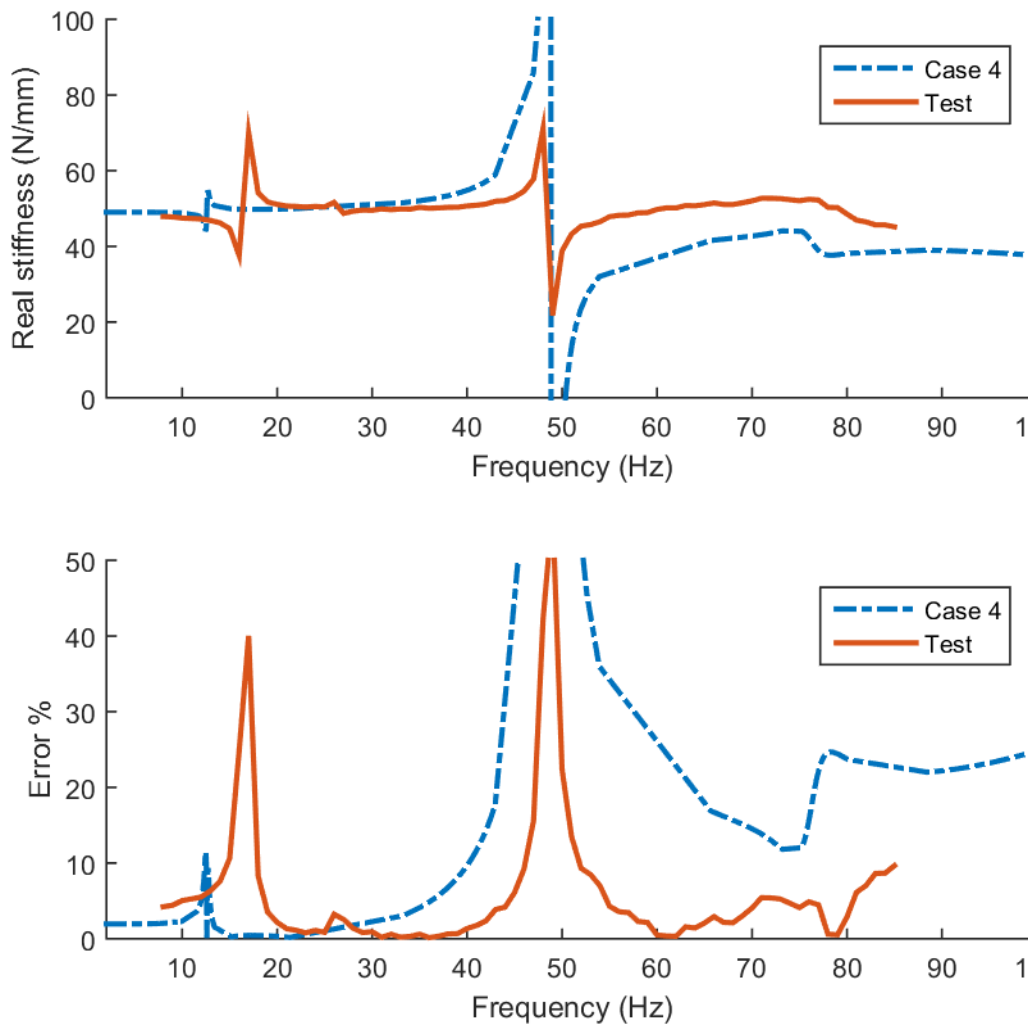


Figure 4.98. Real stiffness measurements and deviation from the reference value, 50N/mm

Stiffness measurements are obtained within 5% error within the sweep range except in some frequencies. Measurements are distorted significantly at frequency values 16, 28, 48 and 78Hz. These are due to coupling effects of the structural modes, evaluated in previous sections. Same frequency values correspond to distortions in the analysis model as well, except for 28Hz.

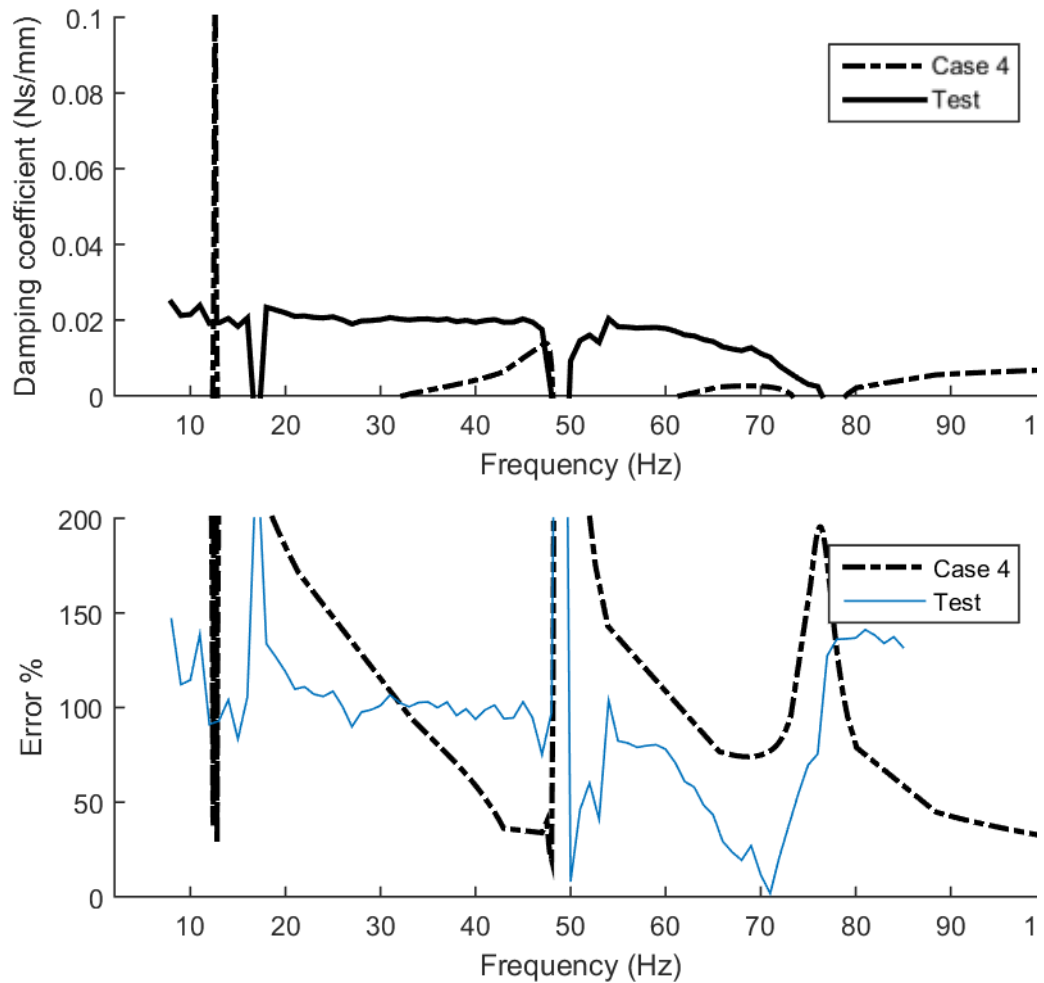


Figure 4.99. Damping coefficient measurements and deviation from the reference value, 0.01N.s/mm

For damping coefficient measurements deviation is significantly high for all frequency range. This may be due to the error in the test system or specimen. Although the test specimen is metallic and expected damping is close to zero, the bolted joints used to assembly the flexible element to connection block may increase damping of the specimen. Spikes within the sweep range are consistent with analysis results.

In addition, test results with some elastomer specimens are provided in Appendix A. The stiffness values of the specimen used in these measurements are not known prior to testing, so they will only be compared with the results obtained with the setup designed in Chapter 3.

4.7. Conclusions

As a result of this study, the effects of some structural features of the test fixture on the results are shown. If the fixture is rigid or the actuator is decoupled, the bending modes of the transmission rods do not influence on the results. However, bending motion of transmission rods is coupled with axial motion if fixture is resilient in transverse direction. Coupling effects are more significant if transverse motion is unconstrained.

In the case where the actuator is connected to the fixture and the force axis is offset, reaction forces excite the bending-induced modes of the transmission rods. To conclude, correct assembly of the actuator is important with respect to coupling of transverse motion. It is also important to prevent the movement of the fixture in the direction of the force application axis.

Following conclusions could be made in this section:

- The effect of transmission rods on measurements depends on the presence and stimulation of those modes.
- If the displacement along the force axis is measured independently from the transverse motion the bending effects on the measurements disappears.
- Transmission rods should be mounted coaxially perfect in order to avoid creating coupling moment that causes bending.
- If the perfect alignment is not possible bending modes should be out of frequency range of interest or damped.

At the end of the study, the questions in 4.5 could be answered as following:

- The fixture should be fixed to the ground. This will eliminate the SDOF-like mode of the fixture on flexible mounts, where large distortion occurs at the measurements. In addition, fixing increase the fixture bending modes.

- Misalignment on the transmission rods will excite the bending modes of the transmission rods. The presence of bending modes on transmission elements does not influence on results if they are not excited.
- The sensors are located on a position where transverse motion is minimum. This could be achieved by placing the sensors as close as possible to the line of action. If it is not possible, multiple sensors could be used to eliminate transverse motion by averaging the measurements.
- Based on the calculations the results are sensitive to the effective mass of the part of the fixture between specimen and the force transducer.

CHAPTER 5

CONCLUSION

Two studies are performed within the scope of the thesis. These studies are aimed to design test systems for dynamic characterization of viscoelastic materials and components. These studies are focused on different aspects for the mechanical design of these systems. However, in these two studies, problematic results were obtained due to unforeseen conditions at the initial phase of the design. Efforts to solve these problems constitute a part of this study.

In the first study, a previously established viscoelastic characterization test setup is modified in order to introduce a preloading mechanism. A manual preloading mechanism is designed, and specific part of the structure is modified. In the validation phase of the design, unexpected measurements are obtained at some frequencies due to decoupling springs, then efforts have been made to solve this problem. Influence of dynamic character of the decoupling springs is treated as a possible source of error on the dynamic stiffness measurements. The study is proceeded on determination of internal resonance frequencies of decoupling springs. As a result, the presence of internal resonance frequency of decoupling springs within the frequency range of interest may influence on the dynamic stiffness measurements. In addition, using elastomeric materials are shown as a design alternative since they have higher natural frequency compared to coil springs.

In the second study, a test setup design was made from scratch. This setup is aimed to measure the frequency and temperature-dependent dynamic resistance of elastomer vibration isolators, which will be designed in the scope of a project. It can also be used to measure the complex modulus of viscoelastic materials from material specimen if desired. This test system is planned as an alternative to the revised test system in Chapter 3. Therefore, a mechanical design study was carried out to eliminate the structural modes under the restrictions created by the equipment used. Initially,

preloading mechanism design with coil springs did not work properly, so tests were continued after the spring mechanism was removed from the system. Subsequently, some inconsistencies were observed in the stiffness and loss factor measurements, and the reason for these was considered to be the structural features which were not taken into account. Consequently, an error analysis study was conducted and inferences about which structural component is effective on the measurements were tried to be made.

As a result of error analysis, the effects of some structural features of the test fixture on the results are shown. If the fixture is rigid or the actuator is decoupled, the bending modes of the transmission rods do not influence on the results. However, bending motion of transmission rods is coupled with axial motion if fixture is resilient in transverse direction. Coupling effects are more significant if transverse motion is unconstrained. In the case where the actuator is connected to the fixture and the force axis is offset, reaction forces excite the bending-induced modes of the transmission rods. Therefore, correct assembly of the actuator is important with respect to coupling of transverse motion. It is also important to prevent the movement of the fixture in the direction of the force application axis.

In order to test findings stated above, a metal spring specimen with a stiffness value was designed and frequency-sweep tests were performed using this specimen. As a result of frequency-sweep tests, consistent behaviors with the analysis studies were observed. However, there were unsolved inconsistencies in damping measurements.

As a future work, a functional preloading mechanism for second design could be made and the reasons which cause inconsistent damping measurements could be determined.

REFERENCES

- Abaqus 2016 Documentation Guide. (n.d.).
- Allen, B. (1996). A direct complex stiffness test system for viscoelastic material properties. *Proceedings of Smart Structures and Materials*.
- Aluminum 6061-T6; 6061 T651. (n.d.). Retrieved from Matweb: <http://asm.matweb.com/search/SpecificMaterial.asp?bassnum=ma6061t6>
- APS 400 ELCTRO-SEIS Long Stroke Shaker with Linear Ball Bearings Datasheet. (2013).
- ASTM D4065 – 12 Standard Practice for Plastics: Dynamic Mechanical Properties: Determination and Report of Procedures. (2012).
- (2011). *ASTM D5992 - Standard Guide for Dynamic Testing of Vulcanized Rubber and Rubber-Like Materials Using Vibratory Methods*.
- ASTM E756 - 05 Standard method for measuring vibration-damping properties of materials. (2005).
- Bagley, R. L. (1989). Power Law and Fractional Calculus Model of Viscoelasticity. *AIAA Journal* (27).
- Banks, H. T., Pinter, G. A., Potter, L. K., Gaitens, M. J., & Yanyo, L. C. (2013). Modelling of Nonlinear Hysteresis in Elastomers.
- Bilgi, E. B. (2016). *Design and Development of a Modular Dynamic Test System for Resilient Mechanical Components and Viscoelastic Materials*. M.Sc Thesis, Gradual School of Natural and Applied Sciences, METU .
- Bower, A. F. (2010). *Applied Mechanics of Solids*. CRC Press.

- Budynas, R. G., & Nisbett, J. K. (2006). *Shigley's Mechanical Engineering Design, 8th Ed.* McGraw Hill.
- Da Silva (ed), C. (2005). *Vibration and Shock Handbook.* CRC Press.
- Diani, J., Fayolle, B., & Gilormini, P. (2008). A review on the Mullins effect. *European Polymer Journal*, 601-612.
- Erol, F. (2014). *Development of a Test System for Viscoelastic Material Characterization.* M.Sc. Thesis, Gradual School of Natural and Applied Sciences, METU .
- Ferry, J. (1980). *Viscoelastic Properties of Polymers, 3rd ed.* Wiley.
- Frampton, R. C. (n.d.). *The Dynamic Testing of Elastomers.* Davenport-Nene Testing Systems.
- ISO 10546-3:2002 Acoustics and vibration -- Laboratory measurement of vibro-acoustic transfer properties of resilient elements -- Part 3: Indirect method for determination of the dynamic stiffness of resilient supports for translatory motion. (2002).
- ISO 10846-2:2008(E) Acoustics and vibration – laboratory measurement of vibro-acoustic transfer properties of resilient elements – part 2: direct method for determination of the dynamic stiffness of resilient supports for translatory motion. (2008).
- ISO 10846-5:2008(E) Acoustics and vibration – laboratory measurement of vibro-acoustic transfer properties of resilient elements – part 5: driving point method for determination of low-frequency transfer stiffness of resilient supports for translatory mot. (2008).
- ISO 18437-3:2005(E) Mechanical vibration and shock – characterization of the dynamic mechanical properties of visco-elastic materials – part 4: dynamic stiffness method. (2005).

- ISO 4664-1:2011 Rubber, vulcanized or thermoplastic -- Determination of dynamic properties -- Part 1: General guidance. (2011).
- ISO 6721-1:2019 Plastics -- Determination of dynamic mechanical properties -- Part 1: General principles. (2019).
- Jones, D. I. (2001). *Handbook of Viscoelastic Damping*. Wiley.
- Kunz, J., & Studer, M. (2006). *Determining the Modulus of Elasticity in Compression via the Shore A Hardness*. Munich: Carl Hanser Verlag.
- Lakes, R. (2004). Viscoelastic measurement techniques. *Review of Scientific Instruments*, 4(75), 797-810.
- Liu, G. R., & Quek, S. S. (2003). *The Finite Element Method - A Practical Course*.
- Nashif, A., Jones, D. I., & Henderson, J. P. (1985). *Vibration Damping*. Wiley.
- Oberst, H., & Frankenfeld, U. (1952). Über die Dämpfung der Biegeschwingungen dünner Bleche durch festhaftende Beläge. *Acustica*(2), 181-194.
- Ogden, R. W. (2013). *Non-Linear Elastic Deformations*. Courier.
- Ozgen, G. O. (2005). Design and Development of a Complex Shear Modulus Measurement Setup For Viscoelastic Materials. *SAE Noise and Vibration Conference and Exhibition*.
- Ozgen, G. O., Erol, F., & Batihan, A. C. (2012). Dynamic Stiffness-Based Test Systems for Viscoelastic Material Characterization: Design Considerations. *Topics in Modal Analysis I, Vol 5*, 287-297.
- Pritz, T. (1980). Transfer function method for investigating the complex modulus of acoustic materials: spring-like specimen. *J Sound Vibration*, 3(72), 317-341.
- Roland, C. M. (2016). *Reinforcements of Elastomers*. Elsevier.
- Semat, H., & Katz, R. (1958). Wave Motion. In *Physics* (pp. 367-388).

SIMULIA. (2016). *Testing and Analysis of Elastomers with Abaqus*.

Uz, C. (2013). *Design of a Test Setup for the Characterization of Vibration Isolators*.
M.Sc. Thesis, Gradual School of Natural and Applied Sciences, METU .

Williams, M. L., Landel, R. F., & Ferry, J. D. (1955). The Temperature Dependence of Relaxation Mechanisms in Amorphous Polymers and Other Glass-forming Liquids. *J of American Chemistry Society*, 77(14), 3701-3707.

A. COMPARISON OF DYNAMIC STIFFNESS MEASUREMENTS MADE USING THE TWO TEST SETUPS STUDIED IN THIS THESIS

In this section some tests performed on various specimens with the setups designed in the scope of this thesis are presented. A vibration isolator LORD AM-009 and a custom-made elastomeric isolator are the test specimens for comparative tests.

First comparative tests are performed on a LORD AM-009 vibration mount in the setups represented in Chapter 3 and Chapter 4. Real stiffness measurements for room temperature are given in Figure A.1 and measurements for loss factor are given in Figure A.2. The label “Ds1” and “Ds2” are used for the setups represented in Chapter 3 and Chapter 4 respectively. Displacement amplitude is not controlled during these tests. In addition same specimen is tested with a commercial test setup, MTS 831.50 with controlled amplitude 0.01 mm peak-to-peak.

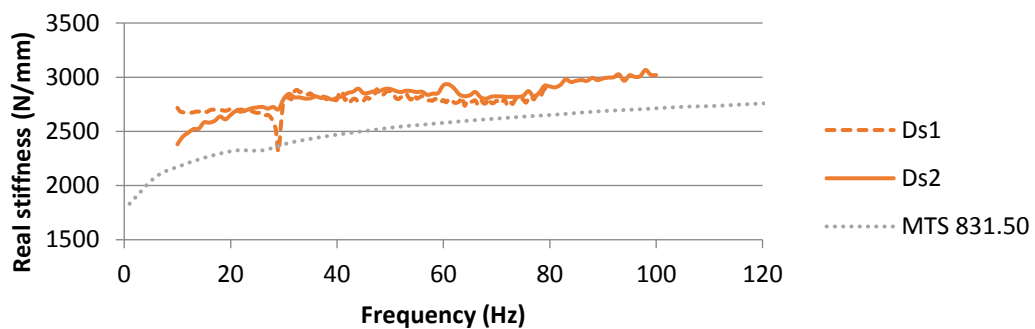


Figure A.1. Real stiffness measurements for LORD AM-009

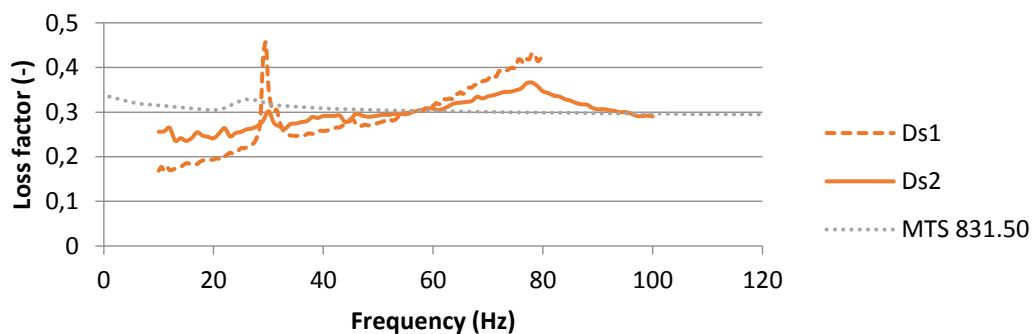


Figure A.2. Loss factor measurements for LORD AM-009

Other tests are performed on a custom-made vibration mount in the setups represented in Chapter 3 and Chapter 4, at two different temperatures. Real stiffness and loss factor measurements are represented for room temperature in Figure A.3-Figure A.4 and for 70°C in Figure A.5-Figure A.6. The labels “Ds1” and “Ds2” are used for the setup represented in Chapter 3 and Chapter 4 respectively. In these measurements both test systems show similar results for same specimen.

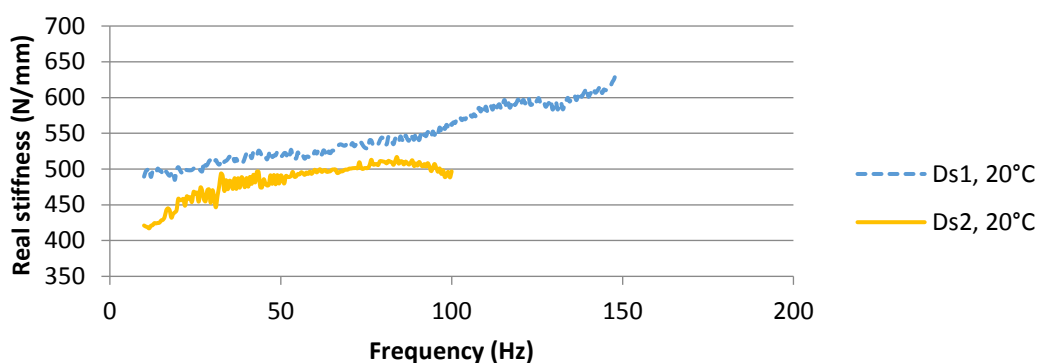


Figure A.3. Real stiffness measurements for custom-made vibration mount, room temperature

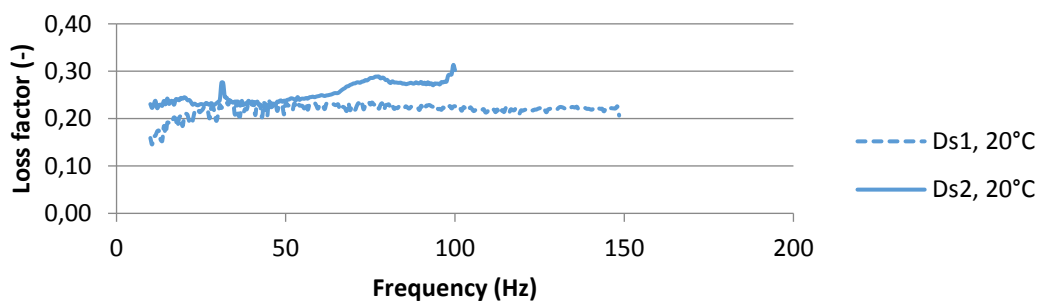


Figure A.4. Loss factor measurements for custom-made vibration mount, room temperature

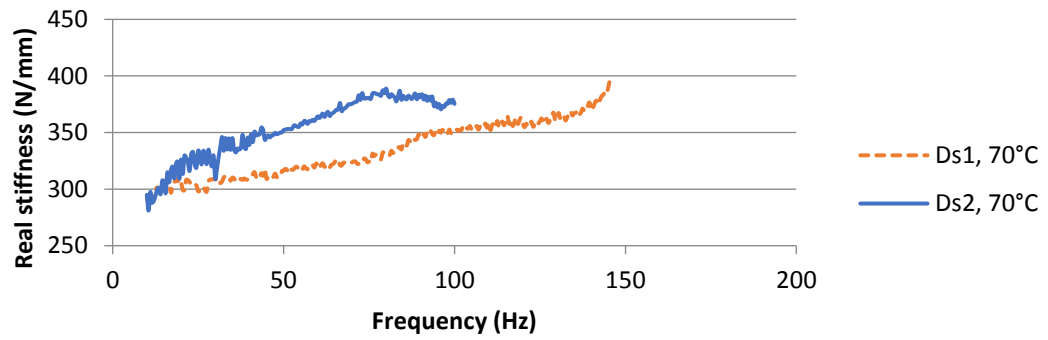


Figure A.5. Dynamic stiffness measurements for custom-made vibration mount, 70°C

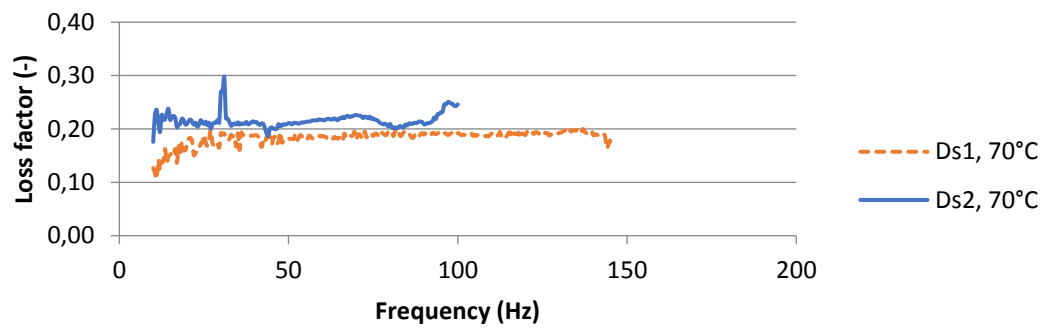


Figure A.6. Loss factor measurements for custom-made vibration mount, 70°C